Oxidovanadium Complexes with N-Donor Heterocyclic Chelates

by

Thulani Innocent Hlela

Submitted in partial fulfilment

of the requirements for the degree of

Masters of Science

in the School of Chemistry and Physics at the

University of KwaZulu-Natal

September 2013

Supervisor: Dr Irvin N. Booysen

As the candidate's supervisor I have approved this dissertation for submission:

Signed:_____   Date:_____

Table of contents

Chapter 1

Introduction

Chapter 2

Experimental

Chapter 3

Novel Vanadium Compounds with 2-Pyridylbenzimidazole

Chapter 4

Oxidovanaduim(IV/V) Compounds with 2-Substituted Phenylheterocyclic Chelators

Chapter 5

Attempted Synthesis of a Dioxidovanadium(V) complex bearing a Uracil Schiff base chelate: Intraligand Cyclization

Chapter 6

Conclusion and Future Work

Declaration - Plagiarism

I, Thulani Innocent Hlela, declare that

1. The research reported in this dissertation, except where otherwise indicated, is my original research.

2. This dissertation has not been submitted for any degree or examination at any other university.

3. This dissertation does not contain other persons' data, pictures, graphs or other information, unless specifically acknowledged as being sourced from other persons.

4. This dissertation does not contain other persons' writing, unless specifically acknowledged as being sourced from other researchers. Where other written sources have been quoted, then:

   a. Their words have been re-written but the general information attributed to them has been referenced

   b. Where their exact words have been used, then their writing has been placed in italics and inside quotation marks, and referenced.

5. This thesis does not contain text, graphics or tables copied and pasted from the Internet, unless specifically acknowledged, and the source being detailed in the thesis and in the References sections.

   Signed: _____

Declaration - Research Outputs

Manuscripts published:

1.   Booysen I.N., Hlela T.I., Gerber T.I.A., Munro O., Akerman M.P., Novel vanadium compounds with 2-pyridylbenzimidazole, *Polyhedron,* 2013, **53**, 8.

2.   Booysen I.N., Hlela T.I., Soares A., Gerber, T.I.A., Hosten E., Betz R., Refinement of the crystal structure of 2-{2-[2-(1*H*-benzo[*d*]imidazol-2-*yl*phenyl)disulfanyl]phenyl}-1*H*-benzo[*d*]imidazole-*N*,*N'*-diium sulfate tetrahydrate, $[C_{26}H_{20}N_4S_2][SO_4] \times 4H_2O$ *at* 100 K*, Z. Kristallogr*., 2011, **226**, 639.

3.   Booysen I.N., Hlela T.I., Ismail M.B., Gerber T.I.A., Hosten E., Betz R., 8-(2-Hydroxyphenyl)-1,3-dimethyl-1*H*-purine-2,6-(3*H*, 7*H*)-dione, *Acta Crystallogr.,* 2011, **E67**, o2347.

Manuscripts in preparation:

4.   Booysen I.N., Hlela T.I., Akerman M.P., Xulu B., Poly- and mononuclear oxidovanadium(IV/V) complexes with N,O-donor heterocyclic chelates, *Inorg. Chem. Comm.*, 2013.

5.   Booysen I.N., Hlela T.I., Akerman M.P., Masubuyane C., Mokotedi L., Xulu B., Anti-diabetic activity of oxidovanadium compounds with 2-pyridylbenzimidazole (Hpybz): synthesis, spectral characterization and crystal structure of $[VO(Hpbyz)_2SO_4].H_2O$, *J. Inorg. Biochem*., 2013.

All the experimental work was conducted by me. My supervisor and I jointly wrote up the publications as well as manuscripts 4 and 5 in preparation. The single crystals in the previous documents were run and resolved by Dr Matthew Akerman and Prof Orde Munro. Single crystal XRD analysis of the compounds in publication 2 and 3 were done by Dr Richard Betz and Dr Eric Hosten from the Nelson Mandela Metropolitan University. The published structure reports were compiled by Dr Richard Betz. The crystal structure descriptions of compound 4 in Chapter 4 and compound in Chapter 5 were given as in the respective publications. I did all the synthesis as well as characterization of these compounds.

Signed:_____

Acknowledgements

Abstract

The growing significance of vanadium in medicinal inorganic chemistry is due to the diverse biological activities of its metal complexes, as elaborated in Chapter 1. These biological activities stem from the fact that vanadium is an essential trace element as well as its ability to form active pro-drugs under physiological conditions. To improve the bio-availability of these potential metallopharmaceuticals, the use of biologically relevant ligand systems such as heterocyclic ligands were considered. These chelators should provide the stability and the ability to promote absorption through cell-membranes. The techniques as described in Chapter 2 were employed to analyze and characterize the formulated heterocyclic ligands and their metal complexes. The attained research findings are mainly divided into two studies which involve the explorative coordination chemistry of two classes of ligands: 2-pyridylbenzimidazole (see Chapter 3) and 2-phenylsubstituted heterocyclics (see Chapter 4). An additional brief study is described in Chapter 5 which discusses the attempted coordination of a uracil Schiff base ligand.

In Chapter 3, the coordination behaviour of Hpybz (2-pyridylbenzimidazole) towards vanadium in various oxidation states (*i.e.* +III/IV/V) was explored. The six-coordinate complex *cis*-[$V^{V}O_2$(Hpybz)(pybz)] (**1**) was isolated as the $CH_3OH.(H_2O)_2$ hydrate from the reaction of NH_4VO_3 and Hpybz in aqueous methanol. The crystal structure shows that the vanadium is bonded to two *cis*-oxido ligands, and to the two bidentate ligands pybz and Hpybz. This combination of ligands confers six-coordination on the metal centre, which is a rare coordination number for a mononuclear dioxido complex of vanadium(V). From the reaction between Hpybz and VCl_3 the cationic complex salt *cis*-[$V^{III}(OH)_2$(Hpybz)$_2$]Cl (**2**) was formed. The ligands in *cis*-[$V^{III}(OH)_2$(Hpybz)$_2$]Cl exhibits the same coordination behaviour as in **1**, but instead of the dioxido moiety present in **1**, two hydroxyl co-ligands are coordinated to the metal centre, with both chelator ligands neutral. Conductivity measurements in DMF affirmed that the compound is a 1:1 electrolyte. A novel binuclear mixed-valence oxidovanadium compound, (μ-O)[$V^{V}O$(pybz)$_2$.$V^{IV}O$(Hpybz)(acac)] (**3**), was obtained from the reaction of Hpybz with

VO(acac)$_2$. ESR analysis illustrates paramagnetic behaviour typical of a type I dimer. The metal compound, VO(Hpbyz)$_2$SO$_4$ (**4**).H$_2$O was isolated in a good yield from the reaction of two equivalents of Hpybz with vanadyl sulfate.

Chapter 4 reports the isolation of oxidovanadium compounds with 2-phenylsubstituted benz(imidazole/othiazole/oxazole) chelators. The 2:1 molar reaction between NH$_4$VO$_3$ and 2-hydroxyphenylbenzothiazole (Hobs) led to the formation of a polynuclear vanadium(IV) complex, [VO(obs)$_2$]$_n$ (**1**). The atmospheric oxygen-induced oxidation reaction of VCl$_3$ and 2-hydroxyphenyl-1*H*-benzoxazole (Hobo) afforded a similar oxidovanadium compound, [VO(obo)$_2$]$_n$ (**2**). A characteristic eight-line isotropic signal was observed in the ESR spectrum of **2** in DMF while, due to the poor solubility of **1**, a singlet was attained upon analysis of the single crystals. A diamagnetic dioxidovanadium(V) complex, *cis*-[VO$_2$(obz)py] (**3**) (Hobz = 2-hydroxyphenyl-1*H*-benzimidazole) was isolated from the reaction of NH$_4$VO$_3$ and Hobz in a methanolic solution. A broad singlet is found in the ^{51}V NMR spectrum at -520.7 ppm for the d^0-vanadium centre. The intra-ligand (π-π*) relaxations [466 nm for **1**, 376 nm for **2** and 469 nm for **3**] could be observed in the emission spectra which were obtained in anhydrous DMF. In an effort to synthesize a coordination compound of vanadium, the reaction of a heterocyclic ligand, 2-mercaptophenyl-1*H*-benzimidazole (Hsbz) with vanadyl sulfate resulted in an unexpected reaction product, [C$_{26}$H$_{20}$N$_4$S$_2$].[SO$_4$].4H$_2$O (**4**).

In Chapter 5, the metal-induced cyclization of 5-amino-6-[(*Z*)-(2-hydroxybenzylidene)amino]-1,3-dimethylpyrimidine-2,4-(1*H*, 3*H*)-dione (H$_3$duo) by NH$_4$VO$_3$ resulted in the formation of a cyclized benzimidazole derivative, 8-(2-hydroxyphenyl)-1,3-dimethyl-1*H*-purine-2,6-(3*H*, 7*H*)-dione (**1**). The IR spectra of H$_3$duo and its cyclized form are nearly identical where only minor shifts in the significant bands are observed. The molecular transformation was more evident when comparing the ^{1}H NMR spectra of H$_3$duo and **1**.

Keywords: Vanadium, Oxido, Dioxido, N-donor Heterocyclic ligands, Benzimidazole, Benzothiazole, Benzoxazole, Bidentate, Crystal Structure, Spectral Characterization

Crystallographic Data

Supplementary data for all the crystal structures that were determined in this study are stored on the compact disk that is included in this dissertation (attached to the inside back cover).

These data include the:

- Final crystal data and details of the structure determinations;
- Final coordinates and equivalent isotropic displacement parameters of the non-hydrogen atoms;
- Hydrogen atom positions;
- Isotropic displacement parameters;
- All bond distances and bond angles;
- Torsion angles;
- Contact distances;
- Hydrogen-bonds.

Chapter 1

Introduction

1.1   General Background

Vanadium is a $3d$ transition element with an atomic number of 23. Of the six known isotopes which exist only two are natural occurring, ^{50}V and ^{51}V. The percentage abundance of ^{50}V is 0.24% with a nuclear spin of 6 while ^{51}V is in the majority (99.76%) with a nuclear spin of 7/2. Vanadium is the 22nd most abundant element in the earth's crust. Furthermore, it is regarded as a universal element since it is also found to exist on the moon, in meteorites and hypothesized to be existent on the sun [1, 2]. Vanadium sources on earth are found in concentrated ores (*e.g.* patronite and roscoelite) and crude oil deposit [3]. Pure vanadium is obtained by heating vanadium residues to produce V_2O_5 which is then reduced to V(0) with molten calcium. It can also be obtained by the process of electrolysis of vanadium halides, or reducing vanadium halides with hydrogen, magnesium or carbon [4].

This transition metal has the electronic configuration of [Ar]$3d^34s^2$ and therefore has a highest oxidation state of +V when all the d and s orbital valence electrons partake in bonding. This d-bock metal exhibits a wide range of different oxidation states, from -III to +V. Variable valency accompanied with rapidly interconverting oxidation states is highly pH dependent which results in complex redox chemistry (especially in aqueous media). Oxidation states of natural occurring vanadium sources are +IV and +V and to a lesser extent +III [2, 3 and 4].

The discovery of protein tyrosine phosphatase (PTP) inhibition by vanadate $[VO_4]^{3-}$ has changed the façade of vanadium, since it has long been known as a toxic and carcinogenic element. However, vanadium has now been approved as an essential trace element. In addition, selected vanadium compounds have shown to exhibit a wide range of biological activities which include antitumour and antibacterial activity [5, 6].

1.2 Aim and Motivation

Heterocyclic compounds have been widely investigated in medicinal chemistry due to their range of applications. Pharmaceutically relevant compounds with heterocyclic moieties including benz(imidazole/oxazole/othiazole) (see **Figure 1.1**) have shown to exhibit an array of biological activities, such as anti-microbial [**7**, **8**], anti-oxidant [**9**] and anti-helminthic activities [**10**]. It has been reported that substitution at the positions 1, 2 and 5 of the benzimidazole ring has significance influence on their pharmacological activity [**11**]. For example, Mebendazole [methyl-(5-benzoyl-1*H*-benzimidazol-2-*yl*)carbamate] is a 2,5-substituted benzimidazole which is an anti-helminthic drug and is marketed as Vermox [**12**], see **Figure 1.2**.
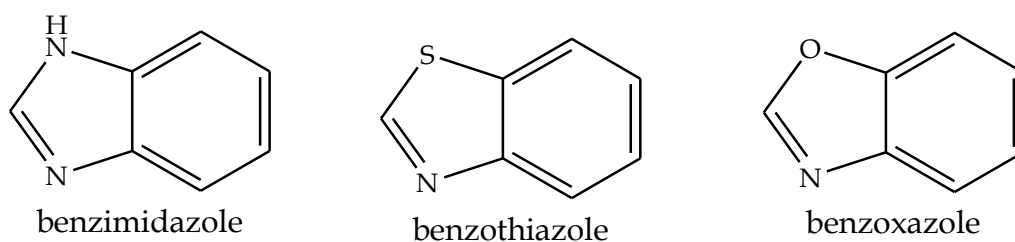
Figure 1.1: *Structures of the respective heterocyclic moieties which will be considered within this study.*
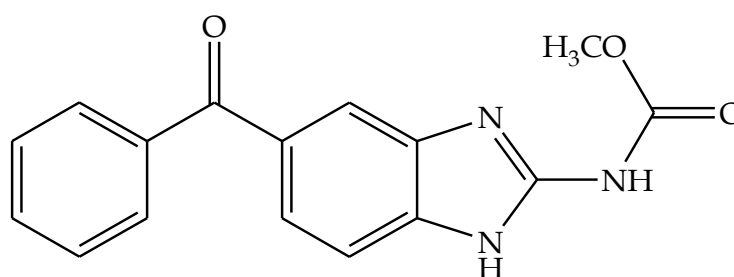
Figure 1.2: *Structure of Mebendazole (methyl-(5-benzoyl-1H-benzimidazol-2-yl)carbamate), also known commercially as Vermox.*

In vivo interconversion between oxidation states of +III, +IV and +V is a common occurrence with potential vanadium pharmaceuticals [**13**]. Meticulous ligand design ensures stability at specific pH values and can avoid biological redox processes associated with ligand exchange

to occur. In addition, selective ligands can provide a balance between (hydro/lipo)philicity for favourable *trans*-membrane transport. These selective ligands can exhibit biological relevance and display activities which may facilitate effective biodistribution. This would ultimately result in an increased bioavailability and minimized toxicity of the vanadium-based pharmaceutical [**14**]. Thus, the development of vanadium metallo-drugs depends on the coordination of diverse ligand systems which inevitably may afford metal complexes with a wide range of biological activity including anti-diabetic, anti-tumour and antibacterial.

Organovanadium compounds have received particular attention as insulin enhancing agents because they have fewer undesirable side effects compared to conventional treatments [**15**]. These orally administered compounds perform as pro-drugs where vanadate acts as the active species at a cellular level. Vanadate is structurally similar to phosphate and is able to inhibit protein tyrosine phosphatase (PTP) which counteracts autophosphorylation effects of insulin, thereby lowering the glucose level in the blood stream. However, these compounds suffer from poor stability in the gastrointestinal (GI) tract and poor absorption through biological membranes at intracellular and extracellular levels [**5**]. In addition, for the successful development of this class of vanadium therapeutic compounds, they need to have specific inherent properties such as a neutral charge, low molecular weight, thermodynamic and kinetic stability, target-specific biodistribution and bifunctional capability for the manipulation of lipophilicity and hydrophobicity [**13**]. Therefore, the biologically relevant ligands, such as the heterocyclic systems (as shown in **Figure 1.1**) will be considered within this study for coordination to the vanadium centre.

Thus the main aim of this research study is:
- To design, synthesize and characterize oxidovanadium(III/IV) as well as dioxido vanadium(V) compounds containing bidentate ligands incorporating heterocyclic chelates.

The coordination behaviour of 2-phenyl- and 2-pyridyl substituted heterocyclic ligands was explored, see **Figure 1.3**. This class of ligands largely afforded monoanionic bidentate chelates (by deprotonating the acidic protons of donor atoms) and in the process coordinating in a "2+2" manner towards the central metal atom. In fact, when similar heterocyclic ligands were used (with no acidic protons), coordination to vanadium in oxidation states +III, +IV and +V did not occur. In a specific case, the unique redox chemistry of vanadium, induced

the dimerization of 2-mercaptophenyl-1*H*-benzimidazole (Hsbz) as well as the cyclization of a uracil Schiff base, 5-amino-6-[(*Z*)-(2-hydroxybenzylidene)amino]-1,3-dimethylpyrimidine-2,4-(1*H*, 3*H*)-dione (H$_3$duo).
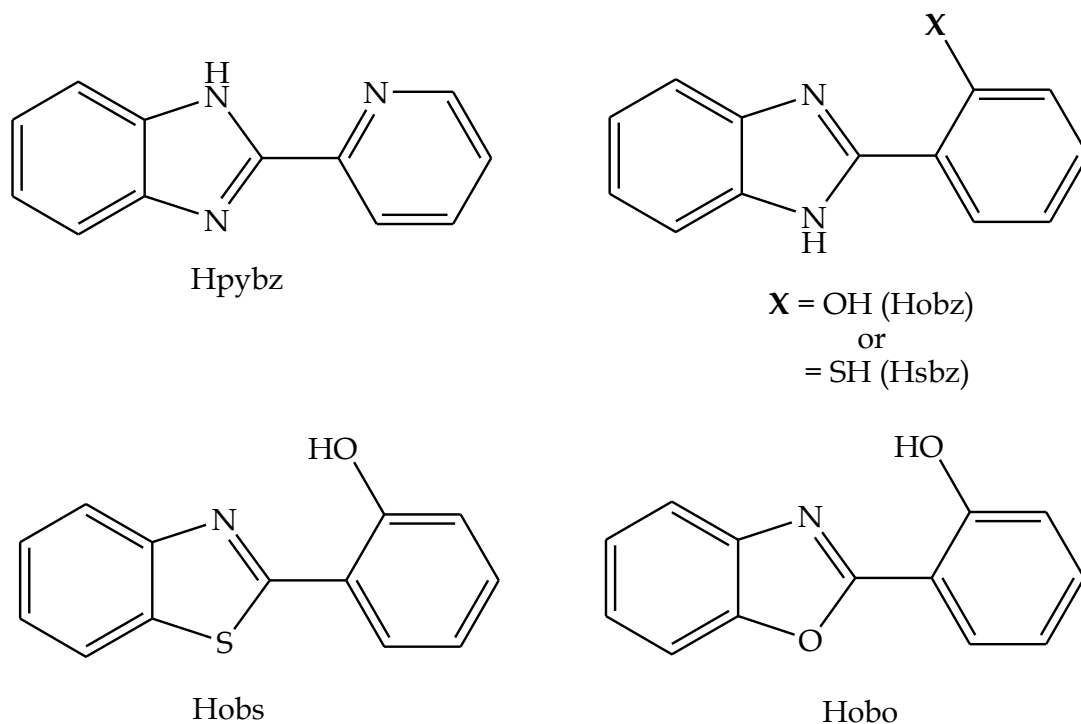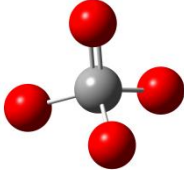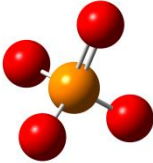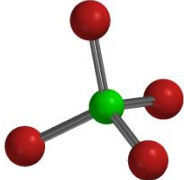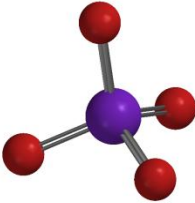
Figure 1.3: *Structures of the heterocyclic ligands utilized within this study: 2-pyridyl-1H-benzimidazole (Hpybz), 2-hydroxyphenyl-1H-benzimidazole (Hobz), 2-mercaptophenyl-1H-benzimidazole (Hsbz), 2-hydroxyphenylbenzothiazole (Hobs) and 2-hydroxyphenylbenzoxazole (Hobo).*

1.3 Vanadium Pharmaceuticals

Vanadate, $[VO_4]^{3-}$, is among several oxidometallates that have been reported to have biological effects. These biological activities arise from the structural and charge resemblance of vanadate to phosphate, $[PO_4]^{3-}$ (see **Table 1.1**) [**16, 17**]. Another example is iodate, $[IO_4]^-$, and perrhenate, $[ReO_4]^-$, which both show high uptake in the thyroid due to their structural similarities [see **Table 1.1**] [**18**]. Typically, vanadate is unstable in the bloodstream and readily coordinates to biogenic ligand systems (*e.g.* gluthathione). As a result, vanadate is typically reduced to vanadyl, $[VO]^{2+}$, under physiological conditions. This resultant species

binds to transferrin and albumin proteins which afford diverse biodistribution patterns [**19, 20**].

Table 1.1: *Structures of vanadate, phosphate, perrhenate and iodate.*

$[VO_4]^{3-}$	$[PO_4]^{3-}$
$[ReO_4]^{-}$	$[IO_4]^{-}$

1.3.1   Development of insulin enhancing vanadium compounds

The glucose lowering effect of oxidovanadium compounds was noticed as early as 1897. It was observed that two out of three individuals with diabetes mellitus who were treated with an aqueous solution of sodium vanadate ($NaVO_3$) showed a lowered blood glucose level. Later, vanadyl sulfate ($VOSO_4$) which is less toxic than vanadate, was found to be more effective in streptozotocin-diabetic (STZ)-rats [**21**]. However vanadyl salts had poor absorption in the small intestine due to formation of insoluble vanadyl hydroxyls at pH 7.2 [**20**].

The poor effectiveness of these common inorganic salts has triggered the use of organic ligands to increase the biological availability of these oxidovanadium species. For this reason, there is currently a huge upsurge in the coordination chemistry of vanadium (predominantly in the oxidation states +IV and +V) with various ligand systems. In fact, the first vanadium compounds that have entered phase II clinical trials are *bis*(maltolato)oxidovanadium(IV)

(BMOV) and its derivative *bis*(ethylmaltolato)oxidovanadium(IV) (BEOV) [see **Figure 1.4**] [**21**, **22**]. These compounds showed higher hypoglemic activity and less toxicity than vanadyl sulfate. Further development of this class of maltol-oxidovanadium complexes have led to the more promising *bis*(allixanato)oxidovanadium(IV) complex which exhibited a much longer residual time within tissues and ultimately resulted in a higher anti-diabetic activity (see **Figure 1.5**) [**5**, **23**].

R = CH$_3$ or CH$_2$CH$_3$
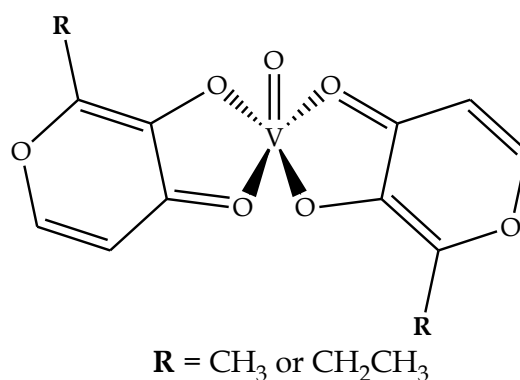
Figure 1.4: *Structures of the BMOV (where **R** = CH$_3$) and BEOV (where **R** = CH$_2$CH$_3$).*
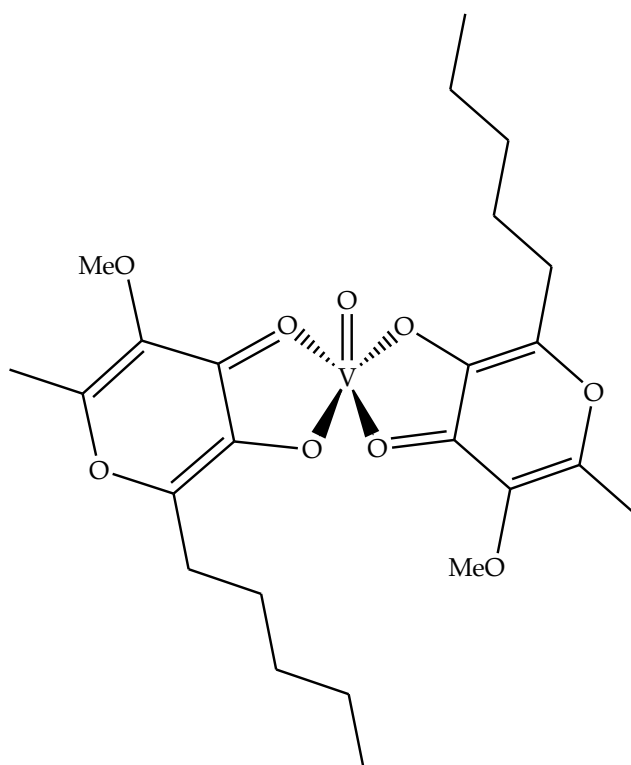
Figure 1.5: *Structure of the bis(allixanato)oxidovanadium(IV) complex.*

1.3.2 Vanadium compounds as potential anticancer agents

Research into the discovery of novel anticancer metallopharmaceuticals has increased due to the multiple adverse side effects of the more established chemotherapeutic drug, *cis*-platin [24]. Peroxidovanadate compounds, like vanadium(V)-betaine-peroxido, (see **Figure 1.6**, structure **A**) has shown therapeutic activity for human breast cancer and lung adenocarcinoma cells [25]. Other vanadium(IV) compounds like vanadocene dichloride (see **Figure 1.6**, structure **B**) as well as a oxidovanadium(IV) complex stabilized by a derivatized heme ligand (see **Figure 1.7**) have shown to exhibit anticancer activity against Ehrlich tumor cells [5].

(**A**)

(**B**)
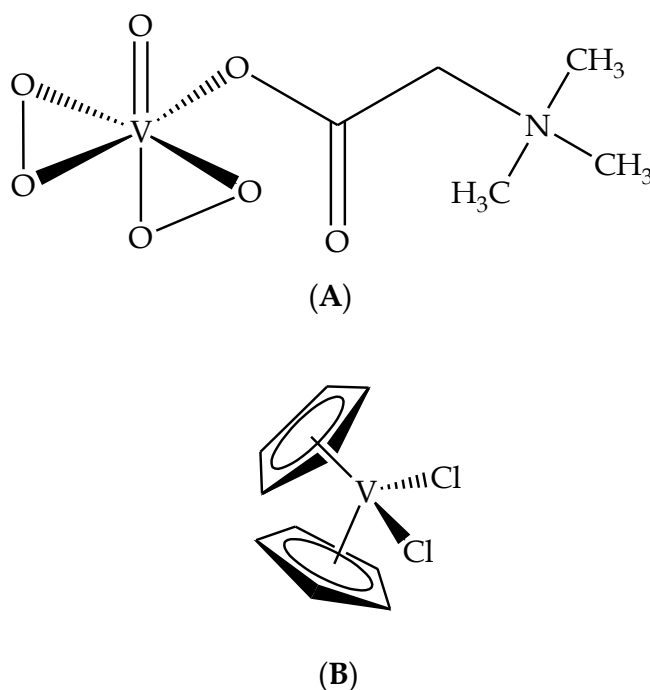
Figure 1.6: *The structure of ternary vanadium-betaine-peroxido (A) and of vanadocene dichloride (B).*

These compounds have shown to be active in all cancer stages (*i.e.* initiation, promotion and progression) on several animal cancer models [27]. The mechanism of activity for the chemotherapeutic vanadium compounds have been assumed to be *via* inhibition of tyrosine phosphatase. Inhibition of tyrosine phosphatase leads to apoptosis or activation of tumour suppressor genes. The mode of action for the vanadium metallocene is through DNA intercalation which results in growth inhibition of the tumor cell [28]. These potential

7

metallo-drugs can also reduce cellular growth rate and modulation of cellular adhesive molecules for the inhibition of metastatic cancer cells. They are also able to reverse antineoplastic drug resistance while still having a lower toxicity for healthy cells in comparison to platinum-based anticancer drugs [**29**, **30**].
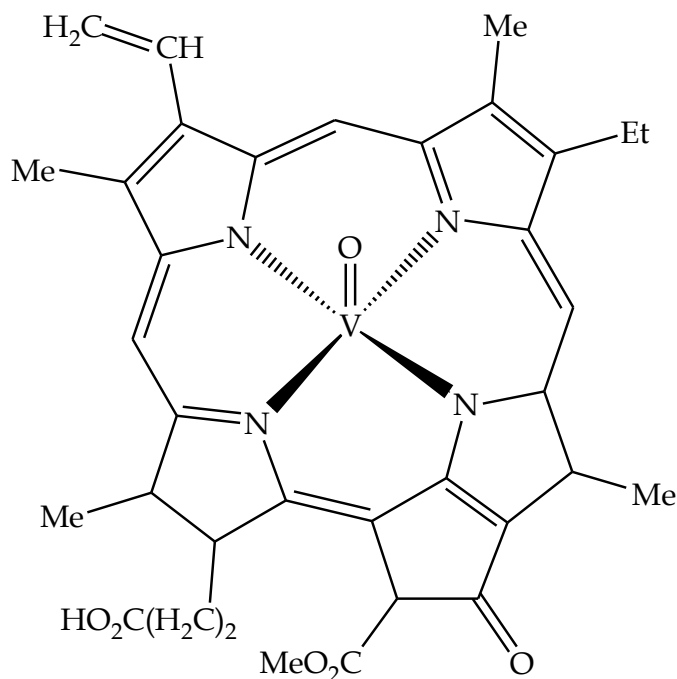
Figure 1.7: *Oxidovanadium(IV) complex stabilized by the derivatized macrocyclic heme ligand.*

1.3.3   Other potential medicinal applications of vanadium compounds

The World Health Organization (WHO) statistics indicated that diseases induced by microorganisms (*e.g.* viruses and parasites) are the most prevalent illnesses worldwide [**31**]. Vanadium compounds have shown potential to act as anti-parasitic agents against microorganisms causing malaria, american trypanosomiasis (chagas disease), Leishmaniasis and Amoebiasis [**32**]. The proposed mechanism of action of these vanadium compounds are *via* the inhibition of parasitic phosphatases. An example is the case of a vanadium compound containing the thiosemicarbazide (see **Figure 1.8**) ligand which showed activity against *Entamoeba histolytica* that causes amoebiasis. *In vitro* studies of a series of oxidovanadium(IV) compounds containing derivatized porphyrins (an example is shown in

Figure 1.9) exhibited anti-HIV-1 activity of 97% inhibition for HIV-1 reverse transcriptase. Interestingly the ligands alone and metal precursor were all found to be inactive [**33**, **34**].
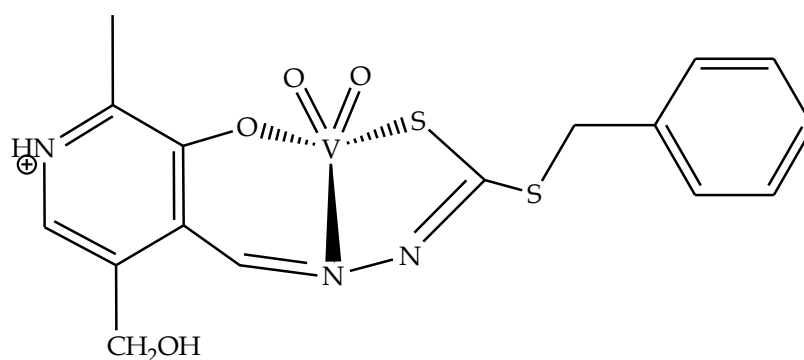
Figure 1.8: *Structure of the dioxidovanadium(V) complex with a thiosemicarbazide ligand.*
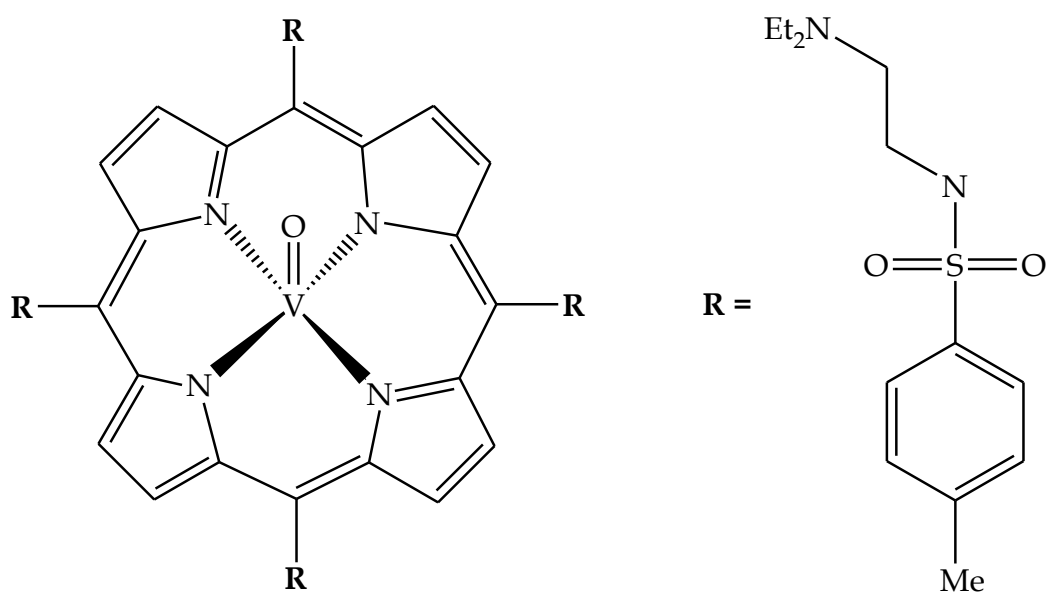
Figure 1.9: *Structure of an oxidovanadium(IV) complex with a derivatized porphyrin tetradentate chelator.*

1.4 General Chemistry of Vanadium (III, IV and V)

1.4.1 Ligand Substitution

The commonly utilized vanadium precursors in oxidation states +III, +IV and +V can readily undergo ligand substitution. For example, the vanadium(III) core can be stabilized by the neutral 1,6-*bis*(2'-pyridyl)-2,5-dithiahexane (N_2S_2) chelating ligand, as illustrated by the following reaction [35]:

$$VX_3(thf)_3 \; [X = Br \text{ or } I] + N_2S_2 \rightarrow [VX_2(N_2S_2)]X + 3thf$$

However, for the more acidic oxidation states, ligand substitution and subsequent metal stabilization requires donating chelating agents. A typical example is the displacement of an acac moiety of the $[V^{IV}O(acac)_2]$ precursor by a monoanionic tridentate aptsc chelator (Haptsc = 2-acetylpyridine thiosemicarbazone), to afford the mononuclear oxidovanadium complex, $[V^{IV}O(acac)aptsc]$ [36] (see **Figure. 1.10**).
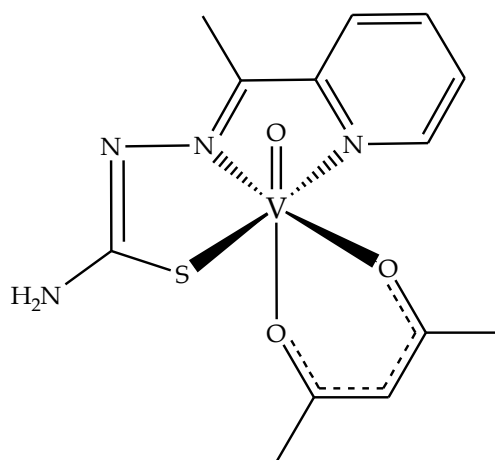
Figure 1.10: *Structure of the oxidovanadium(IV) complex [VO(acac)aptsc].*

1.4.2 Oxidation and reduction

Vanadium complexes are prone to oxidation by atmospheric oxygen. The oxidation of the complex [VO(acac)aptsc] by oxygen in air led to the formation of a five coordinate, *cis*-dioxidovanadium(V) specie, $[VO_2(aptsc)]$ (see **Figure 1.11**).
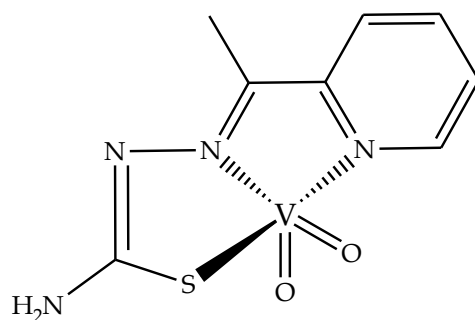
Figure 1.11: *Structure of the cis-dioxidovanadium(V) complex [VO$_2$(aptsc)].*

The unique redox properties of vanadium compounds make them attractive for many catalytic reactions. In fact, the most well-known reduction reaction is the utilization of vanadium pentoxide for the catalytic oxidation of sulfur dioxide within the Contact process for the production of H$_2$SO$_4$

$$SO_2 + V_2O_5 \rightarrow SO_3 + 2VO_2$$
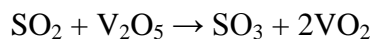
Ligand induced oxidation of the metal centre is a common phenomena in the coordination chemistry of vanadium. One such example is that of the diamagnetic vanadium(V) complex salt (Me$_3$NBz)$_2$[V^V(S$_2$)S$_2$(SPh)] (HSPh = benzenethiol) in which the metal centre is surrounded by sulfur atoms in different coordination modes: the deprotonated thiolate sulfur of the monoanionic SPh moiety, the bridging persulfido (S$_2^{2-}$) and two *cis*-orientated sulfido (S^{2-}) groups [**37**]. This was also observed in the reaction of [VO(acac)$_2$] and *N,N-bis*(2-hydroxy-3,5-ditertiarybutyl)-*N',N'*-dimethyl-ethylendiamine (H$_2$otben) in a methanolic solution which resulted in the formation of a six coordinate complex, [V^{V}O(otben)(OMe)]. The resultant compound readily underwent substitution of the methoxy co-ligand upon reaction with a one molar equivalent of salicylic acid (Hsac) to afford [V^{V}O(otben)(sac)] [**38**].

1.4.3 Disproportionation

Disproportionation reactions of vanadium compounds are not widely observed in the literature. However 1.4.3 disproportionation has been observed with vanadium(III) complexes of H_2salen [39] and derivatives which have been investigated due to their potential electrocatalytic activities. An illustrative example is shown below:

$$2[V^{IV}O(salen)] + 2H^+ \rightarrow [V^{III}(salen)]^+ + [V^VO(salen)]^+ + H_2O$$
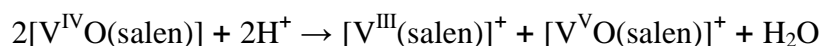
1.4.4 Formation of Polyoxidometallates

The formation of polyoxidometallates is favourable at low pH due to the protonation of oxido ligands followed by dehydration which ultimately induces the condensation of the resulting vanadium species, $e.g.$ a polyoxidometallate compound such as $[n\text{-}C_4H_9N]_4MeCN(V_{12}O_{32})$ is obtained from the heating of $tetra\text{-}n$-butyl ammonium decavanadate salt in refluxing acetonitrile [40]. Vanadium has also been incorporated into heteronuclear polyoxidometallates, largely through hydrothermal synthesis but can also be attained under mild conditions. $[Zn(en)_2]_6[(VO)_{12}O_6B_{18}O_{39}(OH)_3].13H_2O$ (see **Figure 1.12**) is an example of a heteronuclear polyoxidometallate, which was synthesized from the mixing and stirring of $NaVO_3$, H_3BO_3, $Zn(CH_3COO)_2$ and ethylenediamine for two hours at room temperature [41].
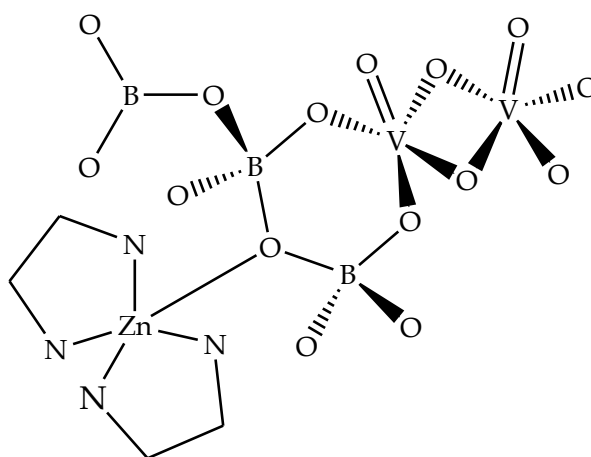
Figure 1.12: *Structure representing the asymmetric unit cell of $Zn_6V_{12}B_{11}$.*

1.5 Coordination Chemistry of Vanadium

1.5.1 Vanadium compounds with N- and N-donor ligands

The first example of a vanadium(III) centre coordinated to two deprotonated diamide moieties was NHEt$_3${$trans$-[V^{III}Cl$_2$(bpb)]}, [H$_2$bpb = 1,2-bis(2-pyridinecarboxamide)benzene] (see **Figure 1.13**). The complex has a distorted octahedral geometry with the chloro co-ligands found in $trans$ axial positions while three constrained five membered chelate rings are formed by the bpb dianionic tetradentate chelator within the equatorial plane. Interestingly, the atmospheric oxidation of the aforementioned complex resulted in the formation of a dimeric oxidovanadium(IV) compound [VOCl(Hbpb)]$_2$ .2MeNO$_2$, where one metal center coordinated in two different manners to the bridging ligands, firstly via the pyridyl nitrogens and secondly via the amide nitrogen and ketonic oxygen [**42**].
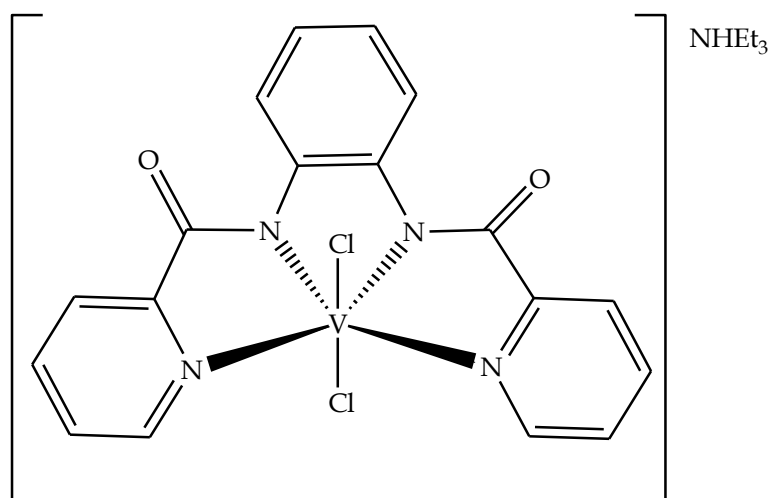
Figure 1.13: *The structure of the vanadium(III) compound, NHEt$_3${trans-[V^{III}Cl$_2$(bpb)]}.*

The reaction of a multidentate *N*-donor benzimidazole ligand, *tris*[benzimidazol-2'-*yl*-methyl]amine (H$_3$ntb, see **Figure 1.14**) with vanadium afforded unique mono oxidovanadium and mixed valence binuclear vanadium compounds. The mixed valence oxidovanadium(IV/V) compound, [(H$_3$ntb)V^{IV}O(μ-O)V^{V}O(H$_3$ntb)](CF$_3$SO$_3$)$_3$ dimer was obtained from the reaction of H$_3$ntb and VO(CF$_3$SO$_3$) in methanol. However, using different

vanadium precursors with H_3ntb resulted in the isolation of only mononuclear species: the reactions with $VOCl_3$, $VOSO_4$ and $VO(acac)_2$ formed $[V^{IV}O(H_3ntb)Cl]Cl$, $[V^{IV}O(H_3ntb)(H_2O)](ClO_4)_2$ and $[V^{IV}O(Hntb)]$ respectively [43]. Interestingly, in the dinuclear compound, the delocalization of the unpaired electron between the two metal centers results in a 15 line-ESR spectrum as opposed to the mononuclear complexes which affords eight-line ESR spectra due to the localization of the unpaired electron at the respective metal centers.
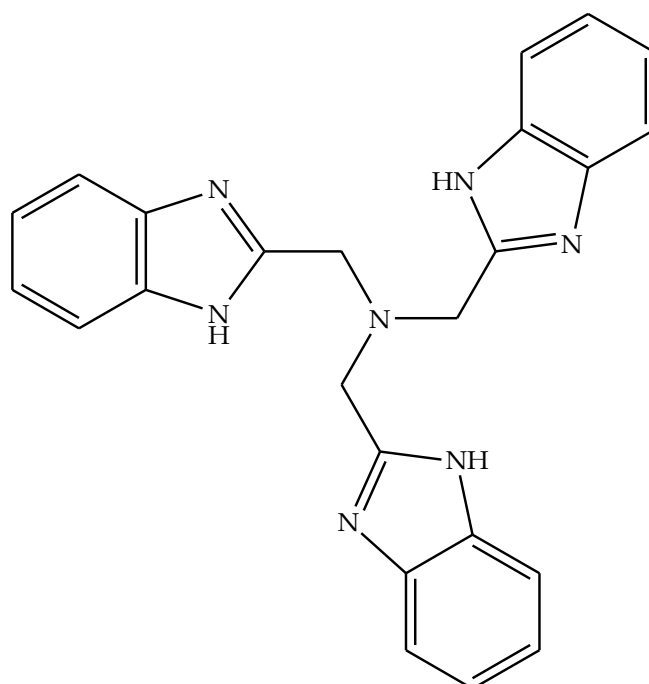
Figure 1.14: *Tripodal structure of tris[benzimidazol-2'-yl-methyl]amine (H_3ntb).*

1.5.2   Vanadium compounds with N- and O-donor ligands

The vanadium compounds in the literature predominatly contain a combination of hard and soft donor atoms (nitrogen and oxygen) [44]. These donor atoms have been incorporated in various classes of ligands, varying from Schiff bases to heterocyclic ligands. In the vanadium(III) complex, $[V(acac)(Hsect)_2]$ {H_2sect = 2-[2-(salicylideneamino)ethylamino]cyclopent-1-*ene*-1-dithiocarboxylate} a unique '2+2+2' coordination is present in which the two Schiff base moieties forms 6-membered chelate rings through their respective imino nitrogens and singly deprotonated phenolic oxygens. It is

also observed that the reduced metal center showed preferential coordination for the N, O donor set while the N, S moiety remains uncoordinated [45] (see **Figure 1.15**).
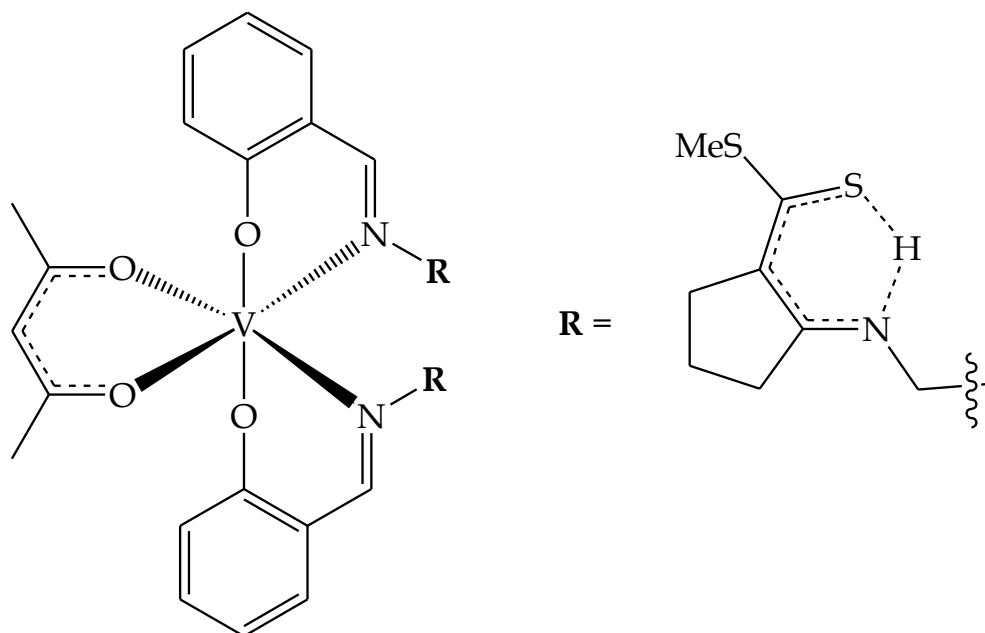
Figure 1.15: *A structure depicting the octahedral geometry around the vanadium(III) centre.*

Recently, a polynuclear vanadium(IV) compound, $(\mu\text{-O})_n[VO(pbx)_2]$ (see **Figure 1.16**) was isolated from the reaction of 2-hydroxyphenyl-1*H*-benzoxazole (Hpbx) and $VO(acac)_2$ [46]. Each metal center is found at the centre of a distorted octahedron and each of the monomeric units stack symmetrically through axially linked oxido-bridged covalent bonds. The symmetry is further emphasized by the nearly equal N-V-O bite angles and coordination bonds. It is suggested that the lowest absorption and luminescence band are due to the electron transfers occurring within $[VO]^{3+}$ moiety. The generation of the excited state specie corresponds to the electron transfer from O^{2-} to V^{4+} while the electron transfer from V^{3+} to O^{-} are due to the formation of the ground state specie.
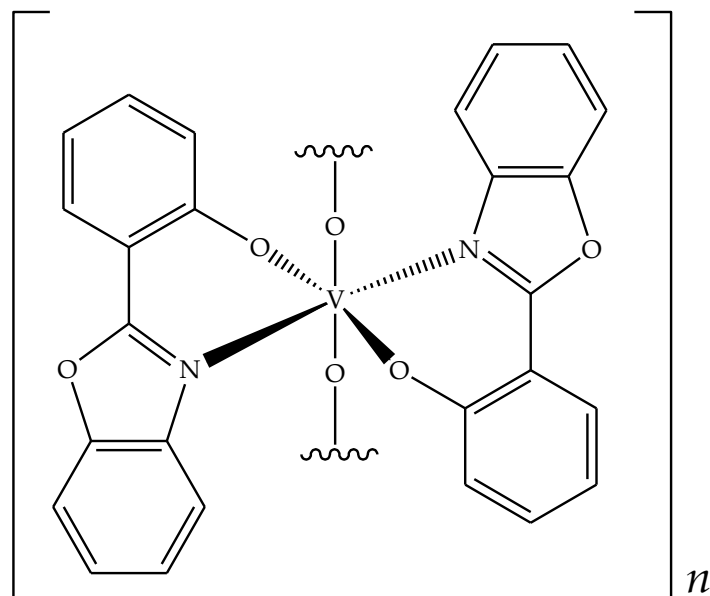
Figure 1.16: *An illustration of a monomer unit of the polynuclear vanadium(IV) compound.*

1.5.3   Vanadium compounds with N- and S-donor atoms

Vanadium compounds with N, S-donor atoms are rare in literature, despite the fact that sulfur is a soft donor atom and readily polarizable. In the dimeric vanadium compound, $[V_2O_2(pyt)_4]$ {Hpyt = pyridine-2-thiol}, vanadium centers are bridged by sulfur atoms which ultimately forms a bridging constrained 4-membered cyclometalled VSVS ring (see **Figure 1.17**) [47]. A rare vanadium(V) *bis*-sulfide complex $(Net_4)[VO(S_2)_2(bpy)]$ with a seven coordination site has been isolated (see **Figure 1.18**). The basal plane is defined by S-donor atoms of the persulfido co-ligands along with one of the nitrogen atoms from the bpy ligand. The other pyridyl nitrogen and oxido oxygen occupies the axial positions [48].
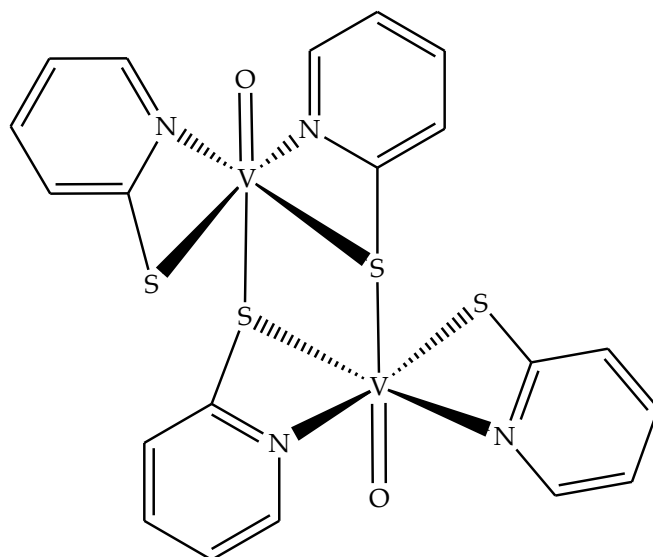
Figure 1.17: *Oxidovanadium(IV) dimer compound with sulfur bridged atoms.*
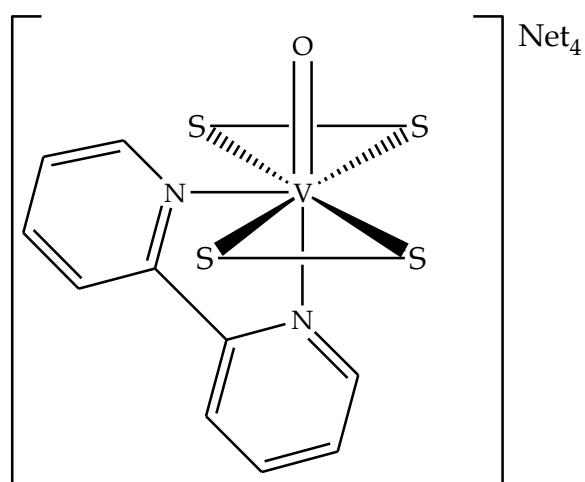
Figure 1.18: *An oxidovanadium persulfide compound (Net$_4$)[VO(S$_2$)$_2$(bpy)].*

1.6   References:

1.   Mukherjee B., Patra B., Mahapatra S., Banerjee P., Tiwari A., Chatterjee M., *Toxicol. Lett., 2*004, **150**, 135.

2.   Lee J.D., *Concise Inorganic Chemistry*, Chapman and Hall, London, 1991, 4th edition.

3.   Moskaly R.R., Alfantazi A.M., *Miner. Eng.*, 2003, **16**, 793.

4.   King B.R., Burdett J.K., Crabtree R.H., Lukehart C.M., Scott R.A., Wells R.L., *Encyclopedia of Inorganic Chemistry,* Wiley, New York, 1995, **8**, 4296.

5.   Rehder D*., Bioinorganic Vanadium Chemistry*, John Wiley and Son, London, 2008.

6.   Scibior A., Zaporowska H., Ostrowski J., Banach A., *Chem. Biol. Interact.,* 2006, **159**, 213.

7.   Pawar N., Dalal D., Shimpi S., Mahulikar P.*, Eur. J. Pharm. Sci.,* 2004, **21**, 115.

8.   Ayhan-Kilcigil G., Altanlar N., *Il Farmaco.,* 2003, **58**, 1345.

9.   Kuş C., Ayhan-Kilcigil G., Özbey S., Kaynak F.B., Kaya M., Çoban T., Can-Eke B., *Bioorg. Med. Chem.*, 2008, **16**, 4294.

10.   Cañete R., Escobedo A., Almirall P., González M., Brito K., Cimerman S., *T.Roy. Soc. Trop. Med. H.,* 2009, **103**, 437.

11.   Tellez F., Sandoval H., Blum S.E., Bahrens N., *Arkivoc,* 2008, 245.

12.   Cózar-Bernal M., Gallardo V., Sáez-Fernández E., Holgado M., Álvarez-Fuentes J., Fernández-Arévalo M., José L., *Int. J. Pharm.,* 2010, **393**, 162.

13.   Rehder D., *Inorg. Chem. Comm.*, 2003, **6**, 604.

14.   Thompson K.H., Orvig C., *J. Chem. Soc., Dalton Trans*., 2000, 2885.

15.   Rehder D., Gaetjens J., Kiss T., *J. Inorg. Biochem.*, 2003, **96**, 14.

16.   Srivastava A.K., Mehdi M.Z., *Diabetic Med*., 2005, **22**, 2.

17.   Willsky G.R., Goldfine A.B., Kostyniak P.J., McNeill J.H., Yang L.Q., Khan H.R., Crans D.C., *J. Inorg. Biochem.*, 2001, **85**, 33.

18.   Abram U., Alberto R*., J. Braz. Chem. Soc.*, 2006, **17**, 1486.

19.   Thompson K.H., Orvig C., *Coord. Chem. Rev.*, 2001, **219–221**, 1033.

20.   Sessler J.L., Doctrow S.R., McMurry T.J., Lippard S.J., *Medicinal Inorganic Chemistry*, American Chemical Society, Washington DC, 2005

21.   Scior T., Hans-Georg M., Garcia J.A.G., Koch W., *Drug Des. Devel. Ther.*, 2008, **2**, 221.

22.   Winter P.W., Al-Qatati A., Wolf-Ringwall A.L., Schoeberl S., Chatterjee P.B., Barisis B.G., Roess D.A., Crans D.C., *Dalton Trans.,*2012, **41**, 6419.

23. Adachi Y., Yoshida J., Kodera Y., Katoh A., Takada J., Sakuria H., *J. Med. Chem.,* 2006, **49**, 3251.

24. Bishayee A., Waghray A., Patel M.A., Chatterjee M., *Cancer Lett.*, 2010, **294**, 1.

25. Pentanidic S.,Kioseoglou E., Hadzopoulou-Cladara M., Salifoglou A., *Cancer Lett.*, 2013, **335**, 387.

26. Vinklarek J., Pavlik I., Cernosek Z., *Met. Based Drugs*, 1997, **4**, 207.

27. Evangelou A.M., *Crit. Rev. Oncol. Hemat.*, 2002, **42**, 249.

28. Chakraborty T., Chatterjee A., Rana A., Dhachinamoorthi D., Kumar A.P., Chatterjee M., *B.B.A.-Mol. B. Dis.*, 2007, **1772**, 48.

29. Shi X., Jiang H., Maoa Y., Yec J., Saffiotti. U., *Toxicol.*,1996, **106**, 27.

30. Petanidis S., Kioseoglou E., Hadzopoulou-Cladaras M., Salifoglou A.*, Cancer Lett.*, 2013, **335**, 387.

31. Gambino D., *Coord. Chem. Rev*., 2011, **255**, 2193.

32. Bharti N., Shailendra M.T., Gonzalez Garza M.T., Cruz-Vega D.E., Castro-Garza J., Saleem K., Naqvi F., Mauryac M.R., Azama A., *Bioorg. Med. Chem. Lett.,* 2002, **12**, 869.

33. Wong S.Y., Sun R.W.Y., Chung N.P.Y., Lin C.L., Che C.M., *Chem. Commun*., 2005, 3544.

34. Maurya M.R., Kumar A., Bhat A.R., Azam A., Bader C., Rehder D.*, Inorg. Chem.*, 2006, **45**, 1260.

35. Nekola H., Wang D., Gruning C., Gatjens J., Behrens A., Rehder D., *Inorg. Chem,* 2002, **41**, 2379.

36. da Mai P.I., Pavan F.R,. Leite C.Q.F., Lemos S.S., de Sousa G.F., Batista A.A., Nascimento O.R., Ellena J., Castellano E.E., Niquet E., Deflon V.M., *Polyhedron*, 2009, **28**, 398.

37. Sendlinger S.C., Nicholson J.R., Lobkovsky E.B., Huffman J.C., Rehder D., Christou G., *Inorg. Chem.*, 1993, **32**, 204.

38. Maity D., Ray A., Sheldrick W.S., Figge H.M., Bandyopadhyay B., Ali M., *Inorg. Chim. Acta,* 2006, **359**, 3197.

39. Liu Z., Anson F.C., *Inorg. Chem.,* 2001, **40**, 1329.

40. Greenwood N.N., Earnshaw A., *Chemistry of Elements*, 2nd edition, Butterworth-Heinemann, Oxford, 1997, 985.

41. Zhang L., Shi Z., Yang G., Chen X., Feng S., *J. Solid State Chem.,* 1999, **148**, 450.

42. Vlahos A.T., Kabanos T.A., Raptopoulou C.P., Terzis A., *Chem. Commun*.,1997, 269.

43. Ghosh S., Nanda K.K., Addison A.W., Butcher R.J., *Inorg. Chem.,* 2002, **41***,* 2243.

44. Maurya M.R., *Coord. Chem. Rev*., 2003, **237**, 163.

45. Bhattacharyya S., Mukhopadhyay S., Samanta S., Weakley T.J.R., Chaudhury M., *Inorg. Chem.*, 2002, **41**, 2433.

46. Back D.F., de Oliveira G.M., Ballin M.A., Corbellini V.A., *Inorg. Chim. Acta,* 2010**, 363**, 807.

47. Reynolds J.G., Sendlinger S.C., Murray A.M., Huffman J.C., Christou G*., Inorg. Chem.,* 1995*,* **34**, 5745.

48. Castro S.L., Martin J.D., Christou G., *Inorg. Chem*., 1993, **32**, 2978.

Chapter 2

Experimental

2.1   Handling of Vanadium

Vanadium occurs naturally as a mixture of two isotopes: a stable ^{51}V (99.75%) and a radioactive ^{50}V (0.25%) which is a weak β-decay radioactive isotope with a corresponding half-life of 1.5 x 10^{17} years [**1**]. Therefore no special precautions were taken in the handling of vanadium.

2.2   Materials

2.2.1   Metal precursors

All the precursor compounds were obtained from Sigma-Aldrich and used without further purifications:

(a)   *Ammonium vanadate (98% purity)*

(b)   *Vanadyl sulfate (95% purity)*

(c)   *Vanadyl acetylacetone (99.9% purity)*

(d)   *Vanadium trichloride (97% purity)*

2.2.2   Commercially obtained ligands and organic precursors

(a)   2-Hydroxyphenylbenzothiazole (Hobz, 98% purity)

(b)   2-Hydroxyphenylbenzoxazole (Hobo, 95% purity)

(c)   Picolinic acid (99% purity)

(d)   Salicylic acid (99% purity)

(e)   2-Mercaptobenzoic acid (97% purity)

(f)   Salicylaldehyde (98% purity)

(g)   5,6-Diamino-1,3-dimethyl uracil (98% purity)

21

All these chemicals were attained from Sigma-Aldrich and used without further purification.

2.2.3   General synthetic procedure of isolated ligands

A mixture of 1,2-diaminobenzene (H$_2$dab) and the relevant 2-substituted-benzoic acid were added in portions over a one hour period to 50 cm^3 hot (250 °C) polyphosphoric acid (PPA), see **Scheme 2.1**. The reaction mixtures were then stirred for a further 5 hours, allowed to cool to room temperature and poured into cold solutions of 10% K$_2$CO$_3$. This general synthetic procedure was adopted from a previously published article [**2**].
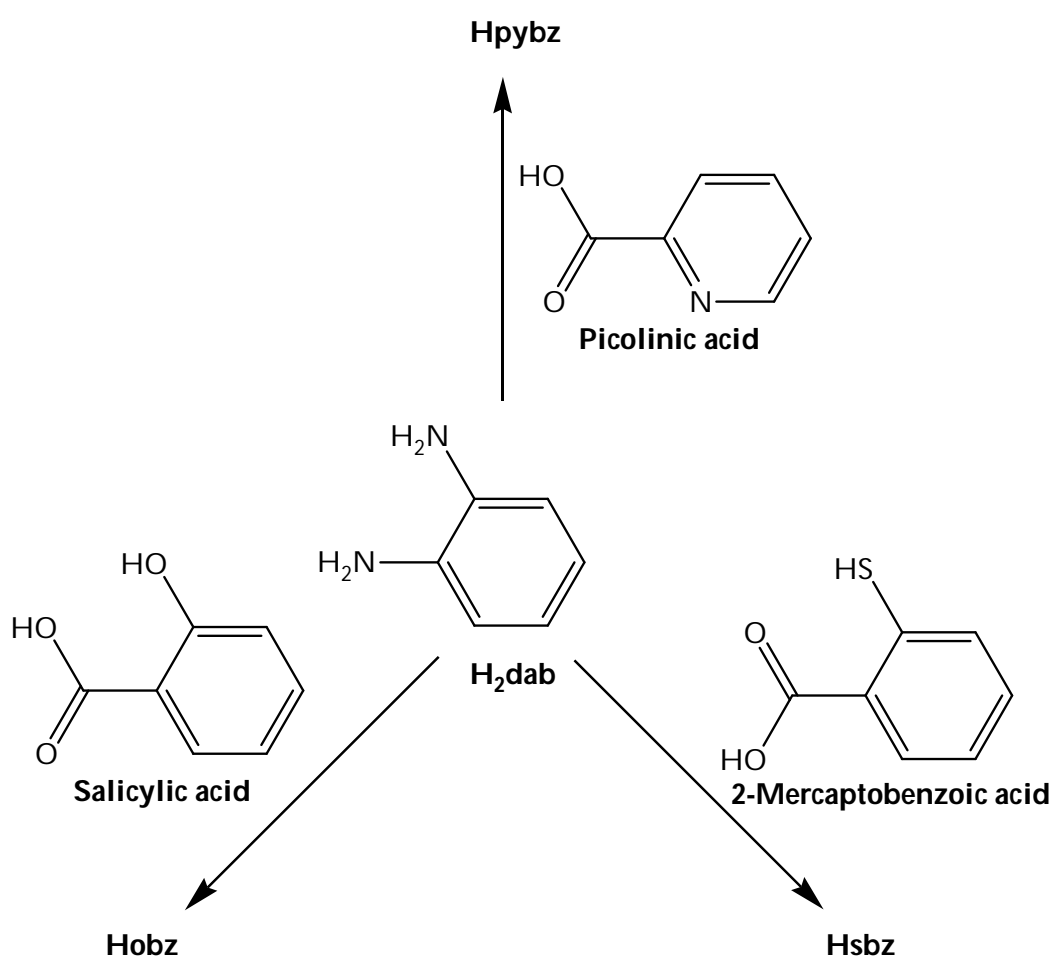
Scheme 2.1: *Formation pathways of the condensation reactions.*

(a)   2-Pyridyl-1H-benzimidazole (Hpybz)

From the condensation reaction between H$_2$dab (2.28 g, 21.08 mmol) and picolinic acid (2.60 g, 21.08 mmol), a purple precipitate was filtered under vacuum and recrystallized from

methanol to afford dark brown crystals. Yield = 81%, m.p. = 224.6 - 229.0 $^{\circ}$C. IR (v_{max}/cm^{-1}): v(N-H) 3063; v(C=N) 1599. ^{1}H NMR (295 K, ppm) 13.08 (br, s, 1H, *NH*); 8.73 (d, 1H, *H1*); 8.32 (d, 1H, *H2*); 7.99 (t, 1H, *H3*); 7.70 (d, 1H, *H4*); 7.49-7.56 (m, 2H, *H5, H8*); 7.18-7.27 (m, 2H, *H6, H7*). UV-Vis (DMF, (λ_{max} (ε, M^{-1}cm^{-1}))): 303 (sh, 4340); 445 (2230).
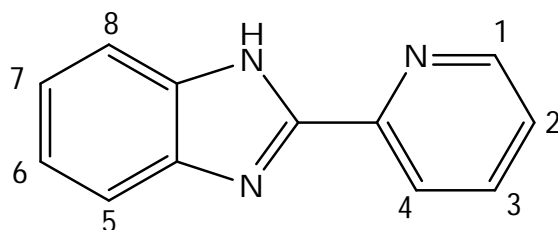
Figure 2.1: *Numbering scheme of Hpybz.*
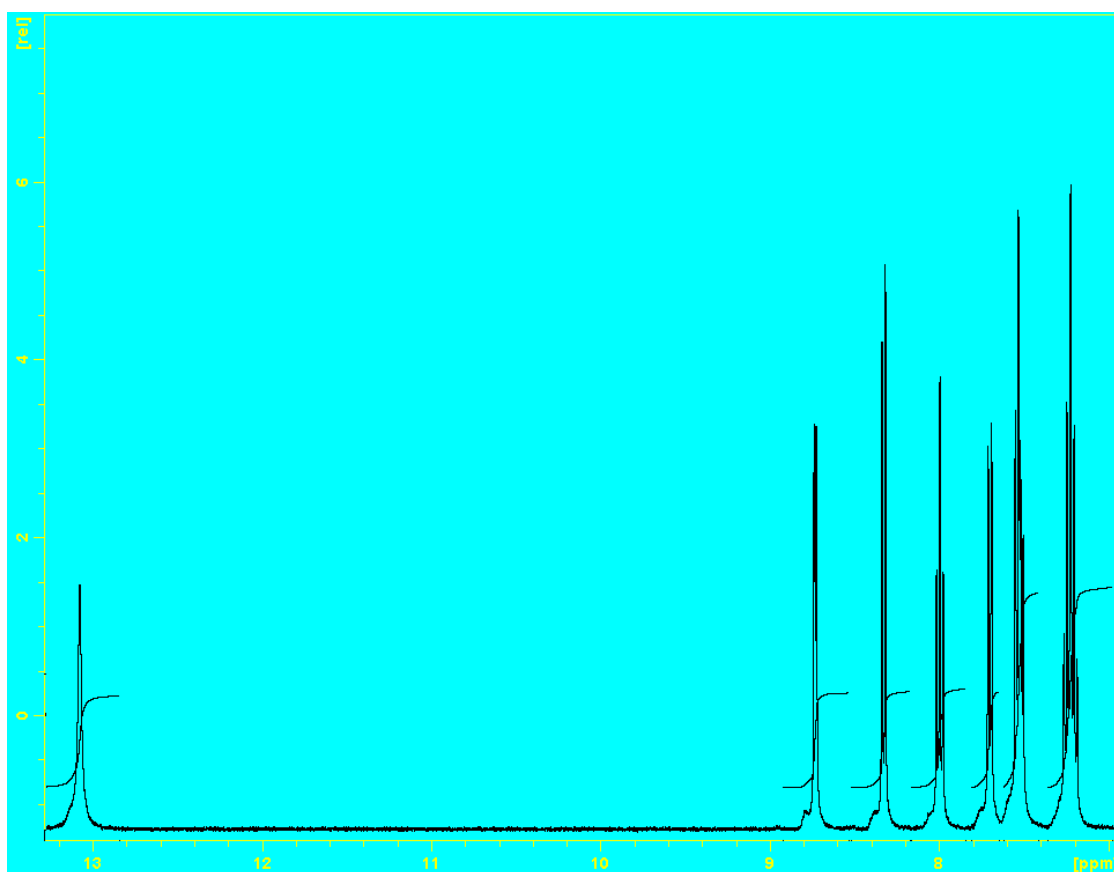
Figure 2.2: *^{1}H NMR spectrum of Hpybz.*

(b)   *2-Hydroxyphenyl-1H-benzimidazole (Hobz)*

Hobz was formed in good yield from the reaction between H_2dab (1.98 g, 18.31 mmol) and salicylic acid (2.53 g, 18.31 mmol). Yield = 75%, m.p. 241.6 - 243.1 ^{0}C. IR (v_{max}/cm^{-1}): v(N-H) 3326; v(O-H) 3240; v(C=N) 1631. ^{1}H NMR (295 K, ppm) 13.17 (br, s, 1H, *NH*); 8.07 (d, 1H, *H4*); 7.64-7.61 (m, 2H, *H5, H8*); 7.32 (t, 1H, *H3*); 7.24-7.19 (m, 2H, *H6, H7*); 7.00-6.92 (m, 2H, *H1, H2*); 4.00 (br, s, 1H, *OH*). UV-Vis (DMF, (λ_{max} (ε, $M^{-1}cm^{-1}$))): 278 (sh, 54110), 291 (sh, 7644); 297 (9033); 321 (10150); 333 (10576); 351 (sh, 2827).
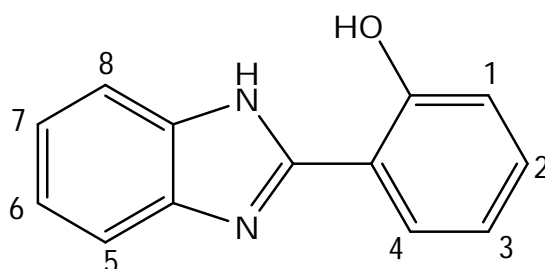
Figure 2.3: *Numbering scheme of Hobz.*
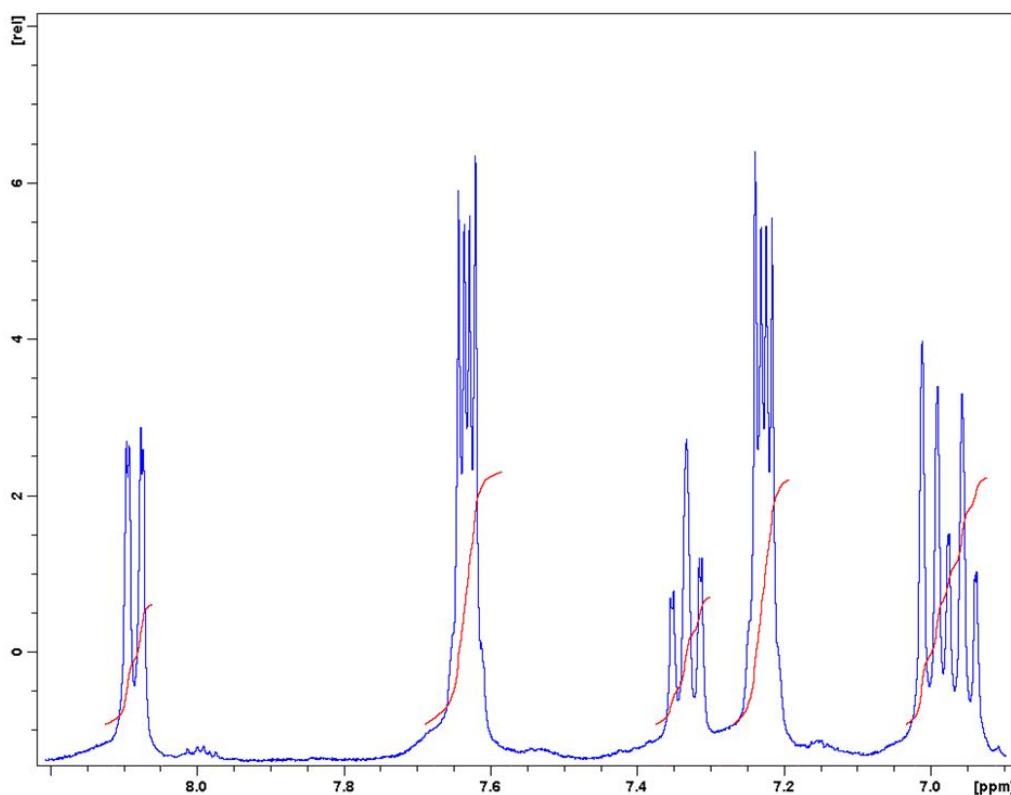
Figure 2.4: *^{1}H NMR spectrum of Hobz, showing the signals of the aromatic protons only.*

24
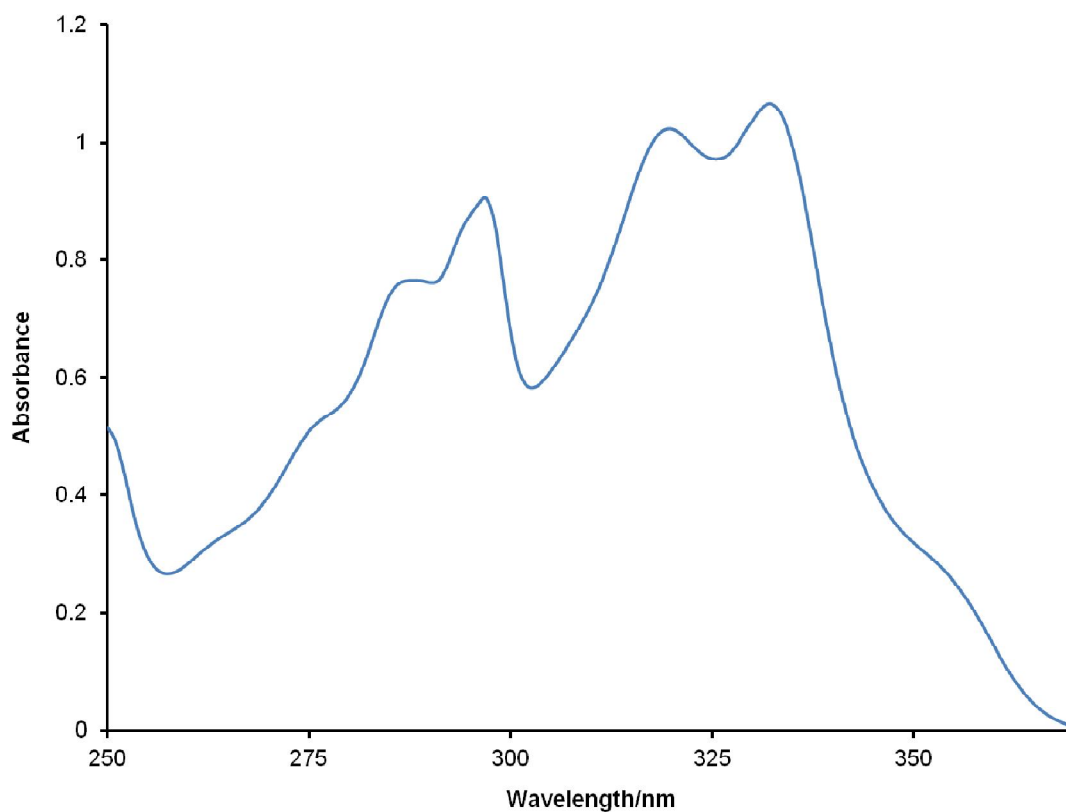
Figure 2.5: *UV-Vis spectrum of Hobz.*

(c)   2-Mercaptophenyl-1H-benzimidazole (Hsbz)

A mixture of 1.75 g (16.18 mmol) of H_2dab and 2.50 g (16.18 mmol) of 2-mercaptobenzoic acid was used as starting reagents. Yield = 63%, m.p. 261.6 - 266.2 $^\circ$C. IR (v_{max}/cm^{-1}): v(N-H) 3059; v(S-H) 2786; v(C=N) 1621. ^{1}H NMR (295 K, ppm) 12.99 (br, s, 1H, *NH*); 7.96 (d, 1H, *H5*); 7.77 (d, 1H, *H8*); 7.69-7.66 (m, 2H, *H6, H7*); 7.46-7.42 (m, 2H, *H1, H4*); 7.30-7.28 (m, 2H, *H2, H3*); 5.01 (br, s, 1H, *SH*). UV-Vis (DMF, (λ_{max} (ε, M^{-1}cm^{-1}))): 298 (sh, 108957); 307 (114312); 321 (sh, 9497); 335 (sh, 6407).
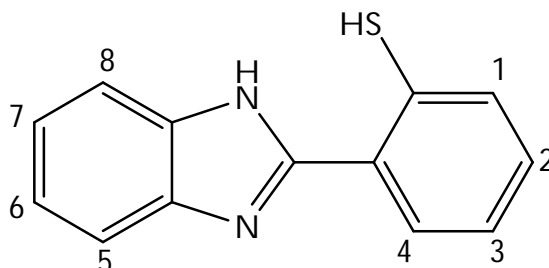
Figure 2.6: *Numbering scheme of Hsbz.*

25
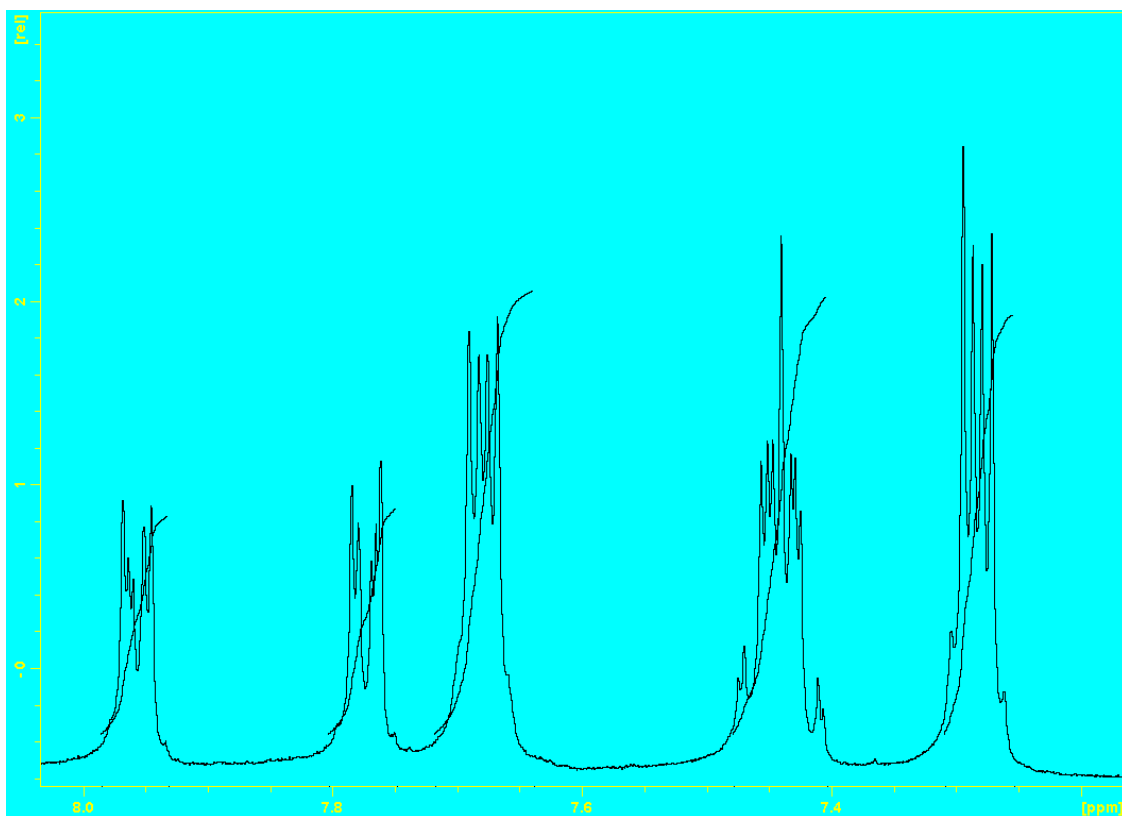
Figure 2.7: *¹H NMR spectrum of Hsbz between 7.15 and 8.05 ppm.*

2.3   Instrumentation

2.3.1   Conventional

A Perkin-Elmer Spectrum 100 FT-IR Spectrometer was utilized for capturing infrared (IR) spectra in the solid state in the range of $650 - 4000$ cm^{-1}. A Varian 500 MHz spectrometer was available for nuclear magnetic resonance (NMR) spectroscopy. Deuterated dimethylsulfoxide (DMSO) was the solvent of choice for both ligands and complexes. Melting points were found using a Stuart SMP3 machine. The electronic properties of the complexes were explored *via* UV/Vis spectroscopy using a PG Instruments Ltd. T80 and a Perkin Elmer Lambda 25 spectrophotometer. Emission spectroscopy was achieved through the utilization of a Photon Technology International, Nanoflash Illuminator. Conductivity measurements were done with a Radiometer Analytical standard Conductivity Electrode equipped on a MeterLab ION450 Ion Analyser instrument. The conductivity meter was calibrated with a standard solution of 0.745 g KCl in 1 L of H_2O.

2.3.2   X-ray crystallography

Single crystal X-Ray diffraction (XRD) analyses were performed using a Bruker Apex Duo diffractometer which was equipped with a three-cycle goniometer, an Apex 2 CCD detector and an Inocoatec M_o (K_α = 0.71073 Å) microsource X-Ray tube operating at 30 W. Data was collected at 10 – 20 second exposure times at mostly 100 K using ω and φ scans at fixed angles of θ. Direct methods were used to solve the structures by applying SIR97 [3] and using SHELXL-97 [4] to refine by least-squares procedures. The hydrogen atoms were calculated in idealized geometrical positions and non-hydrogen atoms were refined anisotropically. Prior to the data being corrected by a numerical absorption correction 10, the crystal shape was optimized with Gaussian 09W [5].

2.3.3   *Computational studies*

The Gaussian 09W programme was used in the computational modelling studies. Geometry optimizations were achieved through Density functional theory (DFT) calculations done with the LAND2Z basis set [6].

2.4   **References**:

1.   Rehder D*., Bioinorganic Vanadium Chemistry*, John Wiley and Son, London, 2008.

2.   Richards M.L., Lio S.C., Sinha A., Banie H., Thomas R.J., Major M., Tanji M., Sircar J.C., *Eur. J. Med. Chem.*, 2006, **41**, 950.

3.   Altomare A., Burla M.C., Camalli M., Gascarano G.L., Giacavazco C., Guagliardi A., Moliterni A.G., Polidori G., Spagna R., *J. Appl. Crystallogr.*, 1999, **32**, 115.

4.   Sheldrick G.M., SHELXL-97, *Programs for Structure Solution and Refinement*, University of Göttingen, Germany, 1997.

5.   Frisch M.J., Trucks G.W, Schlegel H.B., Scuseria G.E., Robb M.A., Cheeseman J.R., Scalmani G., Barone V., Mennucci B., Petersson G.A., Nakatsuji H., Caricato M., Li X., Hratchian H.P., Izmaylov A.F., Bloino J., Zheng G., Sonnenberg J.L., Hada M., Ehara M., Toyota K., Fukuda R., Hasegawa J., Ishida M., Nakajima T., Honda Y., Kitao O., Nakai H., Vreven T., Montgomery J.A., Jr. Peralta J.E., Ogliaro F.,

Bearpark M., Heyd J.J., Brothers E., Kudin K.N., Staroverov V.N., Kobayashi R., Normand J., Raghavachari K., Rendell A., Burant J.C., Iyengar S.S., Tomasi J., Cossi M., Rega N., Millam J.M., Klene M., Knox J.E., Cross J.B., Bakken V., Adamo C., Jaramillo J., Gomperts R., Stratmann R.E., Yazyev O., Austin A.J., Cammi R., Pomelli C., Ochterski J.W., Martin R.L., Morokuma K., Zakrzewski V.G., Voth G.A., Salvador P., Dannenberg J.J., Dapprich S., Daniels A.D., Farkas Ö., Foresman J.B., Ortiz J.V., Cioslowski J., Fox D.J., Gaussian 09 (Revision A.01), Gaussian Inc., Wallingford CT , 2009.

6. Dunning Jr. T.H., Hay P.J., in *Modern Theoretical Chemistry*, Schaefer III Ed. H.F., Vol. 3 (Plenum, New York, 1976) 1.

Chapter 3

Novel Vanadium Compounds with 2-Pyridylbenzimidazole

3.1 Introduction

Vanadium compounds have shown to exhibit a wide range of biological activities which include anti-tumour and antibacterial activity as well as insulin enhancing capabilities for the treatment of diabetes mellitus [1]. Their catalytic properties have also been extensively investigated [2]. Because of these applications there has been renewed interest in the coordination chemistry of vanadium [3].

The compound 2-pyridylbenzimidazole (Hpybz) is a highly versatile ligand system and has been coordinated to an array of transition metals [4]. Studies of this ligand with rhenium(V) metal precursors led to the formation of compounds showing unique redox chemistry. For example, the Re(III) complex [ReCl$_2$(pybz)(PPh$_3$)$_2$] where ReO$_4^-$ is produced as a by-product, was isolated from the disproportionation reaction between *trans*-[ReOCl$_3$(PPh$_3$)$_2$] and Hpybz [5]. Similarly, the cationic complex salt *cis*(Cl), *trans*(P)-[ReCl$_2$(PPh$_3$)$_2$(Hpybz)]Cl was prepared from the reaction of 2-pyridylbenzimidazole with *trans*-[ReOCl$_2$(OEt)(PPh$_3$)$_2$]. However, the reaction of Hpybz with [ReCl$_3$(PhC(O)C(O)Ph)(PPh$_3$)] in the presence of an oxidizing agent, NaOCl afforded a neutral Re(V) compound, [ReCl$_4$(Hpybz)].OPPh$_3$ [6].

Ruthenium complexes of the 2-pyridylbenzimidazole ligand and its derivatives have also been studied, especially with respect to their interesting electrochemical and photoluminescent properties [7]. Titanium dioxide nanocrystals doped with a ruthenium(II) compound, [Ru(NCS)$_2$(L$_1$)(L$_2$)] {L$_1$ = 4,4'-dicarboxy-2,2'-bipyridine and L$_2$ = 1-(2,4,6-trimethylbenzyl)-2-(2'-pyridyl)benzimidazole} showed evidence of optimal

photoelectrochemical activity as a dye sensitized solar cell [8]. Other derivatives of Hpybz such as terpyridyl-imidazole were used to form ruthenium compounds that have been utilized as both electrochemical and lifetime based sensors for anions [9].

Square pyramidal copper complexes of Hpybz have shown to exhibit anticancer activity [10]. These compounds does not show anticancer activity through typical DNA intercalation, like in the case of square planar Pt(II) chemotherapeutic drugs but rather destroy cancer cells through superoxide dismutase (SOD) mimetic activity [11]. Indicative to the above-mentioned, the ligand proved to be an excellent chelator to vanadium. In this chapter, we report the synthesis and characterization of four novel vanadium compounds, *cis*-[VO$_2$(Hpybz)(pybz)] (**1**), *cis*-[V(OH)$_2$(Hpybz)$_2$]Cl (**2**), (μ-O)[VO(pybz)$_2$.VO(Hpybz)(acac)] (**3**) and VO(Hpbyz)$_2$SO$_4$] (**4**).H$_2$O.

3.2   Experimental

3.2.1   *Cis-[VO$_2$(Hpybz)(pybz)] (1)*

A mixture of NH$_4$VO$_3$ (0.100 g, 0.855 mmol) and Hpybz (0.334 g, 1.71 mmol) in 20 cm^3 of a MeOH:water (1:1) *v:v* solvent ratio was heated under reflux for three hours. The resulting yellow solution was allowed to cool to room temperature and yellow, cubic crystals were grown over a four day period *via* the slow evaporation of the mother liquor. Yield (73 %), m.p. = 223 – 225 °C. IR(v_{max}/cm^{-1}): $v($N-H) 3354 w; $v($C=N) 1604 s; $v($V=O$_2$) 875 vs br. ^{1}H NMR (δ, ppm) 13.05 (br, s, 1H, *N6H*); 8.78 (d, 2H, *H1*, *H13*); 8.23 – 8.41 (m, 2H, *H4*, *H16*); 8.05 (t, 2H, *H2*, *H14*); 7.26 – 7.94 (m, 6H, *H3*, *H8*, *H11*, *H15*, *H20*, *H23*); 7.18 (d, 2H, *H10*, *H22*); 7.13 (d, 2H, *H9*, *H21*). ^{51}V NMR (δ, ppm) -588. UV-Vis (DMF, (λ_{max} (ε , M^{-1}cm^{-1}))): 310 (1774); 323 (1512); 354 (270). Conductivity (DMF, 10^{-3} M): 17.08 ohm^{-1}cm^{-2}mol^{-1}.

3.2.2   *Cis-[V(OH)$_2$(Hpybz)$_2$]Cl (2)*

An ethanolic solution (20 cm^3) of Hpybz (0.248 g, 1.271 mmol) and VCl$_3$ (0.100 g, 0.636 mmol) was heated under refluxed for five hours. The volume of the resultant dark green solution was halfed and layered with petroleum ether. Dark green, cubic crystals were obtained which were suitable for X-ray analysis. Yield (78 %), m.p. > 350 °C. IR(v_{max}/cm^{-1}):

v(N-H) 3263 m; v(O-H) 2686, 2682 m; v(C=N) 1603 vs. ^{1}H NMR (δ, ppm) 13.05 (br, s, 2H, *N3H*, *N6H*); 8.73 (s, 2H, *H1*, *H13*); 8.36 (s, 2H, *H4*, *H16*); 8.02 (s, 2H, *H2*, *H14*); 7.51 (s, 6H, *H3*, *H8*, *H11*, *H15*, *H20*, *H23*); 7.61 (br, s, 2H, *O1H*, *O2H*); 7.14 (s, 4H, *H9*, *H10*, *H21*, *H22*). UV-Vis (DMF, (λ_{max} (ε, M^{-1}cm^{-1}))): 311 (3140); 322 (2836); 356 (264). Conductivity (DMF, 10^{-3} M): 39.57 ohm^{-1}cm^{-2}mol^{-1}.

3.2.3 (μ-O)[VO(Hpybz)(pybz).VO(Hpybz)(acac)] (3)

A reaction mixture of Hpybz (0.155 g, 0.796 mmol) and VO(acac)$_2$ (0.100 g, 0.398 mmol) in 20 cm^3 of ethanol was heated under reflux for five hours. After reducing the volume to half, it was layered with petroleum ether. From the solution, XRD quality green needles were obtained. Yield (84 %), m.p. = 277 – 280.5 °C. IR (v_{max}/cm^{-1}): v(N-H) 3058 w; v(C=N) 1604, 1653, 1520 s; v(C=O) 1445, 1366 m; v(V-O) 951, 948 vs; v(V-O-V) 787 m. ^{1}H NMR (δ, ppm) 13.07 (br, s, 1H, *N8H*); 8.70 (d, 4H, *H6*, *H9*, *H16*, *H13*); 8.37 (d, 2H, *H4*, *H12*); 8.09 (d, 2H, *H1*, *H9*); 8.01 (t, 4H, *H2*, *H3*, *H10*, *H11*); 7.45 (t, 4H, *H6*, *H7*, *H14*, *H15*). ^{51}V NMR (δ, ppm) -590.5. UV-Vis (DMF, (λ_{max} (ε, M^{-1}cm^{-1}))): 313 (2780); 327 (2450); 357 (570). Conductivity (DMF, 10^{-3} M): 20.07 ohm^{-1}cm^{-2}mol^{-1}.

3.2.4 VO(Hpbyz)$_2$SO$_4$.H$_2$O (4)

The title compound was formed from the 2:1 molar ratio reaction between Hpbyz (0.239 g; 1.2278 mmol) and VOSO$_4$ (0.100 g; 0.6139 mmol) in 20 cm^3 of a MeOH:water (1:1) *v:v* solvent ratio (after five hours of refluxing). From the slow evaporation of the mother liquor, green, cubic crystals suitable for X-ray analysis were obtained after 3 days. Yield = 87 %, m.p. > 350 °C. IR (v_{max}/cm^{-1}): v(N-H) 3069 (w); v(C=N) 1608 (m); v(V=O) 948 (s). UV-Vis (DMF, (λ_{max} (ε, M^{-1}cm^{-1}))): 303 (sh, 38622); 313 (39835); 360 (sh, 3496). Conductivity (DMF, 10^{-3} M): 27.93 ohm^{-1}cm^{-2}mol^{-1}.

3.2.5 X-ray diffraction

X-ray diffraction data were recorded on an Oxford Diffraction Xcalibur 2 CCD 4-circle diffractometer equipped with an Oxford Instruments Cryojet operating at 120(2) K in the case of compound **1**. The X-ray data for **2**, **3** and **4** were recorded on a Bruker Apex Duo equipped with an Oxford Instruments Cryojet operating at 100(2) K and an Incoatec microsource operating at 30 W power. Crystal and structure refinement data are given in **Table 3.1**. Selected bond lengths and angles are given in **Tables 3.2 and 3.3**. In all three cases the data were collected with Mo Kα (λ = 0.71073 Å) radiation at a crystal-to-detector distance of 50 mm. The data collection on the Oxford diffractometer was performed using omega scans at θ = 29.389° with exposures taken at 2.00 kW X-ray power and 0.75° frame widths using CrysAlis CCD [**12**]. The data were reduced with the programme CrysAlis RED Version 170 [**12**] using outlier rejection, scan speed scaling, as well as standard Lorentz and polarisation correction factors. A semi-empirical multiscan absorption correction [**13**] was applied to the data. The following conditions were used for the Bruker data collection: omega and phi scans with exposures taken at 30 W X-ray power and 0.50° frame widths using APEX2 [**14**]. The data were reduced with the programme SAINT [**14**] using outlier rejection, scan speed scaling, as well as standard Lorentz and polarisation correction factors. A SADABS semi-empirical multi-scan absorption correction [**14**] was applied to the data. Direct methods, SHELXS-97 [**15**] and WinGX [**16**] were used to solve all four structures. All non-hydrogen atoms were located in the difference density map and refined anisotropically with SHELXL-97 [**15**]. All hydrogen atoms were included as idealised contributors in the least squares process. Their positions were calculated using a standard riding model with C-H$_{aromatic}$ distances of 0.93 Å and U_{iso} = 1.2 Ueq. The imidazole N-H atoms as well as the water and methanol solvate O-H hydrogen atoms of **1** were located in the difference density map, and refined isotropically.   In the case of **3**, the O-H hydrogen atoms of first and third ethanol solvent molecules were located in the difference density map and refined isotropically. The O-H hydrogen atom attached to O2S of the second ethanol molecule was refined using a riding model with the torsion angle governed by the experimental electron density (HFIX 83 instruction in SHELX). The third ethanol solvent molecule in the asymmetric unit of **3** (atoms O3-C5S-C6S) exhibited positional disorder for the central methylene group (C5S); this was well-resolved using a simple two-site model with occupancies of 0.37842 (C5S) and 0.62158 (C5S').

3.3 Results and Discussion

3.3.1 Synthesis and spectral characterisation

The metal compounds were isolated in good yields from the reactions of two equivalents of Hpybz with the respective metal precursors. The compounds $1\cdot CH_3OH.(H_2O)_2$, $3\cdot(CH_3CH_2OH)_3$ and $4\cdot H_2O$ compounds dissolve in DMF and DMSO, but they are poorly soluble in other common organic solvents. The solubility of **2** could only be achieved through heating followed by ultrasonication in DMF, DMSO or EtOH but not in chlorinated solvents. Compounds **1**, **3** and **4** are non-electrolytes while compound **2** is a 1:1 electrolyte in DMF [17]. The infrared spectrum of complex $1\cdot CH_3OH.(H_2O)_2$ (see **Figure 3.1**) shows an intense, broad band at 875 cm^{-1} which is well within the region expected for the V=O stretching frequency (860–930 cm^{-1}) [18].
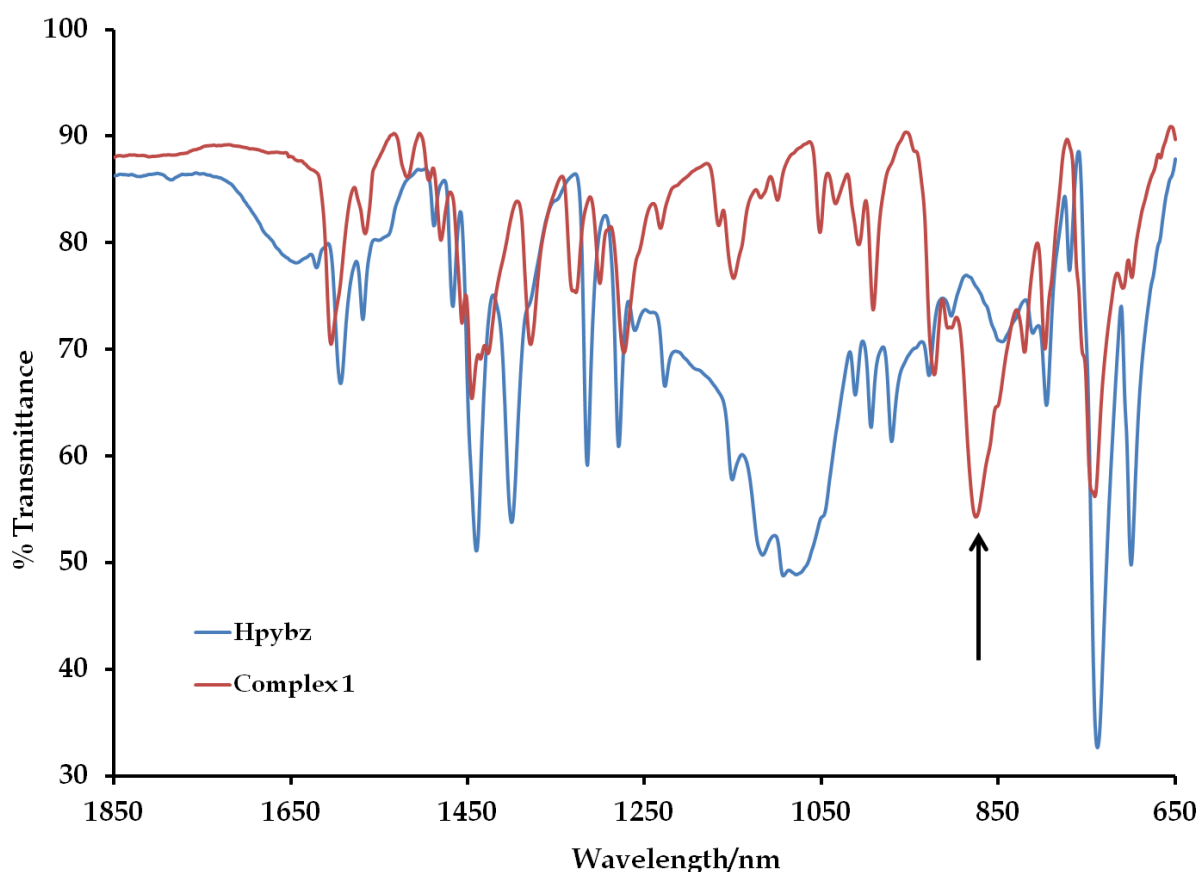

Figure 3.1: *Overlay IR spectra of the free ligand, Hpybz (2-pyridylbenzimidazole) and complex **1** in the range of 1850 and 650 cm^{-1}. The arrow indicates the intense, broad band at 875 cm^{-1} for the V=O stretching frequency.*

For compound **2**, the distinctive feature is two weak intensity stretching frequencies observed at 2686 and 2682 cm^{-1} for the hydroxyl co-ligands (*i.e.* v(O-H)). The N-H vibrations for the chelators in complexes **1**, **2**, **3** and **4** are found at 3554, 3263, 3058 and 3069 cm^{-1} respectively. The IR spectrum of **3** shows high intensity vibrational bands for the oxido-bridged bond (at 787 cm^{-1}), as well as those ascribed to the oxido moieties for the respective metal centres (at 948 and 951 cm^{-1}) which compare well with other oxido-bridged oxidovanadium (IV/V) compounds found in the literature [**19**]. The fact that these V=O bonds vibrate at different frequencies are due to the different coordination environments of the metals. The strong metal oxo-stretching frequency of complex **4** is found at 948 cm^{-1}. All IR spectra shows the presence of an intense stretch for v(C=N); and a weak intensity frequency band for the v(N-H) of the Hpybz/pybz.

The ^{1}H NMR spectrum of complex **1** measured in DMSO-d_6 shows signals in the aromatic region ascribed to the protons of the Hpybz and pybz ligands. However, the signals could not be resolved due to the near equivalence of the two ligands, and so the chemical shifts are listed in the experimental section as averaged values. A broad singlet at 13.05 ppm is readily assigned to the imidazole proton of the Hpybz ligand; note that the signal integrates for one proton, thus confirming that one of the coordinated ligands was deprotonated with the second one remaining in the neutral form. The ^{51}V chemical shifts of -588 (for complex **1**) and -590.5 (for compound **3**) ppm is upfield relative to the values of -540 and -539 ppm reported for *cis*-[VO$_2$(salhyph)]$^-$ (H$_2$salhyph = benzoic acid hydrazide) and *cis*-[NH$_4$]$_2$[VO$_2$(bmidaa)] (H$_3$bmidaa = *N*-(1-carboxymethylbenzimidazol-2-ylmethyl)iminodiacetic acid) respectively [**20, 21**]. The upfield shift reflects a relatively high electron density at the vanadium atom due to the strong σ-donor abilities of the pybz and Hpybz ligands (see the discussion of the crystal structure).

Broad signals were observed in the ^{1}H NMR spectrum of compound **2**, (see **Figure 3.2**) typical of metal centres containing unpaired electrons. Thus the assignments were based on the free ligand. In the case of compound **3**, well resolved proton signals appear in the aromatic region which is associated with the diamagnetic metal centre in combination with broadened signals which are due to the effects of the paramagnetic metal centre (see **Figure. 3.3**). The diamagnetic signals appears as a doublet (d):d:d: triplet (t):t set which integrate to

4:2:2:4:4. A broad singlet is found downfield which is due to the imidazolium proton. The presence of the diamagnetic +V centre was confirmed by ^{51}V NMR, (see **Figure 3.3**) in which the signal at -590.5 ppm was found relatively close to that of complex **1** (at -588 ppm).
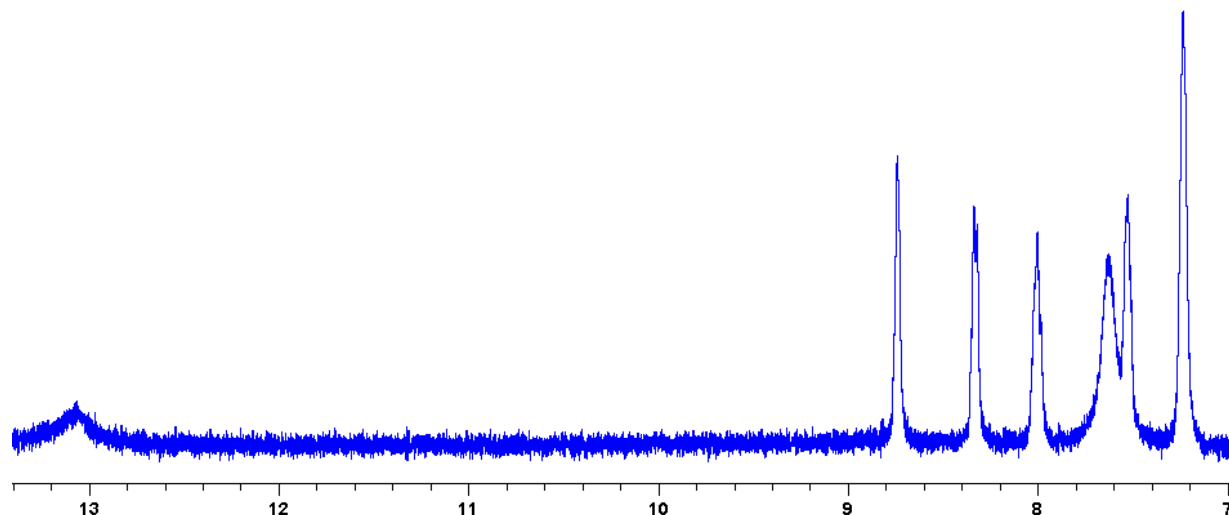
Figure 3.2: *^{1}H NMR spectrum of compound compound 2 illustrating the broad signals in the aromatic region which are due to the paramagnetic influence of the vanadium (III) metal centre.*

The ESR spectrum of compound **3** (see **Figure 3.4**) shows eight well-defined isotropic signals which confirm that no delocalization occurs between the metal centres. It is classified as a type I dimer since the metal centres are within different coordination environments as confirmed by NMR, IR, ESR spectroscopy and the crystal structure. Similar g-values and hyperfine coupling constants were found for other bimetallic oxidovanadium (IV/V) compounds as in compound **3** (g_{iso} = 1.921 and A = 102 G) [**22**]. Indicative to compound **3**, the mononuclear vanadium complex **4** showed an analogous ESR spectrum. The UV-Vis spectra of the compounds shows similar electronic transitions all ascribed to ligand based (π-π^*) transitions due to the highly delocalized nature of the chelator [**23**] (see **Figure 3.5**).
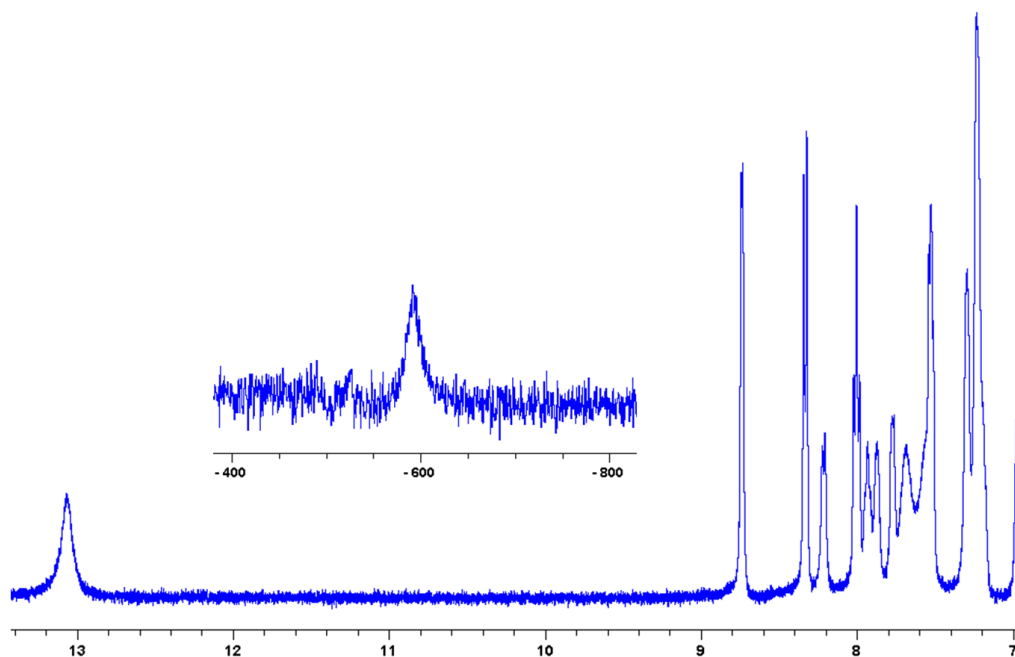
Figure 3.3: *^{1}H NMR of compound **3** illustrating both sharp and broad signals within the aromatic region due to the presence of both vanadium(IV) and -(V) metal centres. **Inset:** The signal at -590.5 ppm in the ^{51}V NMR confirms the presence of the vanadium(V) metal center.*
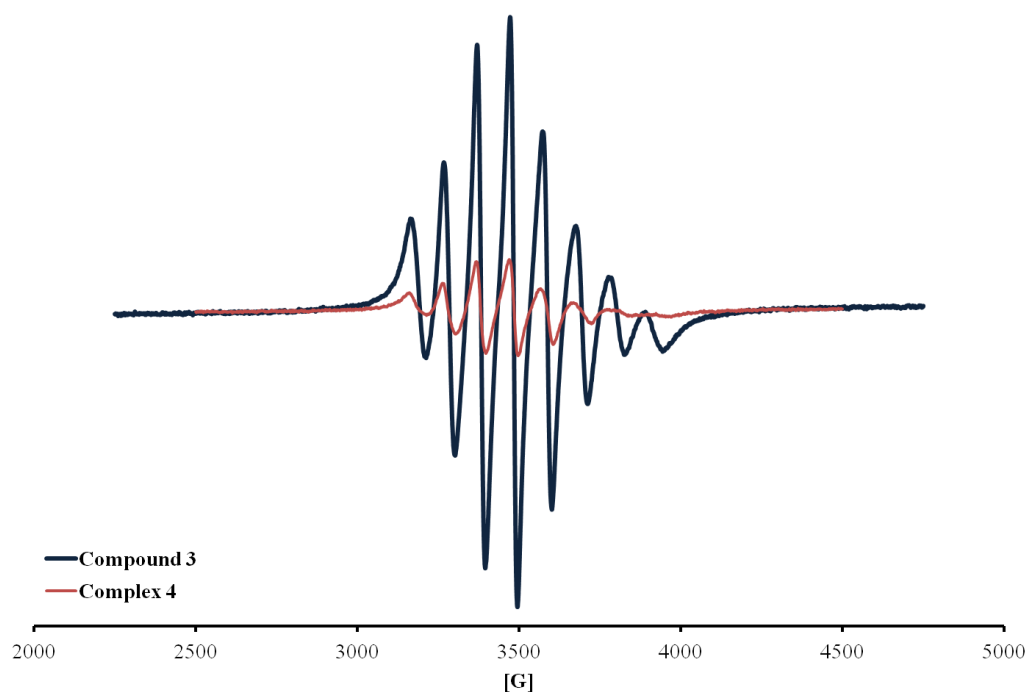
Figure 3.4: *X-band EPR spectra of compound **3** and complex **4** at 298 K. Instrument settings: microwave bridge frequency, 9.8 GHz; microwave bridge attenuator, 20 dB; modulation frequency, 100 kHz; modulation amplitude, 5 G; centre field, 3500 G.*
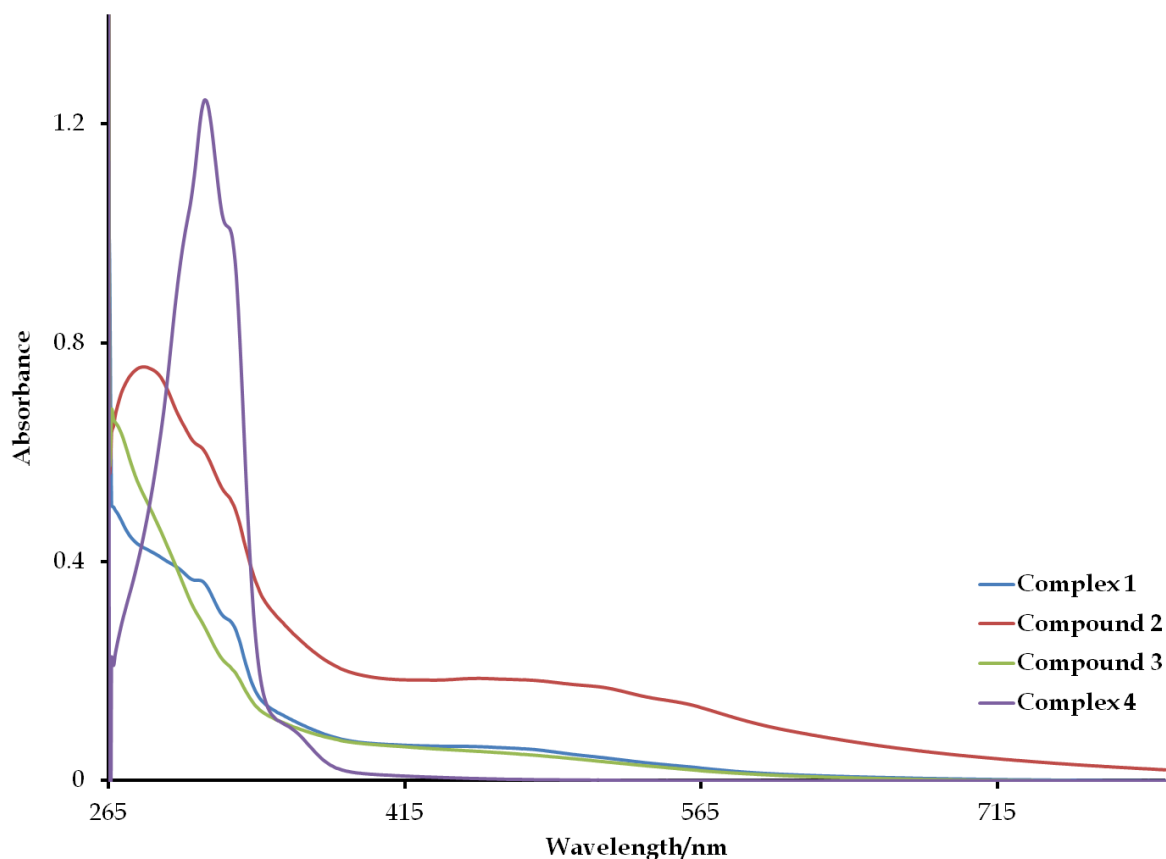
Figure 3.5: *Overlay UV-Vis spectra of the respective compounds.*

3.3.2 Structure of complex 1

The *cis*-[VO$_2$(Hpybz)(pybz)] (complex **1**) crystallizes as the CH$_3$OH·(H$_2$O)$_2$ hydrate with two independent complex molecules per asymmetric unit. The two complexes have very similar geometrical parameters and for this reason, we have averaged the bond lengths and angles (**Table 3.2**) for the purpose of the discussion. A perspective view of the complex is given in **Figure 3.6** along with the atom labelling scheme. The vanadium is octahedrally coordinated by two adjacent oxido groups (O1 and O2), by the pyridyl nitrogen (N1), an imidazole nitrogen (N2) of the anionic pybz ligand, the pyridyl nitrogen (N4) and an imidazole nitrogen (N5) of the protonated Hpybz ligand.

The oxido groups are *cis* relative to each other and *trans* to the pyridyl nitrogen atoms. Distortions from a regular octahedral geometry are apparent from the angles subtended at the vanadium atom, for *e.g*. for the two bidentate ligands: the N1-V-N2 and N4-V-N5 bite angles

are only 72-74°. This is due to the geometric constraints imposed by the ligands that are rigid and planar: the maximum deviation of an atom from a mean plane drawn through the non-hydrogen atoms of the pybz ligand is only 0.104(1) Å; and for the Hpybz ligand it is 0.190(3) Å. The 'trans' O1-V-N1, O2-V-N4 and N2-V-N5 angles also show marked deviations from the idealised octahedral bond angles (*i.e.* 180°)
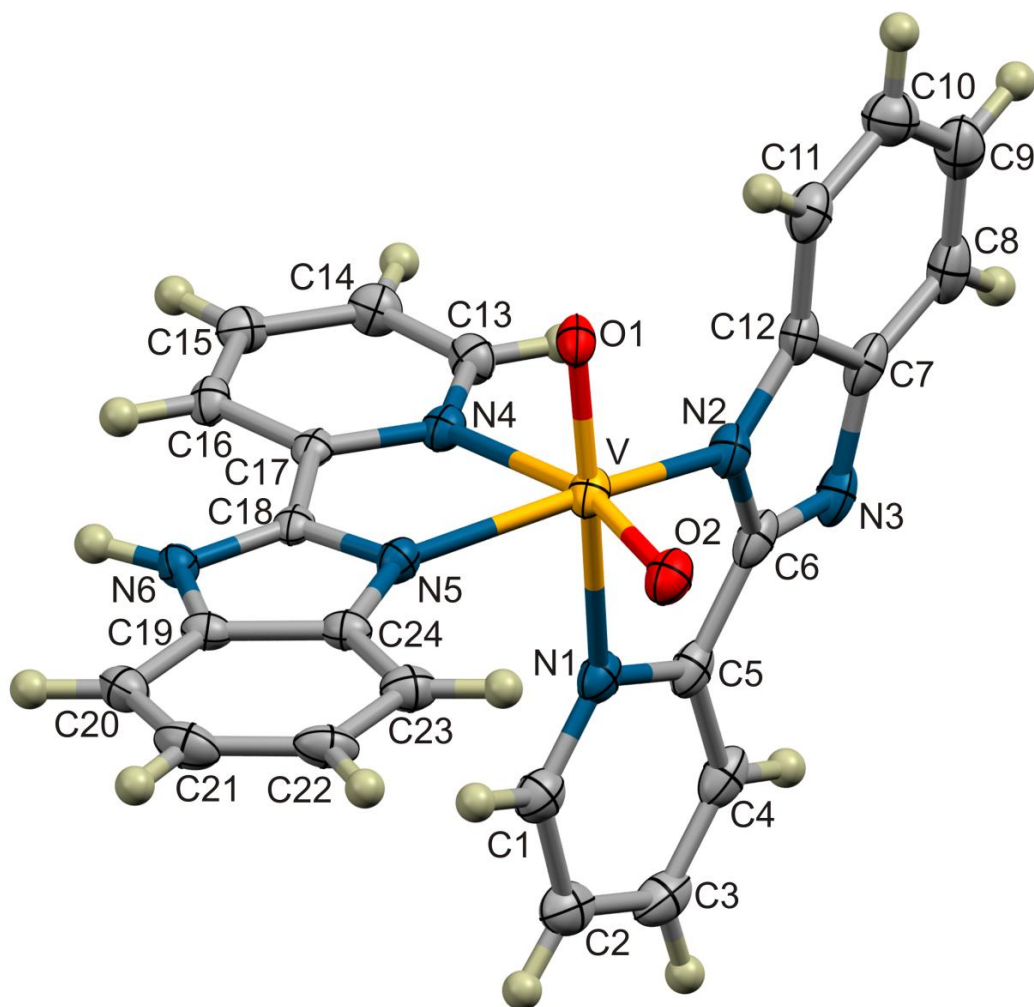
Figure 3.6: *An ORTEP view of complex **1** showing 50 % probability displacement ellipsoids and the atom labelling. The other independent molecule of complex **1** and the solvent molecules of crystallization are omitted for clarity.*

Octahedral coordination for a mononuclear dioxidovanadium(V) complex is unusual and we found only two examples reported in the literature, *viz cis*-[VO$_2$(EDDA)]$^-$ (H$_2$EDDA = ethylenediamine-*N*,*N'*-diacetate acid) [**24**] and *cis*-[VO$_2$(X)] (X = monoanionic tetradentate Schiff base) [**25**]. The octahedral coordination of the VO$_2^+$ core in each of these two

examples is completed by a tetradentate ligand, whereas in complex **1** it is completed by two bidentate ligands. Thus, the combination of ligands in complex **1** is the first of its kind to be reported for an octahedral complex of vanadium(V). Although octahedral mononuclear dioxidovanadium compounds (as in complex **1**) are rarely found in the literature, binuclear dioxidovanadium(V) compounds adopting octahedral geometries with respect to each metal centre are common [**26**]. For example, the coordination reactions with tridentate Schiff base ligands (HX) afforded the formation of centrosymmetric dinuclear dioxidovanadium(V) compounds, (μ-O)$_2$[V$_2$O$_2$X$_2$] where X = [2-(2-(methyl/ethyl/isopropyl)methylaminoethylimino)methyl] phenolate. In all three compounds, each vanadium atom occupies the centre of an octahedron with the chelators acting as monoanionic tridentate (X) moieties and the remaining coordination sites occupied by the oxido moiety as well as two oxido-bridged moieties [**27**].

The two V=O bond lengths of 1.621(3) Å (O1) and 1.638(4) Å (O2) are comparable with values found in the literature. For example, an average V=O bond length of 1.62 Å has been reported for *cis*-[VO$_2$(salhyph)]⁻ [**21**]; while for *cis*-[VO**₂**(Hpmide)]·4H$_2$O (H$_2$pmide = *N*-(2-pyridylmethyl)iminodiethanol) the V=O bond lengths are 1.634(1) and 1.664(1) Å [**20**]. More interesting are the V-N distances listed in **Table 3.2**. Starting with the pyridyl nitrogens, we note a significantly shorter distance to the anionic pybz ligand [V-N1 = 2.308(2) Å] as compared to the corresponding distance of the neutral Hpybz ligand [V-N4 = 2.384(2) Å]. With the imidazole nitrogens, there is also a shorter V-N distance for the anionic pybz ligand [V-N2 = 2.032(2) Å] compared to the neutral Hpybz ligand [V-N5 = 2.092(2) Å]. These V-N bond lengths show that the anionic pybz ligand functions as a stronger σ-donor ligand than the neutral Hpybz ligand, both through the pyridyl and imidazole nitrogen donor atoms. Interestingly, other authors have also reported metal-nitrogen bond lengths that reflect the stronger σ-donor ability of the nitrogen atoms of the anionic pybz ligand, as compared to those of the neutral Hpybz ligand, *e.g.* in the [Gd(Hpybz)(pybz)$_3$] complex, the Gd-N(pyridyl) bond lengths average 2.566(8) Å for the pybz ligand, a shorter distance than the Gd-N(pyridyl) distance of 2.593(9) Å for the Hpybz ligand [**28**].

In order to fully understand the difference in electron density at the nitrogen donor atoms of the protonated and deprotonated 2-pyridylbenzimidazole ligands, DFT calculations were

carried out on the Hpybz and pybz ligands. A plot of the results of the DFT calculations is shown in **Figure 3.7**. As the results in the plot show, there is good agreement between the calculated C-C and C-N bond lengths of the imidazole moieties and those obtained from the crystal structure determination. This suggests that the LANL2DZ basis set used for the DFT calculations is suitable, and that the net charges calculated for the nitrogen atoms are reliable estimates. We first examine the electron density on the imidazole nitrogens of the neutral ligand. The net charge of -0.433 electrons on the protonated nitrogen (N6) is higher than the net charge of -0.289 electrons on the coordinated nitrogen (N5). However, the lone pair on the protonated nitrogen is not available for bonding to the metal and, perforce, a bond between N5 and the vanadium is formed.
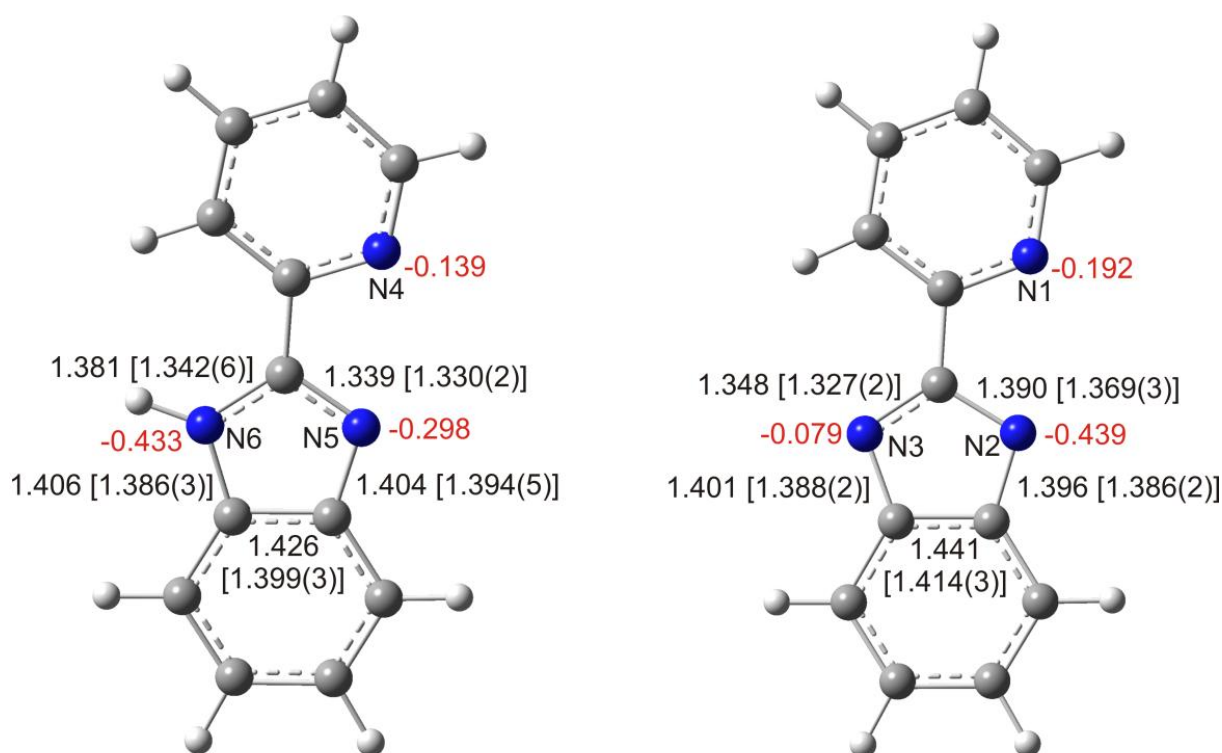
Figure 3.7: *DFT calculated Hpybz and pypz ligands of the vanadium complex. The calculated bond angles are shown adjacent to each bond and the experimental values are given in parentheses. The charge on the nitrogen atoms (electrons) are shown in red.*

The same restriction does not apply to the imidazole nitrogens of the anionic ligand, since *both* have lone pairs available for bonding to the metal. However, they carry very different net charges: the net charge of -0.439 electrons on N2 is much higher than the net charge of -

0.079 electrons on N3, as expected, since N2 carries a formal negative charge after loss of the proton. It is also significantly higher than the net charge on the donor atom of the neutral ligand (N5). On this basis N2 is expected to be a stronger N(σ) donor than N5 and, therefore, the DFT results predict a V-N2 bond that will be stronger and shorter than the V-N5 bond, consistent with the measured V-N2 and V-N5 bond lengths of 2.032(3) and 2.092(3) Å respectively. The calculated net charges on the pyridyl nitrogen atoms of the two ligands were then examined. As the DFT results show, the net charge of -0.192 electrons on the pyridyl nitrogen atom of the anionic ligand (N1) is higher than the net charge of -0.139 electrons on the pyridyl nitrogen atom of the neutral ligand (N4). The former atom is therefore expected to be the stronger σ-donor, and to form the stronger and shorter bond to the vanadium, consistent with the measured V-N1 and V-N4 distances of 2.308(2) and 2.384(2) Å respectively. In fact, all the V-N distances fit a pattern where an increase in net charge on the donor nitrogen atom leads to a shorter V-N bond length.

In the crystal packing it is noteworthy that the two crystallographically independent molecules of complex **1** in the asymmetric unit adopt different packing motifs. The molecules denoted as *A* stack in columns parallel to the [*b*]-axis (see **Figure 3.8**). Successive molecules in a column are linked through a centre of inversion, and in an alternating fashion by either π(pybz)-π(pybz) or π(Hpybz)-π(Hpybz) interactions. These are stabilizing π- π interactions in view of the relative orientations of the ligands within the adjacent pybz/pybz and Hpybz/Hpybz pairs, and the short perpendicular distance of *ca.* 3.3 Å between their planes.

The molecules denoted as *B* also stack in columns parallel to the [*b*]-axis, but in this case successive molecules in a column are linked through hydrogen bonds; also molecules from adjacent columns are linked by hydrogen bonds, thus effectively forming sheets of molecules parallel to the *ab* plane (see **Figure 3.9**). Details of the hydrogen bonding are given in **Table 3.4**. It can be seen in **Figure 3.10** that molecules from adjacent rows are cross-linked through a series of hydrogen bonds (**Table 3.4**). The columns of molecules *A* and molecules *B* stack in alternating layers to give the three-dimensional structure.
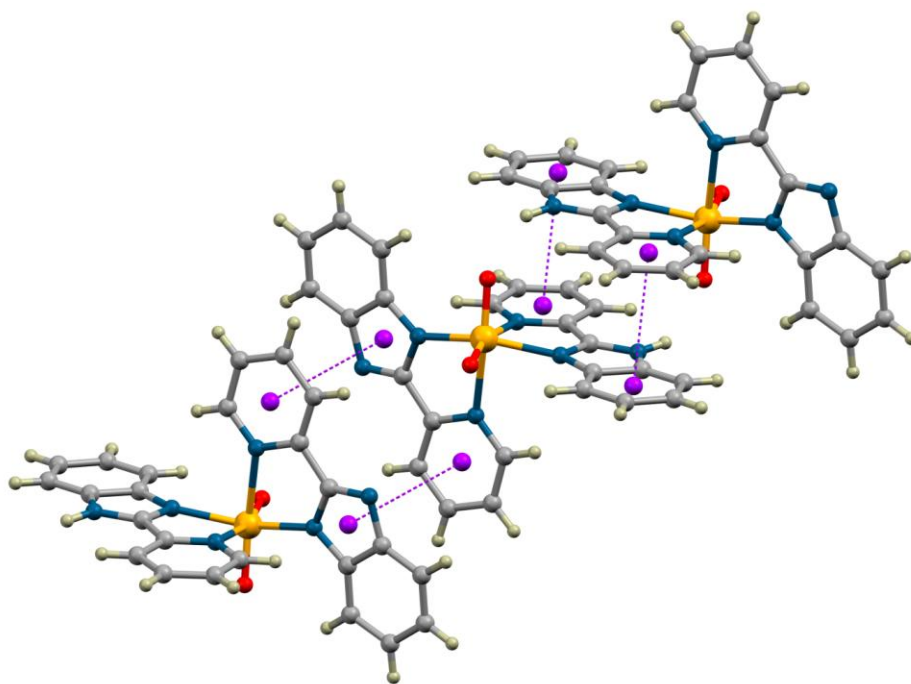
Figure 3.8: *One-dimensional chains of molecules A, showing centroid-centroid contacts. The chains are supported by pi-pi stacking.*
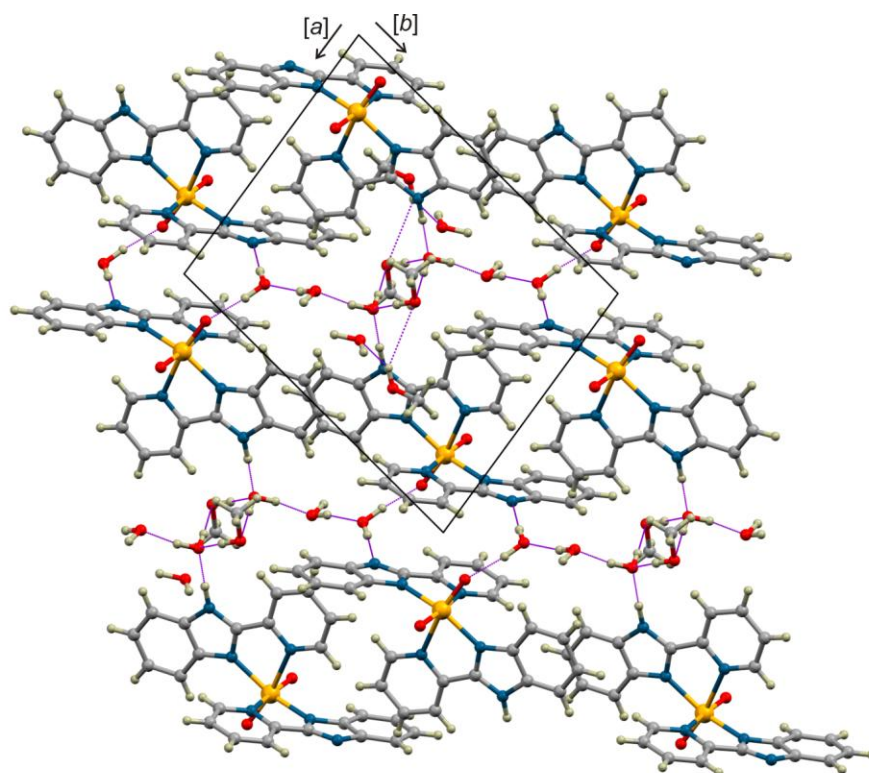
Figure 3.9: *Two-dimensional network of molecules B supported by extensive hydrogen bonds (shown as dashed, purple lines).*
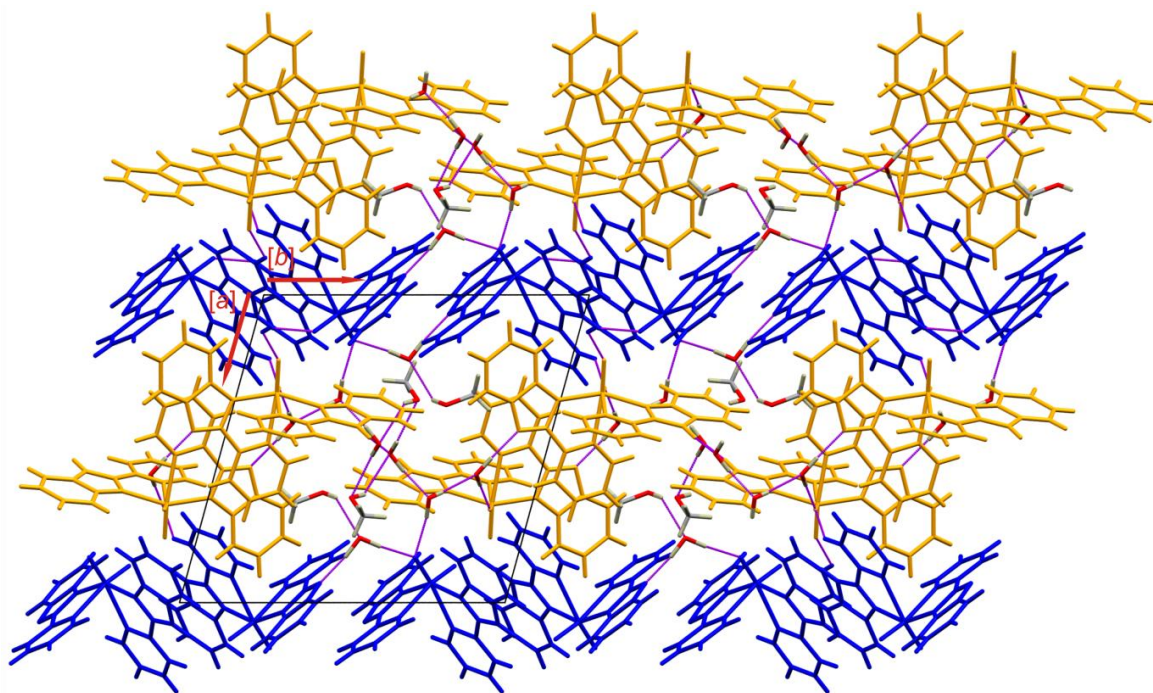
Figure 3.10: *Three-dimensional network of complex* ***1.***CH₃OH·(H₂O)₂ *viewed down the [a]-axis. The network is completed by hydrogen bond cross-links between the molecules in the columns of molecule A (shown in blue) and molecule B (shown in yellow).*

3.3.3   Structure of compound 2

The compound *cis*-[V(OH)₂(Hpybz)₂]Cl (compound **2**) exhibits a distorted octahedral geometry (see **Figure 3.11**). Selected bond distances and angles are given in **Table 3.2**. The Hpybz ligands act as bidentate chelators through the two neutral pyridyl (N1, N4) and imidazolium nitrogens (N2, N5).   These ligands afford 5-membered chelate rings with constrained bite angles [N1-V-N2 = 73.04(9)° and N5-V-N4 = 73.31(9)°] inducing octahedral distortion with the O2-V-N4 = 161.8(1)°, O1-V-N1 = 165.1(1)° and N2-V-N5 = 151.2(1)° angles deviating significantly from linearity. The metal centres of compounds **1** and **2** have very similar coordination environments, with oxido groups that are required for the +V oxidation state of the (d⁰) metal centre (in complex **1**) and are replaced with hydroxyl groups (in compound **2**) which is suitable for low oxidation stabilization. In addition, in compound **2,** both chelating ligands act as neutral bidentate ligands (*i.e.* Hpybz) whereas complex **1** has a neutral and a monoanionic (*i.e.* pybz) bidentate chelator. Thus these compounds have comparable geometrical parameters.   For example, the *cis* hydroxyl co-

ligands in compound **2** affords a slightly wider O1-V-O2 angle of 108.1(1)° compared to the average O1-V-O2 angle [105.6(1)°] formed by the *cis* oxido co-ligands in complex **1**.

Figure 3.11: *An ORTEP view of compound 2, showing 50 % probability displacement ellipsoids and the atom labelling.*

As expected, the V-O double bond lengths in complex **1** [V-O1 = 1.621(3) Å and V-O2 = 1.638(4) Å] are shorter than the V-O single bond lengths in compound **2** [V-O1 = 1.759(3) Å and V-O2 = 1.809(2) Å], and the Hpybz chelators affords similar bite angles in both complex **1** [N4-V-N5 = 72.36(9)°] and compound **2** [N1-V-N2 = 73.04(9)° and N5-V-N4 = 73.31(9)°]. More interestingly, the V-N bond lengths were similar for both metal compounds despite having different oxidation states. In fact, the *trans* V-N(pyridyl) bond lengths are similar to vanadium(III) compounds found in the literature: $V^{III}(qn)_3$ (Hqn = quinoline) as well as the series of complex cations, $[VX_2N_2S_2]X$ (where X = Br or I), [**29**] which were synthesized from the *tri*-halide vanadium precursor, $VX_3(thf)_3$, and the neutral tetradentate chelator, 1,6-*bis*(2'-pyridyl)-2,5-*di*thiahexane (N_2S_2) [**30**].

Unlike in complex **1**, where a network of hydrogen bonding stabilized the crystal lattice, only two classical hydrogen bonds are observed for compound **2** between the chloride counter-ions

and the respective N-H bonds of the chelates, (refer to **Table 3.5** and **Figure 3.12**). Weak intermolecular interactions occur between the C19 to C24 phenyl rings of respective molecules with centroid to centroid distances of 4.012 Å. Consequently, these interactions results in a three dimensional network with a series of polymeric chains running at $ca = 60°$ with respect to the [c]-axis.
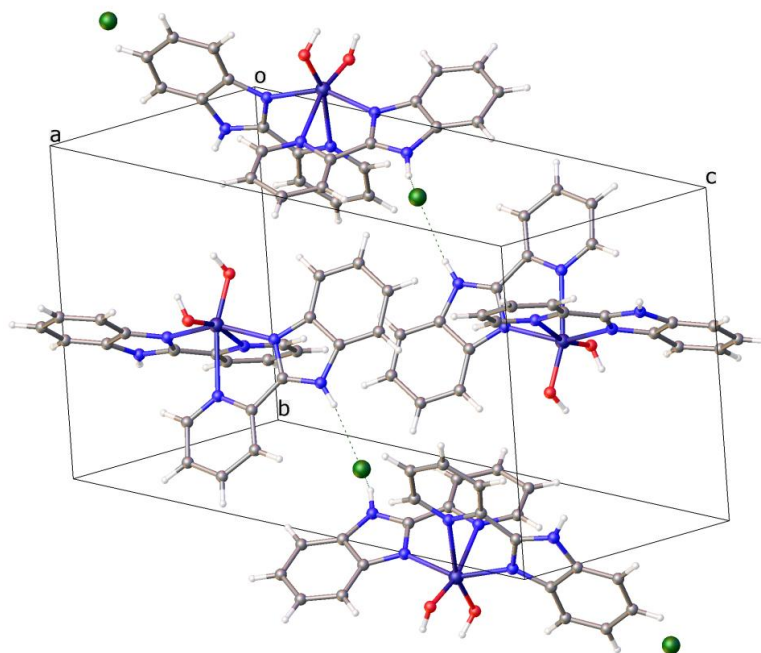
Figure 3.12: *A perspective view of the unit cell for compound **2**, showing the classical hydrogen-bonding.*

3.3.4   Structure of compound 3

The crystal structure of compound **3** with the atom numbering scheme is shown in **Figure 3.13**. Compound **3** crystallized with three ethanol solvent molecules. The crystal structure is stabilized by various classical hydrogen bonding interactions (refer to **Table 3.6**) and π-π interactions ($ca = 3.5$ Å) between two co-planar Hpybz and pybz ligands of the respective metal atoms.

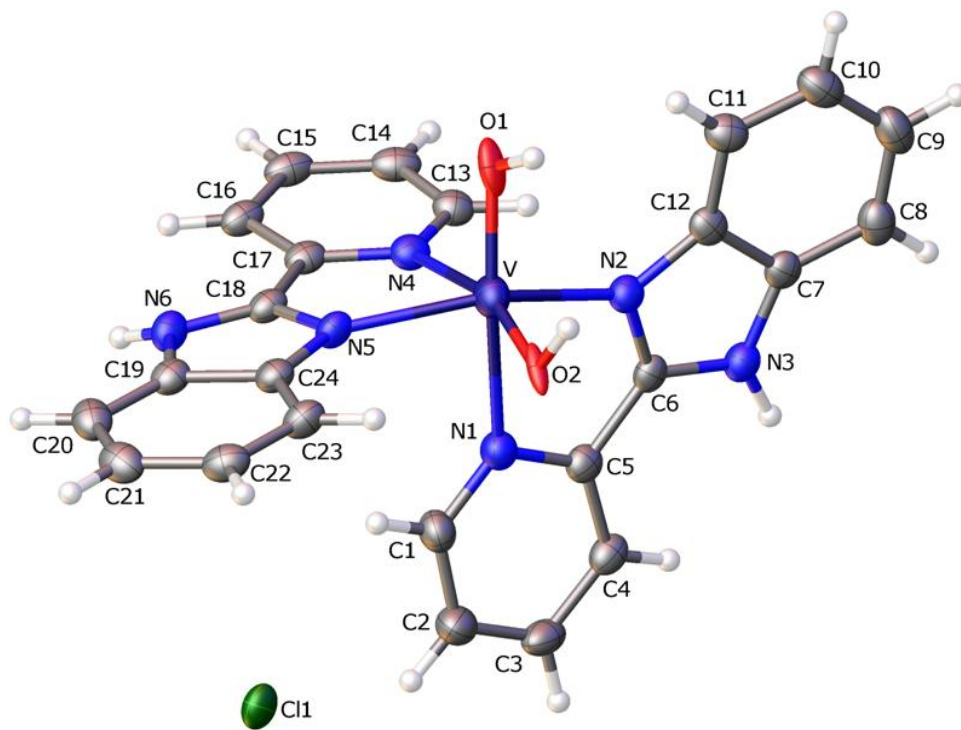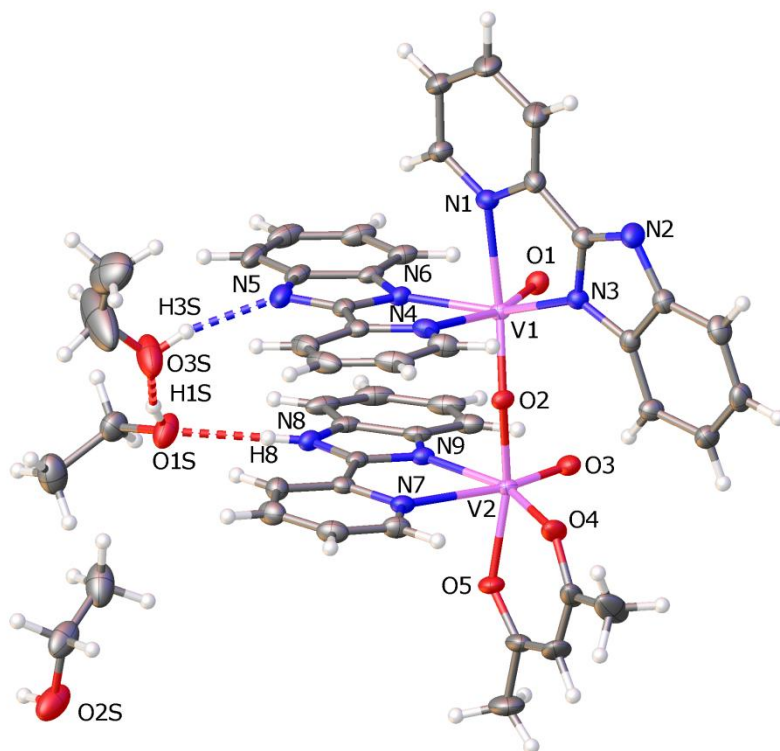**Figure 3.13**: *An ORTEP view of compound **3** showing 50 % probability displacement ellipsoids and the atom labelling.*

The metal atoms are at the centres of distorted octahedrons with a central oxido-bridge O2 [V1-O2-V2 equal to 151.81(9)°]. The deviation of this angle from linearity is ascribed to the variable valences of the metal atoms. The (μ-O)(VO)$_2$ backbone has a *syn*-angular orientation given by the angles of O1-V1-O2 = 105.50(7)° and O3-V2-O2 = 98.60(7)° which is significantly larger than the ideal 90°. Variable valency is also evident from the difference in bond lengths within the oxido-bridged moiety [V1-O2 = 1.683(1) Å and V2-O2 = 1.958(1) Å]. However the V=O bond lengths [V1-O1 = 1.606(1) Å and V2-O3 = 1.602(1) Å] were found to be essentially identical. These bond lengths were comparable with the bond length of 1.607(1) Å for (NH$_4$)[(μ-O)V$_2$O$_2$(Hhida)$_2$]·H$_2$O (H$_3$hida = *N*-(2-hydroxyethyl)iminodiacetic acid [**14**].

The pybz ligands around the V1 atom are coordinated bidentately through the pyridyl (N1, N4) and deprotonated imidazolate (N3, N6) nitrogens of the respective pybz moieties, with bite angles of N1-V1-N3 = 74.26(6)° and N4-V1-N6 = 73.41(6)°. The difference in the bite angles could be due to the stronger *trans* effect experienced by the V1-N4 bond [2.341(2) Å]

which is *trans* to the oxido group [O1] compared to the V1-N1 [2.284(2) Å] which is *trans* to the oxido-bridged group [O2]. Around the V2 atom the ligand forms a 5-membered chelate ring through the pyridyl (N7) and neutral imidazolium (N9) nitrogens with a bite angle, N7-V2-N9 = 72.28(6)°. A six-membered chelate ring is also afforded by the bidentate coordination of the monoanionic acetylacetone (acac) moiety through the oxygens (O4, O5) where the slight difference in the bond lengths V2-O4 = [1.977(2) Å] and V2-O5 = [2.006(1) Å] is accounted to the variable *trans*-influence experienced by the donor atoms.

Although spectral characterization support the presence of different oxidation states for the metal centres, an argument arises that charge neutrality can be achieved through protonation of the N2 atom. This argument is also proven contradictory when considering the C6-N2 [1.324(3) Å] bond which exhibits double bond character and is significantly shorter than the C6-N3 [1.356(3) Å] bond which implies that the latter is a single bond. Furthermore, the C6-N2 bond distance is also comparable with the other two C=N [C18-N5 = 1.335(3) Å and C30-N9 = 1.329(3) Å] bonds found within the Hpybz and pybz ligands respectively. In addition, the coordination bond lengths to the imidazolate nitrogens [V1-N3 = 2.051(2) Å and V1-N6 = 2.031(2) Å] are significantly different.

Despite the fact that most mixed valence oxidovanadium compounds have been formed from oxygen-donor ligands, nitrogen-donor ligands have also proved to be excellent chelators. The isolation of the novel binuclear vanadium (II/III) compounds, $[(PY5Me_2)V^{II}(\mu\text{-}L_{br})V^{III}(PY5Me_2)]^{4+}$ (PY5Me$_2$ = 2,6-*bis*(1,1-*bis*(2-pyridyl)ethyl)pyridine) with different N-donor (L$_{br}$) bridges were described [31]. Another example is the benzimidazole ligand, Me$_3$ntb [*tris*(*N'*-methylbenzimidazol-2'-*y*l-methyl)amine] which was reacted with VO(CF$_3$SO$_3$)$_2$ to afford the binuclear compound, $[(Me_3ntb)V^{IV}O(\mu\text{-}O)V^VO(Me_3ntb)](CF_3SO_3)_3\cdot2H_2O$ [32]. Nitrogen and oxygen-donor Schiff base ligands derived from salicylaldehyde and various aliphatic diamines forms tetradentate chelators which readily coordinate to vanadium affording mixed binuclear oxido-bridged vanadium compounds [33], *e.g.* $[(salen)V^{IV}\text{-}O\text{-}V^V\text{=}O(salen)][ClO_4]$; H$_2$salen = *N,N'*-ethylene-*bis*(salicylideneimine). A further study involves the chelation of one heptadentate N$_4$O$_3$ donor ligand to two vanadium centers, which led to the formation of the vanadium(IV/V) dimer, $(\mu\text{-}O)[V_2O_2(oap)]$; H$_3$oap = 2,6-*bis*[{{(2-hydroxybenzyl)(*N,N'*-(dimethylamino)ethyl)}amino}methyl]-4-methylphenol [22]. In addition, the strong affinity of N, O chelator ligands to vanadium often allows the formation of multinuclear, mixed

valence vanadium compounds. For example, the reaction of vanadyl sulfate and *N*-acetylsalicylhydrazidate (H$_3$ashz) formed a hexanuclear vanadium compound, [V$_3$O$_3$(OEt)(ashz)2(μ-OEt)]$_2$ [**34**].

3.3.5   Structure of complex 4

Complex **4** has similar structural features as all the previous vanadium complexes **1 – 3** and for this reason a detailed comparative description of complex **4** will not be given. The '2+2' coordination mode of the neutral Hpybz ligands affords two five-membered rings with bite angles of 73.20(8)˚ [N1-V-N2] and 77.07(9)˚ [N4-V-N5] (see **Figure 3.14**). These constrained bite angles results in the formation of a distorted octahedron with the N2-V-N4 [159.22(9)˚], N1-V-O1 [170.1(1)˚] and O2-V-N5 [157.25(9)˚] angles severely deviating from linearity.

As expected, the differences between the respective neutral V-N$_{py}$ [V-N1 = 2.350(3) Å and V-N4 = 2.146(2) Å] and V-N$_{hetero}$ [V-N2 = 2.080(2) Å and V-N5 = 2.115(2) Å] coordination bonds are attributed to the different *trans*-effects experienced by the donor atoms. Furthermore, the V-O1 [1.582(2) Å] has a bond order of 2 due to its shorter bond distance V-O2 [1.984(2) Å]. More interestingly, the aforementioned coordination bond (*i.e.* V-O2) induces a longer S-O2 [1.515(2) Å] than all the other intraligand S-O [S-O3 = 1.449(3) Å, S-O4 = 1.461(3) Å and S-O5 = 1.473(2) Å] bonds within the sulfate co-ligand. This implies that the latter exhibits double bond character and that an electron is delocalized over these intraligand bonds.

The crystal lattice of complex **4** is stabilized by the intermolecular interactions between the two co-planar N4/N5-Hpybz moieties of adjacent molecules [average centroid to centroid distance = 5.630 Å]. In addition, the presence of the water molecule of recrystallization and sulfate co-ligand allows the formation of three classical hydrogen bonds (refer to **Table 3.7** and **Figure 3.15**).
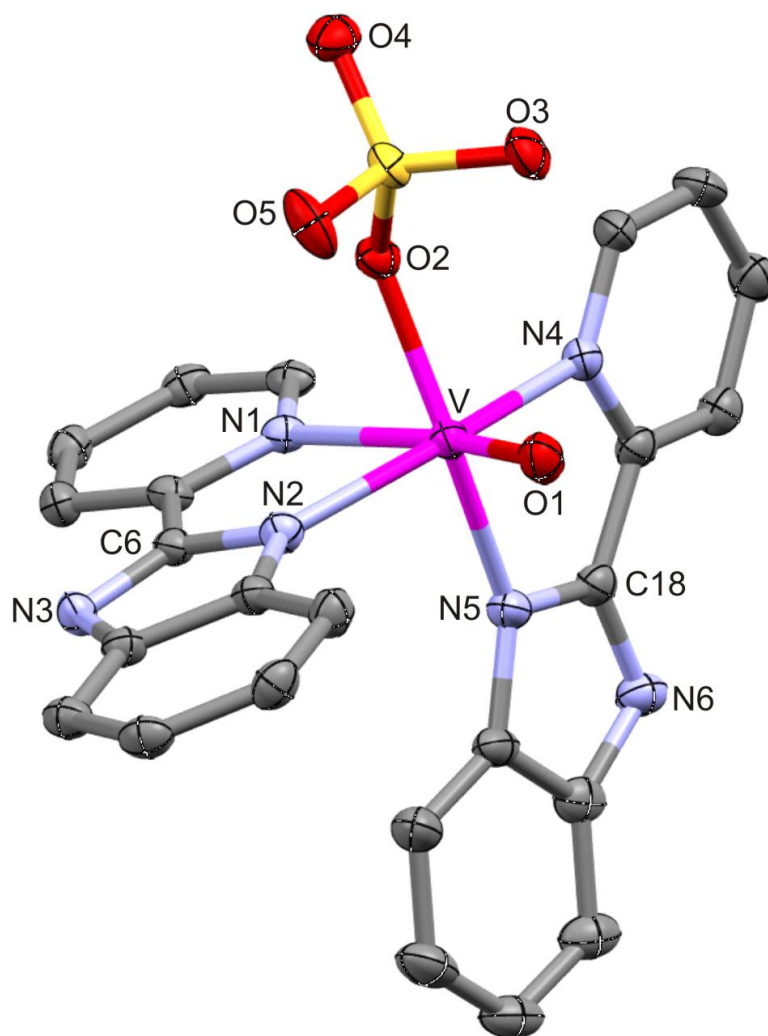
Figure 3.14: *An ORTEP view of complex **4** showing 50 % probability displacement ellipsoids and the atom labelling. Hydrogen atoms have been omitted for clarity.*
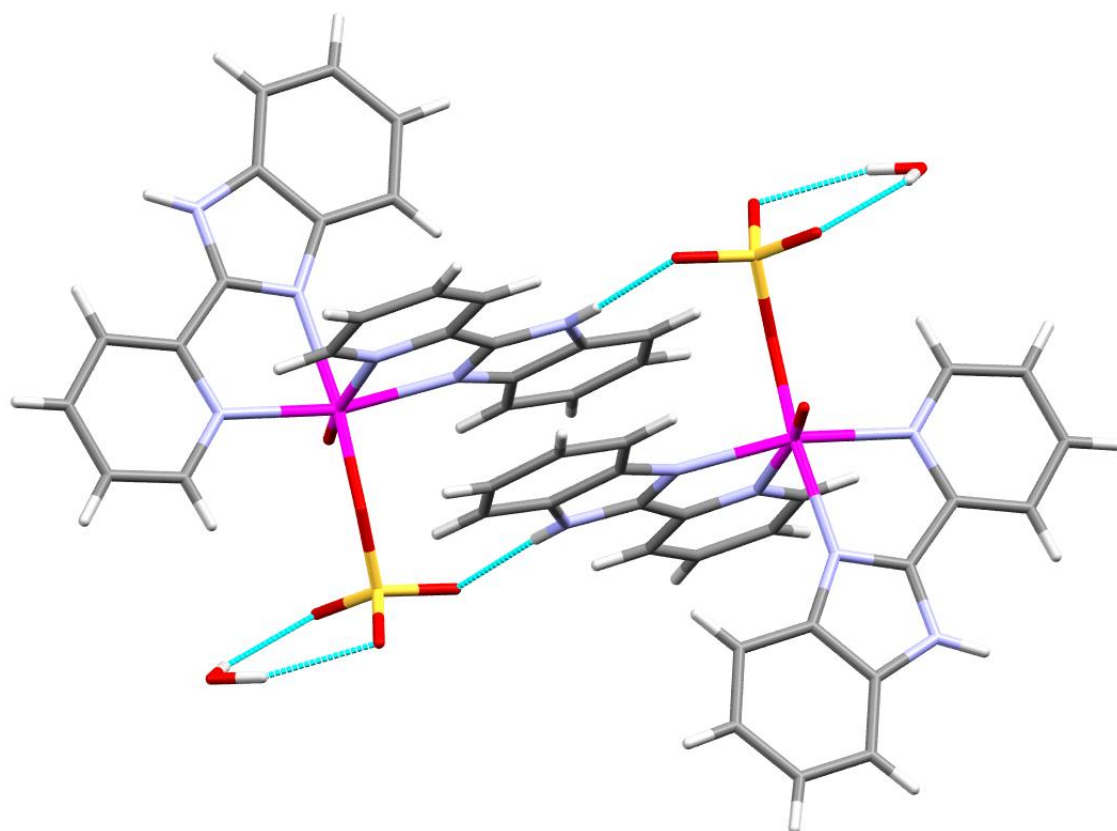
Figure 3.15: *A perspective view of complex **4**, showing the hydrogen-bonding and the two co-planar N4/N5-Hpybz moieties of adjacent molecules.*

3.4   References:

1.   (a) Rehder D., *Inorg. Chem. Comm.,* 2003, **6**, 604, 1(b) Evangelou A.M., *Crit. Rev. Oncol. Hemat.,* 2002, **42**, 249.

2.   Ligtenbarg A., Hage R., Feringa B., *Coord. Chem. Rev.,* 2003, **237**, 89.

3.   Thompson K.H., Orvig C., *Coord. Chem. Rev.,* 2001, **219–221**, 1033.

4.   Zhou Y., Li X., Zhang H., Fan C., Zhang H., Wu B., *J. Coord. Chem.,* 2011, **64**, 4066.

5.   Gerber T.I.A., Mayer P., Tshentu Z.R., *J. Coord. Chem.,* 2006, **59**, 1509.

6.   Sokolov M.N., Fedorova N.E., Peresypkina E.V., Pätow R., Fedorov V.E., Fenske D., *Inorg. Chim. Acta,* 2005, **358**, 3914.

7.   Baggaley E., Weinstein J.A., Gareth J.A., *Coord. Chem. Rev.,* 2012, **256**, 1762.

8.   Sahin C., Ulusoy M., Zafer C., Ozsoy C., Varlikli C., Dittrich T., Cetinkaya B., Icli S., *Dyes Pigments,* 2010, **84**, 88.

9.   Bhaumik C., Maity D., Das S., Baitalik S., *Polyhedron,* 2013, **52**, 890

10. Lu Y.M., Chen Y.H., Ou Z.B., Chen S., Zhuang C.X., Le X.Y., *Chin. J. Chem.*, 2012, **30**, 303.

11. Devereux M., Shea D.O., Kellett A., McCann M., Walsh M., Egan D., Deegan C., Kędziora K., Rosair G., Müller-Bunz H., *J. Inorg. Biochem.,* 2007, **101**, 881.

12. Oxford Diffraction, *CrysAlis CCD and CrysAlis RED*. Oxford Diffraction Ltd, Yarnton, England, 2008.

13. Blessing R.H., *Acta Cryst.,* 1995, **A51**, 33.

14. Bruker APEX2, *SAINT and SADABS*. Bruker AXS Inc. (2010) Madison, Wisconsin, USA.

15. Sheldrick G.M., *Acta Cryst.,* 2008, **A64**, 112.

16. Farrugia L.J., *J. Appl. Cryst.,* 2012, **45**, 849.

17. Asif I., Ali S., Shahzadia S., Mahmood S.*, J. Chin. Chem. Soc.,* 2007, **54**, 23.

18. Maurya M.R., Kumar A., Abid M., Azam A., *Inorg. Chim. Acta,* 2006, **359**, 2439.

19. (a) Mahroof-Tahir M., Keramidas A.D., Goldfarb R.B., Anderson O.P., Miller M.M., Crans D.C., *Inorg. Chem.,* 1997, **36**, 1657 (b) Nishizawa M., Hirostsu K., Ooi S., Saito K., *J. Chem. Soc. Chem. Comm.,* 1979, 707.

20. Crans D.C., Keramidas A.D., Amin S.S., Anderson O.P., Miller S.M., *J. Chem. Soc. Dalton Trans.,* 1997, 2799.

21.   Plass W., Yozgatli H.*, Z. Anorg. Allg. Chem.,* 2003, **65**, 629.

22.   Mondal A., Sarkar S., Chopra D., Guru Row T.N., Pramanik K., Rajak K.K., *Inorg. Chem.,* 2005, **44**, 703.

23.   Murray K.S., Sheahan R.M., *J. Chem. Soc. Dalton Trans.,* 1973, **11**, 1182.

24.   Crans D.C., Keramidas A.D., Mahroof-Tahir M., Anderson O.P., Miller M.M., *Inorg. Chem.,* 1996, **35**, 3599.

25.   Romanowski G., Kwiatkowski E., Nowicki W., Kwiatkowski M., Lis T., *Polyhedron*, 2008, **27,** 1601.

26.   Kwiatkowski E., Romanowski G., Nowicki W., Kwiatkowski M., *Polyhedron,* 2006, **25**, 2809; Romanowski G., Wera M., *Polyhedron,* 2010, **29**, 2747.

27.   You Z., Sun H., Ding B., Ma Y., Zhang M., Xian D., *J. Coord. Chem.,* 2011, **64**, 3510.

28.   Muller-Buschbaum K., Quitmann C.C., *Z. Anorg. Allg. Chem.,* 2004, **630**, 131.

29.   Manos M.J., Tasiopoulos A.J., Raptopoulou C., Terzis A., Woollins J.D., Slawin A.M.Z., Keramidas A.D., Kabanos T.A., *J. Chem. Soc. Dalton Trans.,* 2001, **10**, 1556.

30.   Nekola H., Wang D., Grunning C., Galtjens J., Behrens A., Rehder D., *Inorg. Chem.,* 2002, **41**, 237.

31.   Bechlars B., D'Alessandro D.M., Jenkins D.M., Lavarone A.T., Glover S.D., Kubiak C.P., Long J.R., *Nature Chem.,* 2010, **2**, 362.

32.   Ghosh S., Nanda K.K., Addison A.W., Butcher R.J., *Inorg. Chem.,* 2002, **41**, 2243.

33.   Tsuchida E., Oyaizu K., *Coord. Chem. Rev.,* 2003, **237**, 213 and references therein.

34.   Sutradhar M., Kirillova M.V., Guedes da Silva M.F.C., Martins L.M.D.R.S., Pombeiro A.J.L., *Inorg. Chem.,* 2012, **51**, 1229.

Table 3.1: *Crystal and structure refinement data*

	1.(H₂O)₂V.(H₂O)₂.CH₃OH	2	3.(CH₃CH₂OH)₃	4.H₂O
Chemical formula	$C_{24}H_{17}N_6O_2V$	$C_{24}H_{20}ClN_6O_2V$	$C_{41}H_{32}N_9O_5V_2$.$(CH_3CH_2OH)_3$	$C_{24}H_{20}N_6O_6SV$
Formula weight	540.44	510.9	970.9	571.5
Temperature(K)	120(2)	100(2)	100(2)	100(2)
Crystal system	Triclinic	Monoclinic	Monoclinic	Triclinic
Space group	P-1	P2₁/c	P2₁/n	P-1
Unit cell dimensions (Å, °)	$a = 11.962(5)$	$a = 8.8535(3)$	$a = 10.0064(3)$	$a = 10.1333(5)$
	$b = 14.728(5)$	$b = 11.2264(4)$	$b = 28.839(1)$	$b = 10.8179(5)$
	$c = 14.846(5)$	$c = 22.2385(7)$	$c = 16.5545(6)$	$c = 13.3804(6)$
	$\alpha = 103.511(5)$	$\alpha = 90$	$\alpha = 90$	$\alpha = 69.040(2)$
	$\beta = 104.504(5)$	$\beta = 90.508(2)$	$\beta = 101.518(1)$	$\beta = 74.293(2)$
	$\gamma = 94.933(5)$	$\gamma = 90$	$\gamma = 90$	$\gamma = 88.224(3)$
V(Å³)	2432.9(6)	2210.26(1)	4681.1(1)	1315.03(15)
Z	4	4	4	2
Density (calc.) (Mg/m³)	1.48	1.53	1.38	1.44
Absorption coefficient (mm⁻¹)	0.811	0.606	0.462	0.507
F(000)	1119.8	1047.8	2019.6	585.9
θ range for data collection (deg)	2.9-26.0	1.8-26.9	2.46-25.48	2.0-27.0
Index ranges	$-14 \leq h \leq 14$	$-11 \leq h \leq 11$	$-11 \leq h \leq 11$	$-12 \leq h \leq 12$
	$-17 \leq k \leq 18$	$-14 \leq k \leq 13$	$-31 \leq k \leq 34$	$-13 \leq k \leq 13$
	$-18 \leq \ell \leq 13$	$-27 \leq \ell \leq 28$	$-19 \leq \ell \leq 20$	$-17 \leq \ell \leq 14$
Reflections measured	18264	17809	24775	16281
Independent reflections	9611	4786	8520	5238
Observed reflections [$I>2\sigma(I)$]	5734	4132	7531	4323
Data/Restraints/parameters	9611/0/651	4786/0/317	8520/3/621	5238/0/359
Goodness of fit on F^2	0.862	1.066	1.052	1.031
Observed R, $_wR^2$	0.049, 0.106	0.057, 0.138	0.037, 0.101	0.045, 0.125
R_{int}	0.048	0.035	0.022	0.026

Table 3.2: *Selected bond lengths [Å] and bond angles [°] for **1**, **2** and **4***

	1	**2**	**4**
V-O1	1.621(3)	1.759(3)	1.582(2)
V-O2	1.638(4)	1.809(2)	1.984(2)
V-N1	2.308(2)	2.334(3)	2.350(3)
V-N2	2.032(2)	2.078(2)	2.080(2)
V-N4	2.384(2)	2.330(2)	2.146(2)
V-N5	2.092(2)	2.090(3)	2.115(2)
N5-C18	1.330(2)	1.335(4)	1.315(3)
N3-C6	1.327(2)	1.342(4)	1.342(3)
N2-C6	1.369(5)	1.336(4)	1.321(4)
N6-C18	1.342(6)	1.342(4)	1.324(3)
S-O2	-	-	1.515(2)
S-O3	-	-	1.449(3)
S-O4	-	-	1.461(2)
S-O5	-	-	1.473(2)
O1-V-N1	164.65(1)	165.1(1)	170.1(1)
N5-V-N2	149.30(1)	151.20(1)	159.22(9)
N4-V-O2	163.15(1)	161.80(1)	157.25(9)
N4-V-N5	72.36(9)	73.31(9)	77.07(9)
N2-V-N1	73.91(9)	73.04(9)	73.20(8)
O1-V-N4	89.12(1)	85.04(9)	97.9(1)
O1-V-O2	105.6(1)	108.10(1)	102.4(1)

Table 3.3: *Selected bond lengths [Å] and bond angles [°] for 3*

	3
V1-O1	1.606(1)
V1-O2	1.683(2)
V2-O2	1.958(2)
V2-O3	1.601(1)
V2-O4	1.977(2)
V2-O5	2.006(2)
V2-N9	2.090(2)
V2-N7	2.372(2)
V1-N6	2.031(2)
V1-N4	2.341(2)
V1-N1	2.284(2)
V1-N3	2.051(2)
C6-N2	1.324(3)
C6-N3	1.355(3)
C18-N5	1.335(3)
C30-N9	1.329(2)
N1-V1-N3	74.26(6)
N4-V1-N6	73.41(6)
O4-V2-O5	86.62(6)
N9-V2-N7	72.28(6)
V1-O2-V2	151.81(9)
O1-V1-N4	165.22(7)
N1-V1-O2	162.71(7)
N3-V1-N6	151.64(7)
O5-V2-O2	163.76(7)
O4-V2-N9	156.47(7)
O3-V2-N7	168.95(7)
O1-V1-O2	105.50(7)
O3-V2-O2	98.60(7)

Table 3.4: *Hydrogen bond lengths and angles for 1·H₂O·CH₃OH*

D-H···A	D-H (Å)	H···A (Å)	D···A (Å)	D-H···A (°)
N6B-H101···O1W	0.99(3)	1.69(3)	2.680(5)	175(3)
O3W-H6W···O2B	0.95(2)	1.88(2)	2.819(3)	171(2)
O3W-H5W···N3B	0.98(4)	1.83(4)	2.814(4)	174(4)
N6A-H102···O1A	0.90(2)	2.05(3)	2.793(3)	140(3)
O2W-H3W···O2A	0.95(1)	1.99(1)	2.923(3)	166(3)
O4W-H7W ···O2A	1.02(1)	1.83(1)	2.847(3)	175(1)
O4W-H8W···N3A	1.04(1)	1.73(1)	2.758(4)	169(1)
O1W-H2W···O1S	0.73(6)	2.24(6)	2.925(6)	158(6)
O2S-H2S···O4W	0.84(1)	2.22(1)	2.897(4)	138(1)
O1W-H1W···O2W	0.98(3)	1.72(2)	2.702(4)	171(1)
O2W-H4W···O3W	0.77(5)	1.98(5)	2.742(4)	169(1)

Table 3.5: *Hydrogen bond lengths and angles for 2*

D-H···A	D-H (Å)	H···A (Å)	D···A (Å)	D-H···A (°)
N3-H3···Cl1	1.00(7)	2.310(7)	3.038(3)	151(5)
N6-H6···Cl1	0.830(4)	2.300(4)	3.112(2)	166(4)

Table 3.6: *Hydrogen bond lengths and angles for 3·(CH₃CH₂OH)₃*

D-H···A	D-H (Å)	H···A (Å)	D···A (Å)	D-H···A (°)
O1S-H1S···O3S	0.81(3)	1.89(3)	2.680(3)	163(3)
O3S-H3S···N5	0.89(4)	1.88(4)	2.751(3)	168(4)
N8-H8···O1S	0.81(3)	1.94(3)	2.757(3)	178(3)
O2S-H2S···N2	0.84(1)	2.08(1)	2.824(3)	148.1(1)

Table 3.7: *Hydrogen bond lengths and angles for 4.H₂O*

D-H···A	D-H (Å)	H···A (Å)	D···A (Å)	D-H···A (°)
NB6-HB6···O3	0.74(5)	2.01(5)	2.749(5)	174(4)
O1S-H2S···O4	0.89(3)	2.08(2)	2.903(3)	154(3)
O1S-H1S ···O5	0.89(3)	2.22(3)	2.991(3)	145(4)

Chapter 4

Oxidovanadium(IV/V) Compounds with 2-Substituted Phenylheterocyclic Chelators

4.1   Introduction

Vanadium compounds have been a focus of research in medicinal inorganic chemistry due to their optimal hypoglycemic activity in the potential treatment of Type II diabetes. To enable targeted uptake as well as secretion of vanadium-containing formulations, fine tuning of the solubility as well as hydrophilicity of the compounds under investigation is necessary. In addition, this class of metallo-pharmaceuticals requires biologically relevant ligand systems that should provide the stability and the ability to promote absorption across cell-membrane transportation [1].

A plausible option for chelators is the utilization of heterocyclic ligands including benz(imidazole/oxazole/othiazole) moieties which have shown an array of biological activities, such as anti-microbial [2], anti-oxidant [3] and anti-helminthic activities [4]. It has been reported that substitution at the positions 1, 2 and 5 of the benzimidazole ring has significant influence on their pharmacological activity. For example, Mebendazole [methyl-(5-benzoyl-1*H*-benzimidazol-2-*yl*)carbamate] is a 2,5-substituted benzimidazole which is an anti-helminthic drug and is marketed as Vermox [5]. In addition, derivatized benzimidazoles have also been commercially used as proton pump inhibitors for the reduction of gastric acid [6].

In this Chapter, the isolation of oxidovanadium(IV) compounds with 2-substituted phenylheterocyclic chelators are reported. The 1:2 molar reaction between NH_4VO_3 and 2-hydroxyphenyl-1*H*-benzothiazole (Hobs) led to the formation of a polynuclear vanadium(IV) complex, $[VO(obs)_2]_n$ (**1**). The atmospheric oxygen-induced oxidation reaction of VCl_3 and

2-hydroxyphenyl-1*H*-benzoxazole (Hobo) afforded a similar oxidovanadium compound, [VO(obo)$_2$]$_n$ (**2**). A diamagnetic dioxidovanadium(V) complex, *cis*-[VO$_2$(obz)py] (**3**) (Hobz = 2-hydroxyphenyl-1*H*-benzimidazole) was isolated from the reaction between NH$_4$VO$_3$ and Hobz in a methanolic solution. The resulting yellow precipitate was then dissolved in a 70% pyridine and 30% THF solution. In an effort to synthesize a coordination compound of vanadium containing the heterocyclic ligand, 2-mercaptophenyl-1*H*-benzimidazole (Hsbz), an unexpected reaction product, [C$_{26}$H$_{20}$N$_4$S$_2$].[SO$_4$]·4H$_2$O (**4**) was isolated.

4.2   Experimental

4.2.1   *[VO(obs)$_2$]$_n$ (1)*

A solution of 0.100 g of NH$_4$VO$_3$ (85.50 µmol) in 5 cm^3 of ultrapure water was added to 0.389 g of Hobz (171 µmol) in 20 cm^3 of pyridine, and the mixture was refluxed for 6 hours. Afterwards, precipitation of an orange compound was induced by adding ethanol dropwise. The precipitate was then filtered and dried under vacuum. The precipitate was then dissolved in a pyridine:thf (7:3, *v:v*) mixture and the resultant mixture was layered with ethanol. From the slow diffusion of ethanol into the solvent mixture, orange needles grew which were suitable for XRD analysis. Yield = 89 %, m.p. = 212.7 – 214.6 °C. IR (v_{max}/cm^{-1}): v(C=N) 1601 (s); v(V=O) 910 (vs). UV-Vis (DMF, (λ_{max} (ε, M^{-1}cm^{-1}))): 291 (1682); 301 (1538); 334 (2074). Emission (DMF): 466 nm. Conductivity (DMF, 10^{-3} M): 14.53 ohm^{-1}cm^{-2}mol^{-1}.

4.2.2   *[VO(obo)$_2$]$_n$ (2)*

A mixture of VCl$_3$ (0.100 g, 63.57 µmol) and Hobo (0.269 g, 127.14 µmol) in ethanol (20 cm^3) was heated under reflux for 6 hours. A brown precipitate was filtered, dried under vacuum and then dissolved in pyridine. From the slow evaporation of the aforementioned solution, brown, cubic crystals were grown. Yield = 95 %, m.p. 282.6 – 283.5 °C. IR (v_{max}/cm^{-1}): v(C=N) 1615 (s); v(V=O) 899 (s). UV-Vis (DMF, (λ_{max} (ε, M^{-1}cm^{-1}))): 273 (2862); 284 (3264); 288 (3252); 296 (4165); 323 (3984); 336 (3538). Emission (DMF): 376 nm. Conductivity (DMF, 10^{-3} M): 17.93 ohm^{-1}cm^{-2}mol^{-1}.

4.2.3 Cis-[VO₂(obz)py] (3)

To a mass of 0.1 g of NH_4VO_3 (85.50 μmol) in 10 cm³ of ultrapure water was added 0.389 g of Hobz in 10 cm³ of methanol which was heated under reflux for 8 hours. The solution was allowed to cool to room temperature and a yellow precipitate was filtered by gravity. This precipitate was dissolved in a pyridine:thf (7:3, *v:v*) mixture and the resultant mixture was layered with ethanol. Yellow needles were isolated from the slow diffusion of ethanol into the solvent mixture. Yield = 87 %, m.p. = 126.6 – 127.5 °C. IR (v_{max}/cm⁻¹): v(N-H) 3070 (w); v(C=N) 1626 (m); v(V=O₂) 951, 871 (w). ¹H NMR (δ, ppm) 13.53 (s, 1H, *NH*); 8.57 (d, 2H, *H14, H18*); 8.08 (d, 1H, *H9*); 7.78 (t, 1H, H*11*); 7.56 (d, 1H, *H12*); 7.32 - 7.49 (m, 5H, *H2, H5, H10, H15, H17*); 7.05 (t, 2H, *H3, H4*); 6.92 (t, 1H, *H16*). ⁵¹V NMR (δ, ppm) -520.7. UV-Vis (DMF, (λ_{max} (ε, M⁻¹cm⁻¹))): 293 (2563); 303 (2649); 323 (sh, 2113); 336 (2748); 361 (sh, 1884). Emission (DMF): 469 nm. Conductivity (DMF, 10⁻³ M): 18.94 ohm⁻¹cm⁻²mol⁻¹.

4.2.4 [C₂₆H₂₀N₄S₂].[SO₄] ·4H₂O (4)

The reaction conducted was aimed at synthesizing a vanadium based coordination compound and the title compound was unintentionally obtained upon reacting Hsbz (277.69 mg, 122 μmol) with vanadyl sulfate (100 mg, 61.35 μmol) in refluxing 20 cm³ methanol/water (*v/v* = 1:1). Crystals were obtained upon free evaporation of the solvent, yield = 65 %, m.p. = 255 – 256.7 °C. IR (v_{max}/cm⁻¹): v(N-H) 3373, 3185 (s); v(C=N) 1627 (s).¹H NMR (δ, ppm) 7.96 – 7.91 (m, 2H, *H12, H33*); 7.83 – 7.77 (m, 2H, *H16, H36*); 7.77 – 7.71 (m, 4H, *H14, H15, H34, H35*); 7.55 – 7.46 (m, 4H, *H23, H26, H45, H46*); 7.46 – 7.39 (m, 4H, *H24, H25, H43, H44*); 5.12 (br, s, 4H, *N1H, N2H, N3H, N4H*).
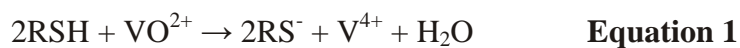
4.2.5 X-ray diffraction

The X-ray data for compounds **1**, **2**, **3** and **4**.3H₂O were recorded on a Bruker Apex Duo equipped with an Oxford Instruments Cryojet operating at 100(2) K and an Incoatec microsource operating at 30 W power. Crystal and structure refinement data are given in **Table 4.1**. Selected bond lengths and angles are given in **Tables 4.2** and **4.3**. In all three cases the data were collected with Mo Kα (λ = 0.71073 Å) radiation at a crystal-to-detector distance of 50 mm. The following conditions were used for data collection: omega and phi scans with exposures taken at 30 W X-ray power and 0.50º frame widths using APEX2 [**7**]. The data were reduced with the programme SAINT [**7**] using outlier rejection, scan speed scaling, as well as standard Lorentz and polarization correction factors. A SADABS semi-

empirical multi-scan absorption correction [7] was applied to the data. Direct methods, SHELXS-97 [8] and WinGX [9] were used to solve all four structures. All non-hydrogen atoms were located in the difference density map and refined anisotropically with SHELXL-97 [8]. All hydrogen atoms were included as idealized contributors in the least squares process. Their positions were calculated using a standard riding model with C-H$_{aromatic}$ distances of 0.93 Å and U_{iso} = 1.2 Ueq. The imidazole N-H atom was located in the difference density map, and refined isotropically. The carbon-bound H atoms of compound **4** were placed in calculated positions with d(C—H) = 0.95 Å and were included in the refinement in the riding model approximation, with U(H) set to 1.2 U_{eq}. The nitrogen-bound H atoms were located from a difference Fourier map and refined freely. The H atoms of the solvent water were located from a difference Fourier map as well and refined using DFIX instructions.

4.3   Results and Discussion

4.3.1   *Synthesis and spectral characterization*

All the coordination reactions were conducted in a 1:2 molar ratio of the metal and the free heterocyclic ligands, which resulted in the formation of the metal complexes in good yields while compound **4** could only be attained at a moderate yield of 65%. The chelating moieties act as monoanionic bidentate chelators (*i.e.* obs, obo or obz) through the deprotonated phenolic oxygens and neutral heterocyclic nitrogens. The 2:1 molar reaction between NH$_4$VO$_3$ and 2-hydroxyphenylbenzothiazole (Hobs) led to the formation of a polynuclear vanadium(IV) compound, [VO(obs)$_2$]$_n$ (**1**). The formation of complex **2** is promoted by the atmospheric oxygen oxidation of the metal precursor, VCl$_3$. Interestingly, complex **2** could also be attained from NH$_4$VO$_3$ and as previously reported, using VO(acac)$_2$ [10]. However, reacting the benzimidazole analogue (*i.e.* Hobz) with NH$_4$VO$_3$ afforded a yellow precipitate which was dissolved in a 70% pyridine and 30% THF solution resulting in   the dioxidovanadium(V) complex, [VO$_2$(obz)py], (**3**). In an effort to synthesize a coordination compound of vanadium by applying the Hsbz heterocyclic ligand featuring a thiol group, the unexpected reaction product **4** was isolated. A mechanism has been proposed for the oxidation of thiophenolates (RSH) to disulfides (RSSR), which is initiated by removal of the oxygen from the vanadyl ion (VO^{2+}) (see **Equation 1**). The resultant reactive V^{4+} cation oxidized the thiophenolates (RSH) to afford the sulfur-bridged specie (RSSR) (see **Equation 2**) [11].

$$2RSH + VO^{2+} \rightarrow 2RS^- + V^{4+} + H_2O \qquad \textbf{Equation 1}$$

$$2V^{4+} + 2RS^- \rightarrow 2V^{3+} + RSSR \qquad \textbf{Equation 2}$$

Complex **1** exhibits partial solubility in pyridine and upon heating in DMSO and DMF, whereas complexes **2** and **3** are only soluble in DMF and DMSO. The molar conductivity values of the metal complexes are typical of neutral vanadium(IV/V) complexes [**12**]. The overlay IR spectra of the metal complexes show the common v(C=N) [1601 cm^{-1} for complex **1**, 1615 cm^{-1} for complex **2** and 1626 cm^{-1} for complex **3**] (see **Figure 4.1**), and the absence of the phenolic stretching frequencies which were originally found in the respective free ligands' IR spectra (*e.g.* 3240 cm^{-1} for Hobz). Similarly, for the dimerized organic compound **4**, the heterocyclic C=N bonds vibrate at 1627 cm^{-1} while the absence of the thiol group of the Hsbz starting material is noted. Another distinctive feature of complex **3** is the weak intensity band for the benzimidazolium N-H vibrating at 3070 cm^{-1}. In addition, the v(V=O$_2$) stretches appears as two weak bands at 951 and 871 cm^{-1}. For the mono-oxo metal cores of complexes **1** and **2**, these bonds vibrate as intense bands at 910 and 899 cm^{-1}, respectively. All these metal-based vibrations were comparable to other di/oxidovanadium(IV/V) complexes found in the literature [**13**, **14**, **15**].
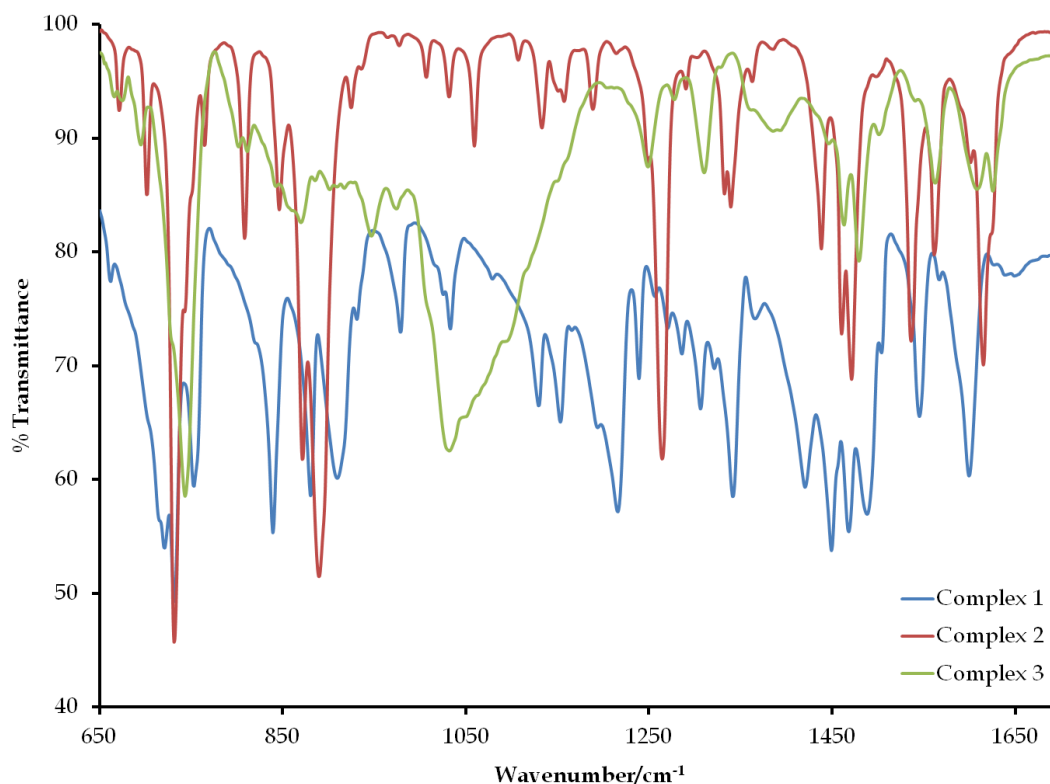

Figure 4.1: *Overlay IR spectra of the complexes 1, 2 and 3.*

The presence of the paramagnetic vanadium(IV) metal centers (*i.e.* in complexes **1** and **2**) were confirmed *via* room temperature X-band ESR spectroscopy. A characteristic eight-line isotropic signal was observed in the ESR spectrum of complex **2** in DMF while, due to the poor solubility of complex **1**, a singlet was attained upon analysis of the single crystals (see **Figure 4.2**). All the experimental g-values (g_1 = 1.97028 and g_2 = 2.00138) were close to the value of a free electron (*i.e.* g_e = 2.0023) which implies that all the electron transitions are metal based. In addition, the g-values and hyperfine coupling constant (95.238 G) of complex **2** were similar to other oxidovanadium species in solution (see **Figure 4.3**) [16, 17]. The well resolved signals in the ^{1}H NMR spectrum of complex **3** is reminiscent of diamagnetism; the benzimidazolium proton occurs as a sharp singlet integrating to one proton which is found downfield at 13.53 ppm (see **Figure 4.4**). In the aromatic region, signals for the pyridyl and obz moieties appear as a doublet, doublet, triplet, doublet, multiplet and two triplets. A broad singlet is found in the ^{51}V NMR spectrum of complex **3** which appears at -520.7 ppm for the d^0-vanadium centre (see **Figure 4.4**). In the ^{1}H NMR spectrum of compound **4**, nearly identical aromatic peaks are observed as the free-ligand Hsbz; except that the aromatic peaks integrates to double the number of protons in comparison to the proton spectrum of Hsbz. In addition, the singlets of the benzimidazolium protons coalesce into a broad singlet at 5.12 ppm (see **Figure 4.5**).
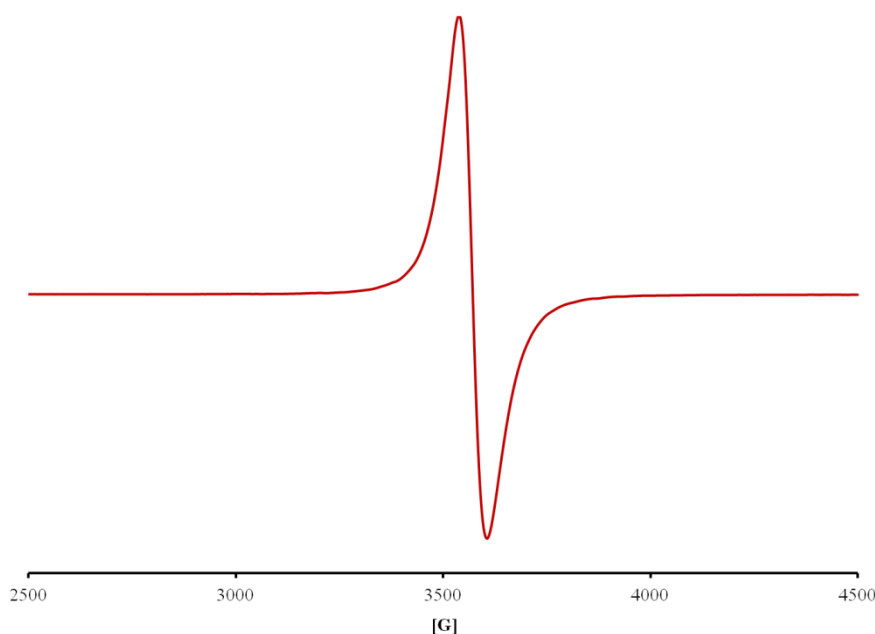

Figure 4.2: *Solid state X-band ESR spectrum of complex **1** at 298 K. Instrument settings: microwave bridge frequency, 9.8 GHz; microwave bridge attenuator, 20 dB; modulation frequency, 100 kHz; modulation amplitude, 5 G; centre field, 3500 G.*
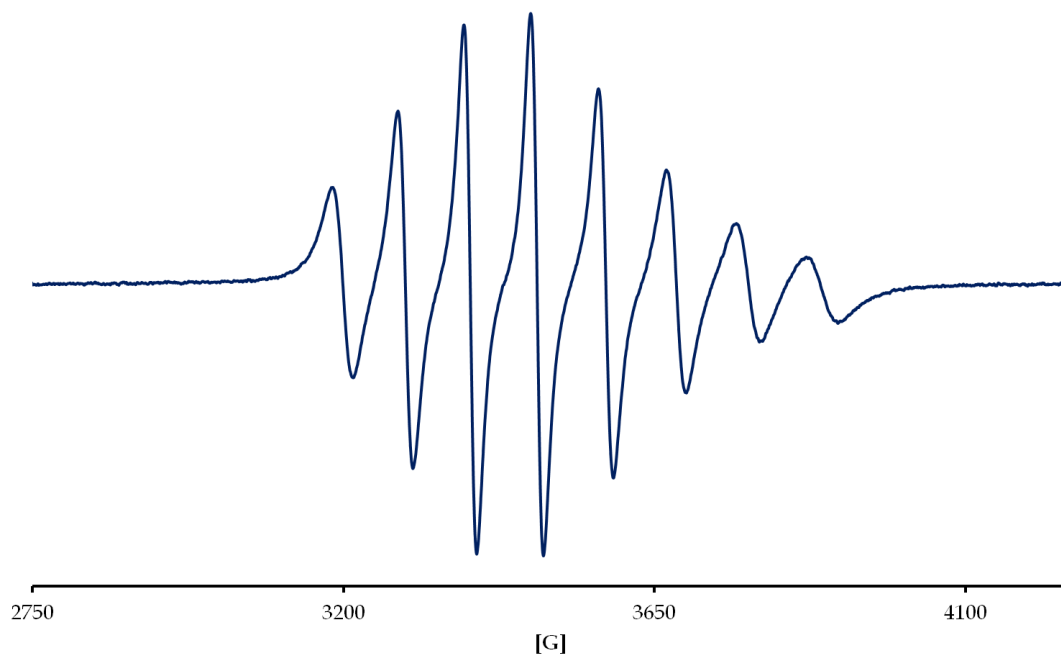
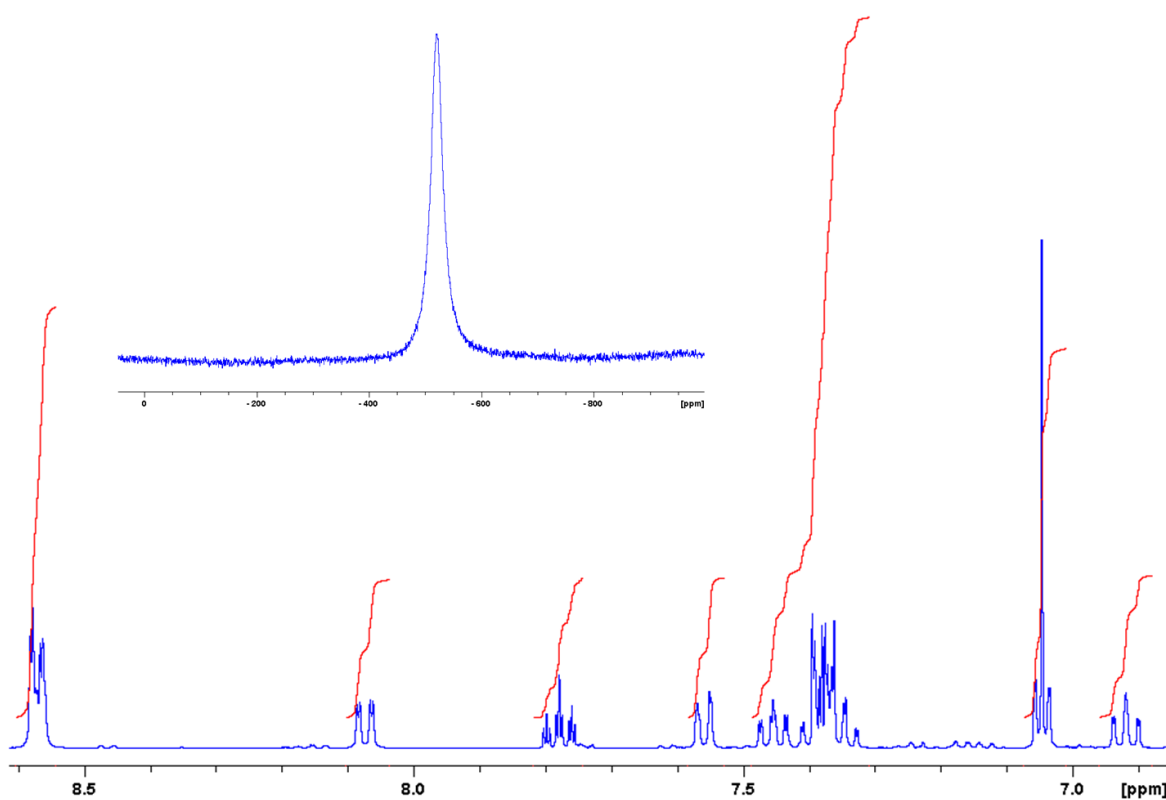**Figure 4.3**: *X-band ESR spectrum of complex **2** at 298 K.*

Figure 4.4: *^{1}H NMR spectrum of complex **3**, showing the aromatic protons of the pyridyl co-ligand and obz chelator. **Inset:** The signal at -520.7 ppm in the ^{51}V NMR confirms the presence of the vanadium(V) metal center.*
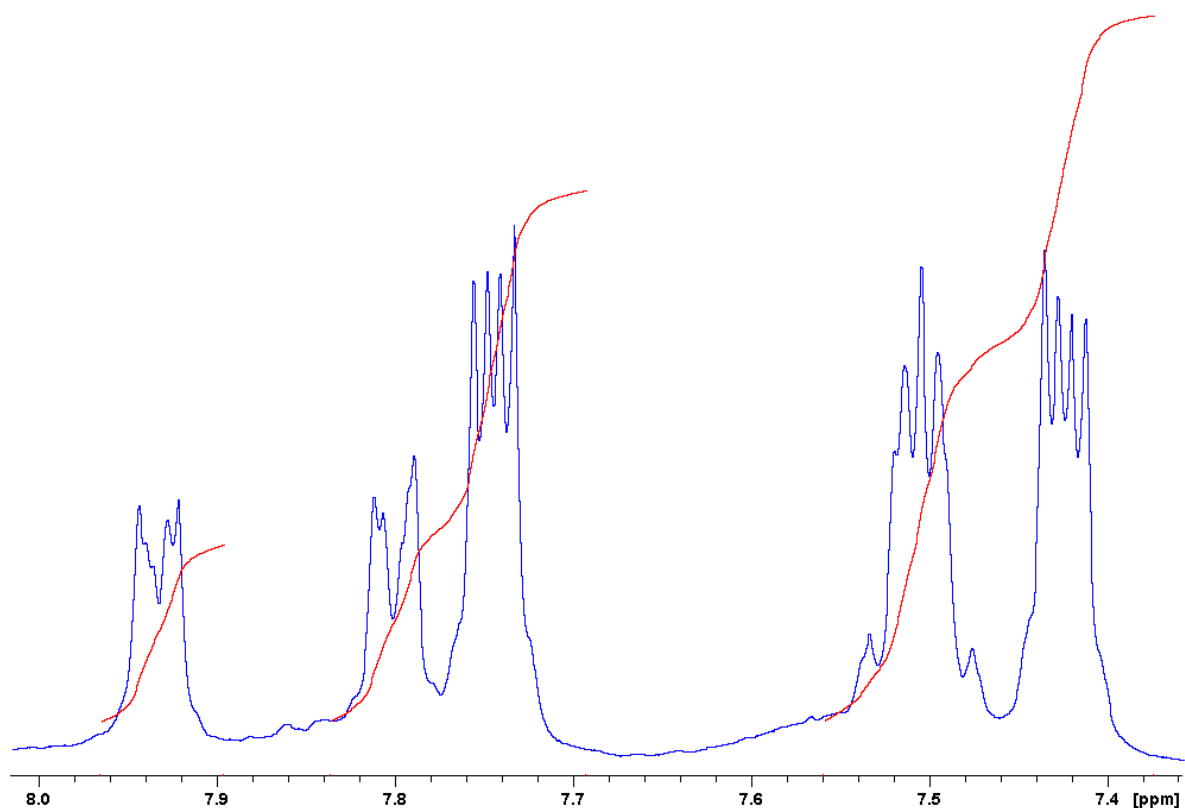
Figure 4.5: *^{1}H NMR of complex **3** between 7.36 – 8.02 ppm.*

The UV-Vis spectra of the metal compounds (see **Figure 4.6 - 4.8**) in DMF are dominated by intense intra-ligand (π-π*) electronic transitions which were similar to those found in the electronic spectra of the corresponding free ligands (refer to **Figure 2.5** in Chapter 2). Similar to all the vanadium complexes in Chapter 3, no ligand-to-metal charge transfer and *d-d* transitions for the d^1 systems (*i.e.* complexes **1** and **2**) and for the d^0 system (*i.e.* complex **3**) could be observed. The corresponding intra-ligand (π-π*) relaxations [466 nm for complex **1**, 376 nm for complex **2** and 469 nm for complex **3**] could be observed in the emission spectra which were obtained in anhydrous DMF. The peak labeled **A** in the emission spectrum of complex **3** occurred as a result of not having a filter near the excitation wavelength to eliminate the replicating effect of the emission spectrometer.
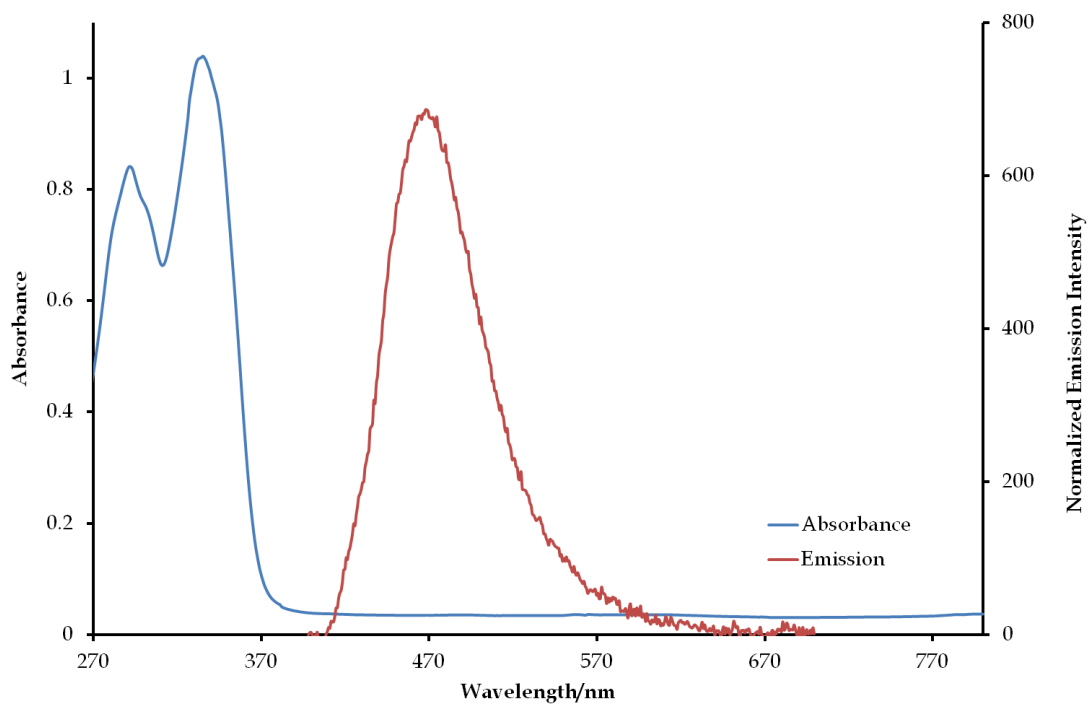
Figure 4.6: *Overlay absorbance and emission spectra of complex **1**. The excitation wavelength was 388 nm.*
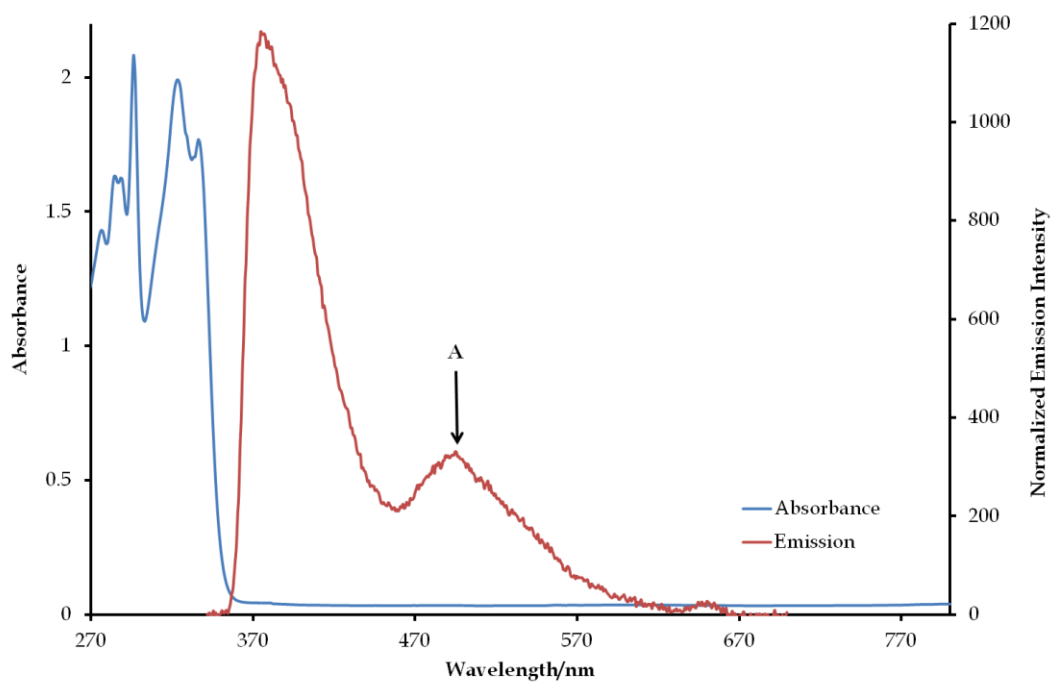

Figure 4.7: *Overlay absorbance and emission spectra of complex **2**. The excitation wavelength was 322 nm. Peak **A** results from instrumental limitations.*
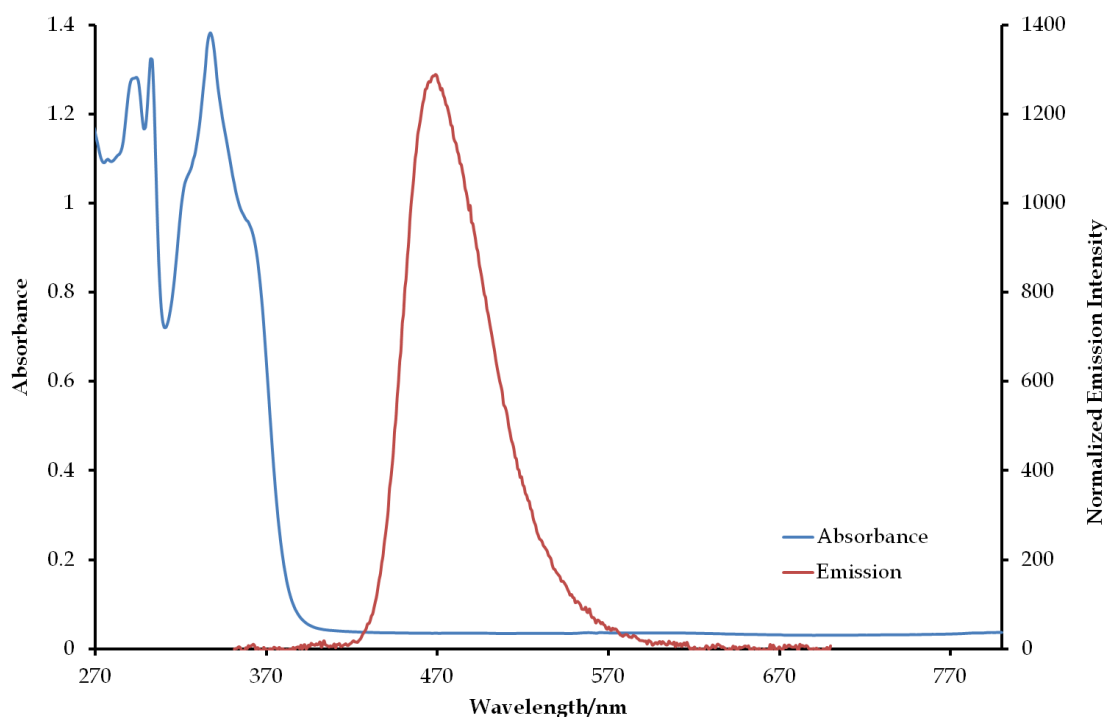
Figure 4.8: *Overlay absorbance and emission spectra of complex **3**. The excitation wavelength was 336 nm.*

4.3.2   Structures of complexes 1 and 2

In compounds **1** and **2**, the vanadium atom is at the centre of an octahedron which is surrounded by two chelators within the equatorial plane and the $[VO]^{2+}$ core occuping one axial position while the remaining axial position is occupied by the $V \cdots O_x$ [3.393(3) Å for complex **1** and 2.257(2) Å for complex **2**] interactions. These axial interactions allow the molecules of **1** and **2** to stack in polymeric columns parallel to the [*b*]-axis (see **Figure 4.9**). Furthermore, the monoclinic unit cells of the complexes have the same number of molecules (*i.e.* Z = 6 for complexes **1** and **2**) with each complex having identical three-dimensional arrangements of their molecules (see **Figure 4.10**).
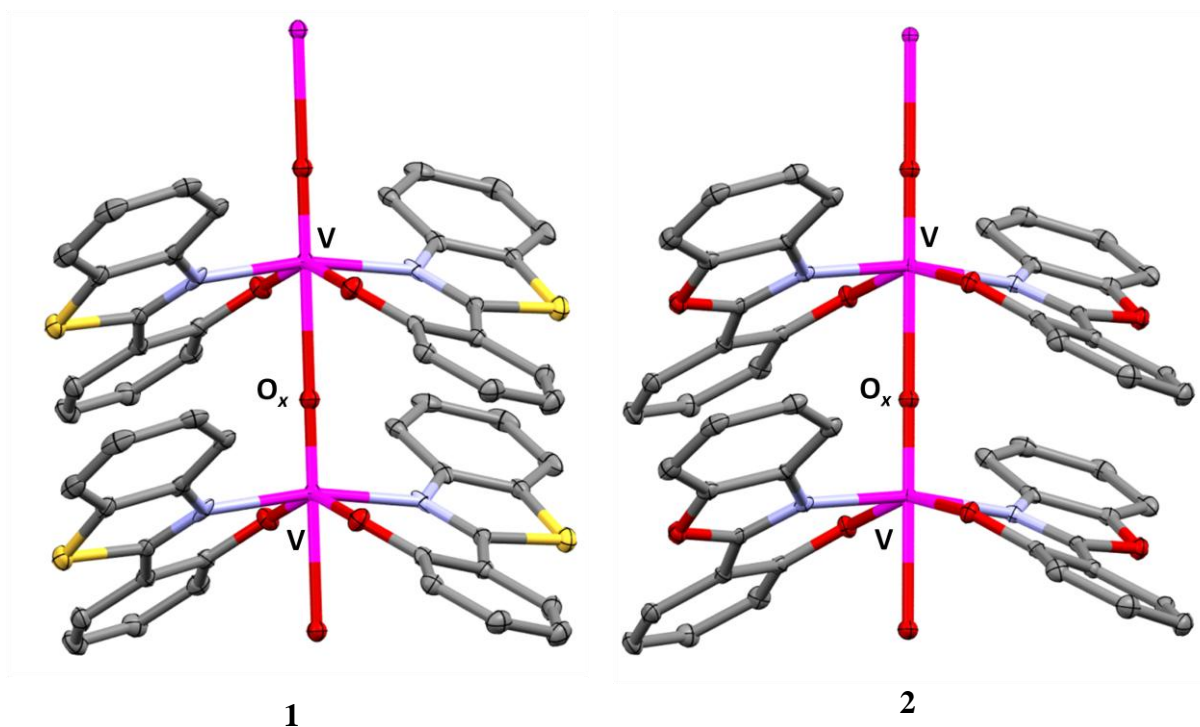
Figure 4.9: *Perspective views of complexes **1** and **2**, illustrating the co-planar obs/obo chelators, as well as the $V_n \cdots O_x$ linkages for the respective molecules.*

The structures are highly distorted due to the influence of the constrained bite angles [O-V-N = 87.6(1)° for complex **1** and 87.07(6)° for complex **2**] in the individual structures which affords large deviations from the idealized 90° for the angles: O1-V-O2/O3 [103.8(1)°] and O1-V-N1/N2 [96.3(1)°] for complex **1** and O1-V-O2/O4 [101.81(7)°] and O1-V-N1/N2 [95.99(7)°] for complex **2** (see **Figures 4.11 and 4.12**). Another contributive factor to the distortion, is the influence of the π-π stacking between the chelators of respective molecules where the interplanar spacings for complexes **1** and **2** are 4.018 Å and 3.881 Å, respectively. In turn, this forces the chelators of the two complexes to have different arrangements as given by the dihedral angles of 63.23° (for complex **1**) and 55.30° (for complex **2**).
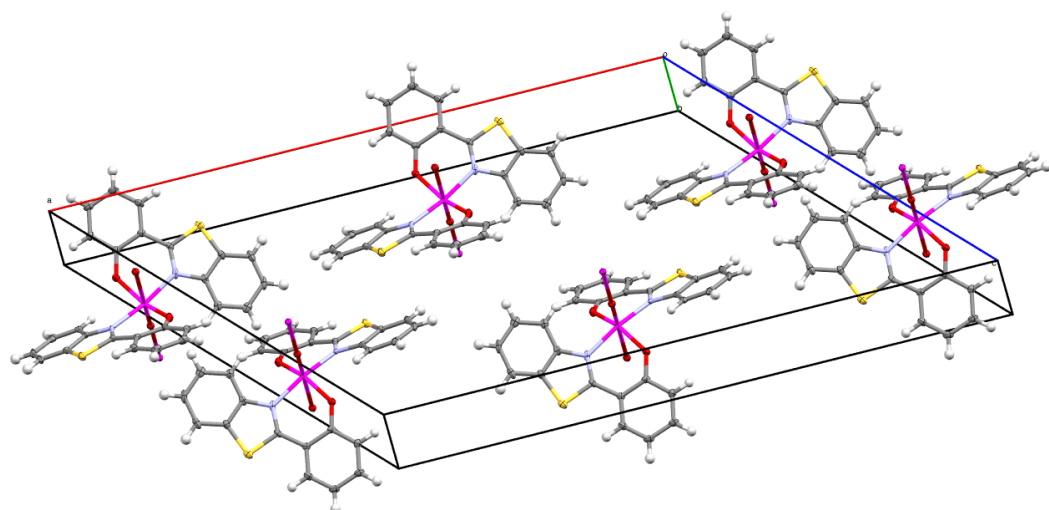
1
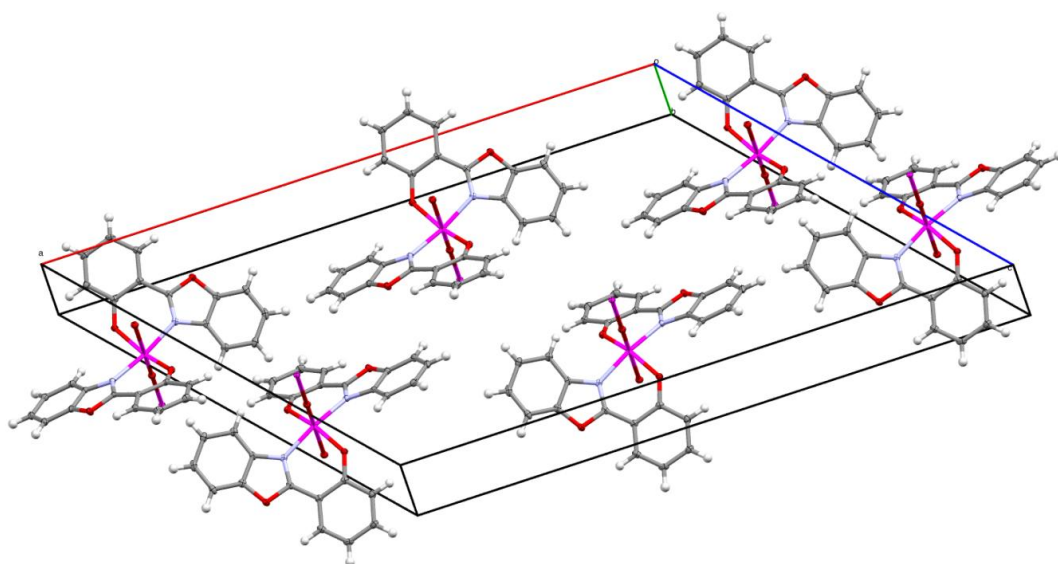
2

Figure 4.10: *The monoclinic unit cells of complexes 1 and 2.*

The ideal axial bond angles [O1-V-O$_x$ = 180°] for complexes **1** and **2** affords inversion of symmetries which is emphasized by the opposing bond distances within the equatorial plane being the same in the individual structures: V-O$_{phenolic}$ [1.923(3) Å for complex **1** and 1.945(2) Å for complex **2**] and V-N [2.087(3) Å for complex **1** and 2.077(1) Å for complex **2**]. The characteristic short and nearly equidistant V-O1 [1.625(3) Å for complex **1** and 1.625(2) Å for complex **2**] bond distances is similar to those found in other oxidovanadium(IV) complexes, *e.g.* the polynuclear oxovanadium(IV) complex [VOL$_2$]$_n$ (L =

(5-bromo-2-hydroxybenzyl-2-furylmethyl)imine) with a V=O bond distance of 1.6247(19) Å [18]. In contrast, the analogous V·····O_x bond of this complex is considerably shorter than found in complexes **1** and **2**. Within the heterocyclic moieties, the bond orders of the C-N bonds are readily distinguishable based on their distances [N1-C1/N2-C14 = 1.408(6) Å for complex **1** and 1.404(3) Å for complex **2**, N1-C7/N2-C20 = 1.355(6) Å for complex **1** and 1.310(2) Å for complex **2**]. In contrast to the C-N bond distance, the C-X (where X = S or O) single bonds [C7-S1/C20-S2 = 1.738(4) Å for complex **1** and C7-O3/C20-O5 = 1.336(2) Å for **2**, C6-S1/C19-S2 = 1.725(4) Å for complex **1** and C6-O3/C19-O5 = 1.387(3) Å for complex **2**] are nearly equidistant.

Interest in polynuclear oxidovanadium complexes largely arises from the potential in developing new functional molecular-based ferromagnetic materials [19, 20]. In particular, vanadium(IV) complexes with *bis*-imines derived from salicylaldehyde have been known to form metal complexes containing the [V=O·····V=O]$_n$ backbone [21, 22]. The general structure includes the tetradentate N_2O_2 chelators occupying the basal plane while the monomeric fragments link through V$_n$·····O_x interactions, similar to those found in complexes **1** and **2**. For example, a study originally conducted by Drake *et.al.* on the temperature-dependance of the magnetic susceptibility of [VO(salph)]$_n$ (H$_2$salph = *N, N'*-disalicylidenepropylenediamine) has sparked wide-spread curiosity in the isolation of new derivatives of this complex [23]. This alteration of the original metal complex includes attaching electron-withdrawing groups on the phenyl substituents to investigate the influence of the stereoelectronic changes on the magnetic properties [24, 25].
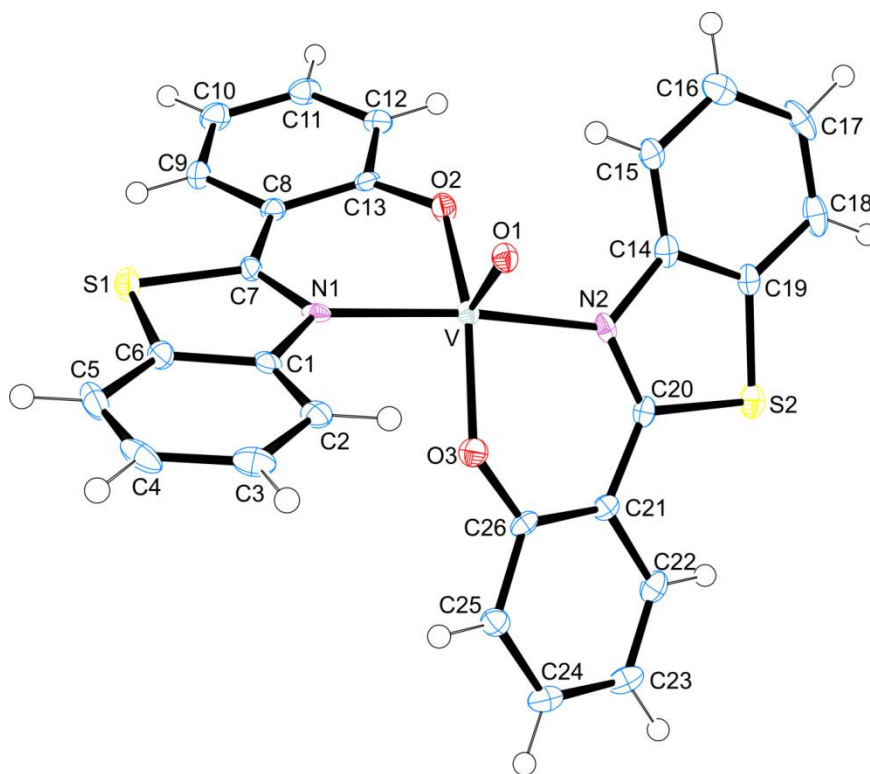
Figure 4.11: *An ORTEP view of the monomeric fragment of complex **1** showing 50 %
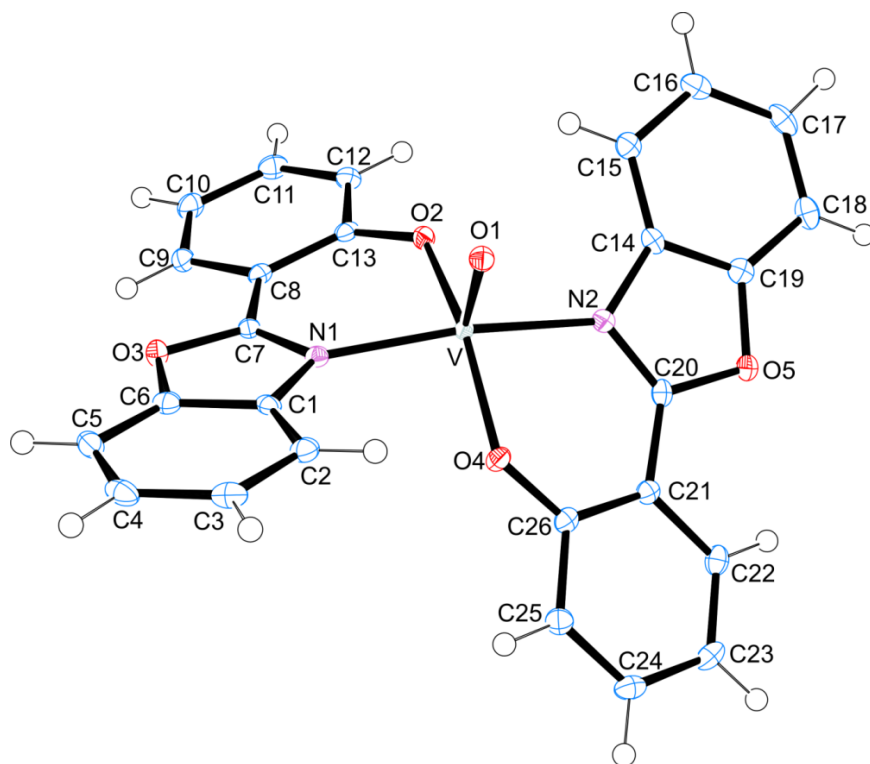probability displacement ellipsoids and the atom labelling.*

Figure 4.12: *An ORTEP view of the monomeric fragment of complex **2** showing 50 %
probability displacement ellipsoids and the atom labelling.*

4.3.3 Structure of complex 3

Complex **3** crystallizes in a P2$_1$/c space group with four crystallographic identical molecules occupying the monoclinic unit cell. The crystal packing is influenced by classical hydrogen bonding [N2-H2A·····O1 = 1.96(3) Å] as well as accompanying intermolecular π-π stacking between pyridyl moieties of adjacent molecules, with interplanar spacing of 4.141 Å (see **Figure 4.13**). The effects of cyclometallation are clearly evident from the distortion of the bond angles compared to the ideal square pyramidal values. The constrained N1-V-O3 [84.15(8)°] bite angle forces the N1-V-N3 [166.02(8)°], O3-V-O1 [126.12(9)°] and [O3-V-O2 = 123.88(9)°] bond angles to be narrower than the idealized 180° (see **Figure 4.14**).
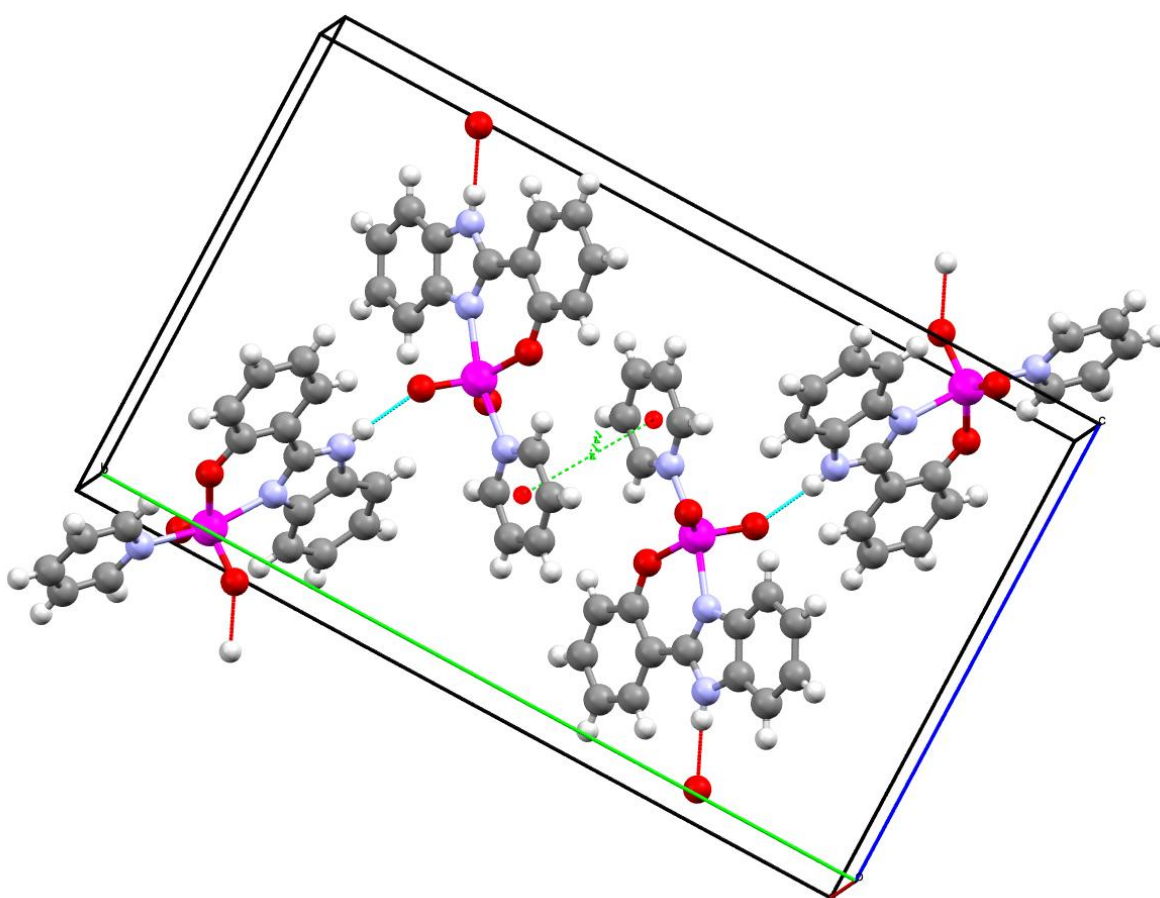

Figure 4.13: *The monoclinic unit cell of complex **3**, showing the classical hydrogen-bonding in blue and the π-π intermolecular interactions between the co-planar pyridyl moieties, shown in green.*
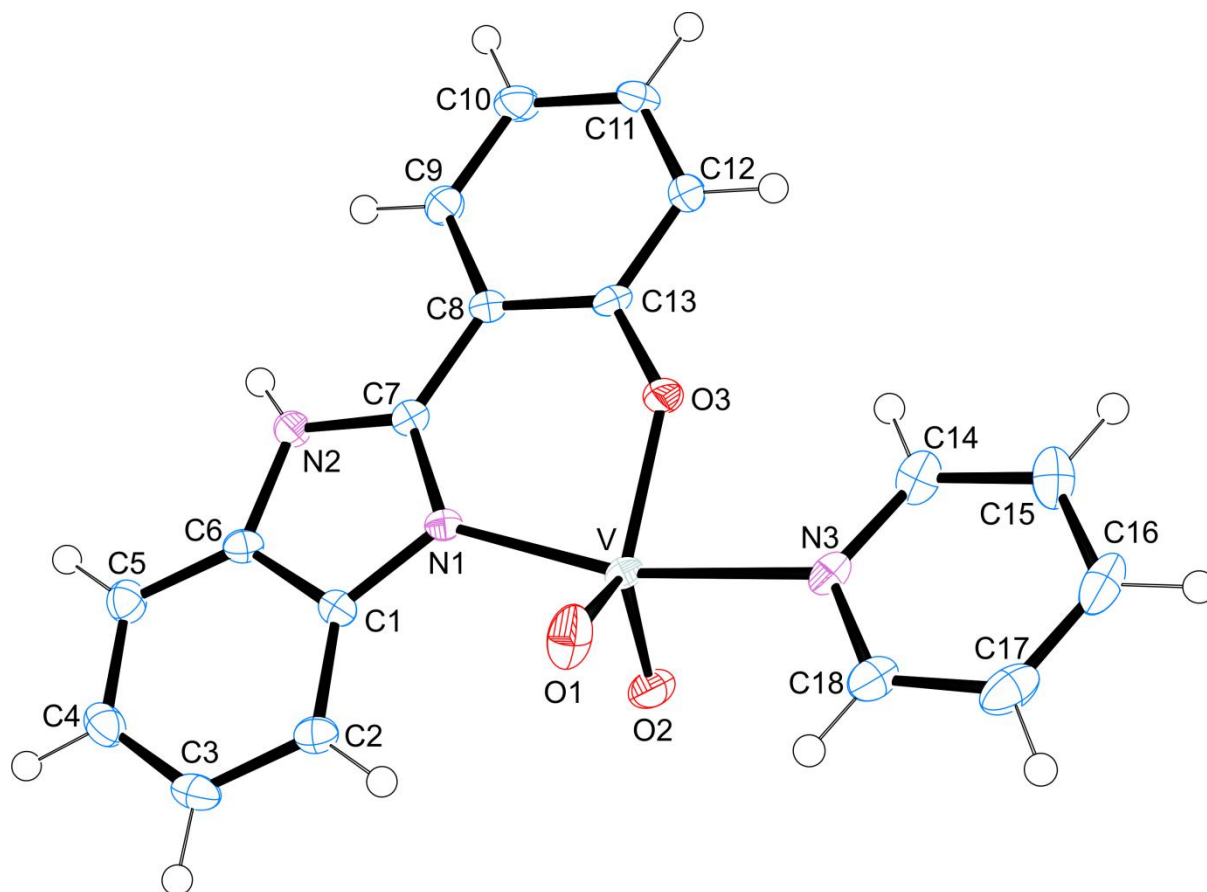
Figure 4.14: *An ORTEP view of complex **3** showing 50 % probability displacement ellipsoids and the atom labelling.*

Evaluating the coordination sphere bonds, the V-O1 [1.625(2) Å] and V-O2 [1.635(2) Å] are different but both are comparable to that found in the mononuclear vanadium(V) complex, *cis*-[VO$_2$(salhyhp)] where salhyhp was isolated from 5-hydroxy-pentane acid hydrazide and salicylaldehyde (1.625(3) Å and 1.647(3) Å), respectively [**26**]. The lower acidic character of the vanadium(V) centre in complex **3** results in shorter V-O3 [1.892(2) Å] and V-N1 [2.068(2) Å] bonds compared to the V-O$_{phenolic}$ [1.923(1) Å for complex **1** and 1.945(1) Å for complex **2**] and V-N [2.087(3) Å for complex **1** and 2.077(1) Å for complex **2**] bond distances of the vanadium(IV) complexes. The V-N3 bond length of 2.191(2) Å is shorter than the V-N$_{pyridyl}$ bond distance found in a similar dioxidovanadium(V) complex, *cis*-[VO$_2$(ads)] (Hads = 2-acetylpyridine-*N,N*-dimethylselenosemicarbazone) due to the difference in *trans*-effect experienced by the pyridyl nitrogens [**27**].

The vast majority of vanadium complexes have N, O-donor ligands due to the preference of the vanadium metal center for this combination of hard and soft donor atoms [28]. An example is the reactions of the bidentate ligands, 2-(2'-hydroxyphenyl)-1R-imidazoline {R = hydrogen, ethyl or ethanol} with VOSO$_4$ whereby a series of five coordinate oxidovanadium complexes formed with a '2+2' coordinate mode of two monoanionic N, O-donor chelators [29].

4.3.4 *Structure of 4*

Compound **4** is a dimer of Hsbs with a S-S bridge which co-crystallize along with three water molecule and one sulfate molecule of crytallization (see **Figure 4.15**). The bond length d(S—S) = 2.0511(6) Å, as well as both angles C$_{ar}$–S–S = 100.77(6)° and 100.99(5)°, (see **Figure 4.15**) respectively, are in good agreement with corresponding values in comparable compounds whose data has been deposited with the Cambridge Structural Database [30]. The least-squares planes defined by the aromatic systems in both halves of the molecule intersect at angles of 50.28(4)° and 44.92(4)° respectively. The planes defined by the atoms of both benzimidazole moieties enclose an angle of 65.20(3)° while the corresponding angle for the planes defined by phenyl moieties was found at only 28.86(3)°.

In the crystal structure, hydrogen bonds between all NH groups as well as all water molecules are present. For two of the NH groups, one O atom of the sulfate anion serves as a two-fold acceptor while the remaining two NH groups apply the oxygen atom of one water molecule each as acceptor. The protons of the water molecules form hydrogen bonds to other water molecules as well as O atoms of the sulfate anion. One of the water molecules span two of the sulfate ion's O atoms. The descriptor for the hydrogen bonding system in terms of graph-set analysis [31] is D on the unitary level. In total, the components of the crystal structure are connected to a three-dimensional network. The closest intercentroid distance between two p-systems was found at 3.4592(9) Å and is apparent between the five-membered part of a benzimidazole moiety and the six-membered part of its symmetry-generated equivalent.
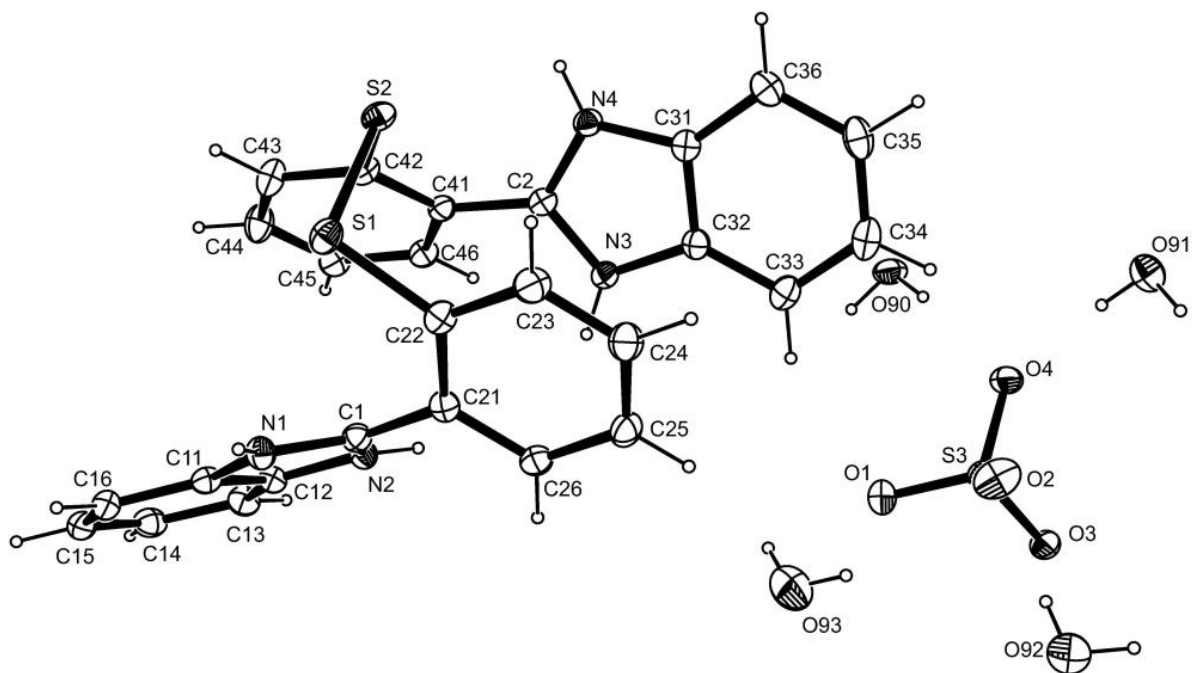
Figure 4.15: *An ORTEP view of **4**.3H₂O showing 50 % probability displacement ellipsoids and the atom labelling.*

4.4   References:

1. Willsky G.R., Chi L., Godzala M., Kostyniak P.J., Smee J.J., Trujillo A.M., Alfano J.A., Ding W., Hu Z., Crans D.C., *Coord. Chem. Rev.,* 2011, **255**, 2258.

2. Bondock S., Fadaly W., Metwally M.A., *Eur. J. Med. Chem.*, 2010, **45**, 3692.

3. Zhou B., Li B., Yi W., Bu X., Ma L., *Bioorg. Med. Chem. Lett.*, 2013, **23**, 3759.

4. Satyendra R.V., Vishnumurthy K.A., Vagdevi H.M., Rajesh K.P., Manjunatha H., Shruthi A., *Eur. J. Med. Chem.*, 2011, **46**, 3078.

5. Dayan A.D., *Acta Trop.*, 2003, **86**, 141.

6. Jain K.S., Shah A.K., Bariwal J., Shelke S.M., Kale A.P., Jagtap J.R., Bhosale A.V., *Bioorg. Med. Chem.*, 2007, **15**, 1181.

7. Bruker APEX2, *SAINT and SADABS*. Bruker AXS Inc. (2010) Madison, Wisconsin, USA.

8. Sheldrick G.M., *Acta Cryst.,* 2008, **A64**, 112.

9. Farrugia L.J., *J. Appl. Cryst.,* 2012, **45**, 849.

10. Back D.F., de Oliveira G.M., Ballin M.A., Corbellini V.A., *Inorg. Chim. Acta*, 2010, **363**, 807.

11. Rehder D., *Inorg. Chim. Acta*, 2003, **6**, 604.

12. Thaker B.T., Barvalia R.S., *Spectrochim. Acta A, 2013, **112**, 101.*

13. Kwiatkowski E., Romanowski G., Nowicki W., Kwiatkowski M., Suwinska K., *Polyhedron*, 2003, **22**, 1009.

14. Romanowski G., Wera M., *Polyhedron*, 2010, **29**, 2747.

15. Kurt Y., İlhan-Ceylan B., Acıkgoz M., Tuzun E., Atun G., Ulkuseven B., *Polyhedron*, 2013, **65**, 67.

16. da Maia P.I., Pavan F.R., Leite C.Q.F., Lemos S.S., de Sousa G.F., Batista A.A., Nascimento O.R., Ellena J., Castellano E.E., Niquet E., Deflon V.M., *Polyhedron*, 2009, **28**, 398.

17. Nejo A.A., Kolawole G.A., Opoku A.R., Wolowska J., O'Brien P., *Inorg. Chim. Acta*, 2009, **362**, 3993.

18. Grivani G., Delkhosh S., Fejfarová K., Dušek M.L., Khalaji A.D., *Inorg. Chem. Comm.*, 2013, **27**, 82.

19. Miller J.S., Epstein A.J., *Angew. Chem. Int. Ed. Engl.*, 1994, **33**, 385.

20. Matsuoka N., Tsuchimoto M., Yoshioka N., *J. Phys. Chem. B*, 2011, **115**, 8465.

21. Kasahara R., Tsuchimoto M., Ohba S., Nakajima K., Ishida H., Kojima M., *Inorg. Chem.*, 1996, **35**, 7661.

22. Fujiwara K., Ishida T., *Polyhedron,* 2011, **30**, 3073.

23. Drake R.F., Crawford V.H., Hatfield W.E., Simpson G.D., Carlisle G.O., *J. Inorg. Nucl. Chem.*, 1975, **37**, 291.

24. Pasini A., Gulloti M., *J. Coord. Chem.*, 1974, **3**, 319.

25. Tsuchimoto M., Yoshioka N., *Chem. Phys. Lett.*, 1998, **297**, 115.

26. Pohlmann A., Nica S., Luong T.K.K., Plass W., *Inorg. Chem. Comm.*, 2005, **8**, 289.

27. Sarkar A., Pal S., *Polyhedron*, 2006, **25**, 1689.

28. Maurya M.R., *Coord. Chem. Rev.*, 2003, **237**, 163.

29. Walmsley R.S., Tshentu Z.R., Fernandes M.A., Frost C.L., *Inorg. Chim. Acta*, 2010, **363**, 2215.

30. Allen F.H., *Acta Crystallogr.*, 2002, **B58,** 380.

31. Bernstein J., Davis R.E., Shimoni L., Chang N.L., *Angew. Chem. Int. Ed. Engl.*, 1995, **34,** 1555.

32. Etter M.C., MacDonald J.C., Bernstein J., *Acta Crystallogr.,* 1990, **B46,** 256.

Table 4.1: *Crystal and structure refinement data*

	1	2	3	4.3H$_2$O
Chemical formula	VS$_2$O$_3$N$_2$H$_{16}$C$_{26}$ *	VO$_5$N$_3$H$_{14}$C$_{18}$ *	VO$_3$N$_3$H$_{14}$C$_{18}$	C$_{26}$H$_{28}$N$_4$O$_8$S$_3$
Formula weight	519.49 *	487.36 *	371.26	620.72
Temperature(K)	296	296	100(2)	100(2)
Crystal system	Monoclinic	Monoclinic	Monoclinic	Monoclinic
Space group	C12/c1	C12/c1	P2$_1$/c1	P12$_1$/c1
Unit cell dimensions (Å, °)	$a = 29.5602(24)$	$a = 29.1740(2)$	$a = 5.9681(9)$	$a = 14.8050(3)$
	$b = 4.0181(4)$	$b = 3.8812(3)$	$b = 23.035(4)$	$b = 15.1570(4)$
	$c = 21.5536(17)$	$c = 21.6008(16)$	$c = 13.914(3)$	$c = 12.3130(3)$
	$\alpha = 90$	$\alpha = 90$	$\alpha = 90$	$\alpha = 90$
	$\beta = 127.454(3)$	$\beta = 90.970(2)$	$\beta = 90.970(2)$	$\beta = 90.206(1)$
	$\gamma = 90$	$\gamma = 90$	$\gamma = 90$	$\gamma = 90$
V(Å^3)	2032.27(59)	1975.00(36)	1910.3(5)	2736.0
Z	6	6	4	4
Density (calc.) (Mg/m^3)	1.70	1.649	1.291	-
Absorption coefficient (mm^{-1})	0.730	0.549	0.539	3.26
F(000)	1059.8	995.8	760	-
Crystal size (mm)	0.60 x 0.06 x 0.03	0.30 x 0.10 x 0.10	0.18 x 0.03 x 0.02	0.256 x 0.441 x 0.536
θ range for data collection (deg)	1.7-26.2	1.7-26.8	1.77-26.0	-
Index ranges	$-36 \leq h \leq 36$ $-2 \leq k < 4$ $-27 \leq \ell \leq 25$	$-36 \leq h \leq 36$ $-2 \leq k < 4$ $-27 \leq \ell \leq 25$	$-3 \leq h \leq 7$ $-28 \leq k < 27$ $-17 \leq \ell \leq 17$	-
Reflections measured	6870	8148	13889	48123
Observed reflections [$I>2\sigma(I)$]	1656	1962	3160	6892
Independent reflections	1947	2079	3740	6306
Data/Restraints/parameters	1947/0/155	2079/0/155	3740/0/231	6306/0/407
Goodness of fit on F^2	1.242	1.057	1.043	-
Observed R, wR^2	0.0532, 0.1620	0.0305, 0.0785	0.0510, 0.1134	0.037; 0.102
R_{int}	0.031	0.019	0.031	-

- = not available,   * = for a mononuclear fragment

Table 4.2: *Selected bond lengths [Å] and bond angles [°] for **1** and **2***

	1	2
V-O1	1.625(3)	1.652(2)
V-O2	1.923(3)	1.945(2)
V-O3	1.923(3)	-
V-O4	-	1.945(2)
V-N1	2.087(3)	2.077(1)
V-N2	2.087(3)	2.077(1)
N1-C7	1.335(4)	1.310(2)
N1-C1	1.408(6)	1.404(3)
N2-C20	1.355(4)	1.310(2)
N2-C14	1.408(6)	1.404(3)
S1-C7	1.738(4)	-
S1-C6	1.725(4)	-
S2-C19	1.725(4)	-
S2-C20	1.738(4)	-
C8-C7	1.452(6)	1.439(3)
C21-C20	1.452(6)	1.439(3)
O1-V-O2	103.8(1)	101.81(7)
O1-V-O4	-	101.81(7)
O1-V-N1	96.3(1)	95.99(7)
O1-V-O3	103.8(1)	-
O1-V-N2	96.3(1)	95.99(7)
O2-V-N1	87.6(1)	87.07(6)
O3-V-N2	87.6(1)	-
O4-V-N2	-	87.07(6)
O3-C7	-	1.366(2)
O3-C6	-	1.387(3)
O5-C19	-	1.387(3)
O5-C20	-	1.366(2)

Table 4.3: *Selected bond lengths [Å] and bond angles [°] for 3*

V-O1	1.625(2)
V-O2	1.635(2)
V-O3	1.892(2)
V-N1	2.068(2)
V-N3	2.191(2)
N1-C1	1.403(8)
N1-C7	1.341(3)
N2-C7	1.357(3)
N2-C6	1.385(3)
N1-V-O3	84.15(8)
O1-V-O2	109.7(1)
N1-V-N3	166.02(8)
O3-V-O1	126.12(9)
O2-V-O3	123.88(9)

Chapter 5

Attempted Synthesis of a Dioxidovanadium(V) complex bearing a Uracil Schiff base chelate: Intraligand Cyclization

5.1   Introduction

Molecular transformations using ammonium metavanadate (NH_4VO_3) has been widely explored [1, 2]. The most common transformation is the formation of α-hydroxy/aminophosphonates which are essential building blocks for many pharmaceutical agents [3, 4]. Recent developments in the isolation of these compounds include the use of solvent-free synthesis at room temperature to form products having higher conversion yields than other oxidants in organic media [5].

Similarly, a study involving the isolation of 2-substituted benzimidazole derivatives from 2-aryl aldehydes and 1,2-diaminobenzimidazole using NH_4VO_3 as a catalyst, have reported minimal formation of Schiff base side products, compared to other synthetic methodologies [6]. In this Chapter, the metal-induced cyclization of 5-amino-6-[(*Z*)-(2-hydroxybenzylidene)amino]-1,3-dimethylpyrimidine-2,4-(1*H*, 3*H*)-dione (H₃duo) by NH_4VO_3 which resulted in the formation of a cyclized benzimidazole derivative, 8-(2-hydroxyphenyl)-1,3-dimethyl-1*H*-purine-2,6-(3*H*, 7*H*)-dione (**1**) is reported (see **Figure 5.1**).
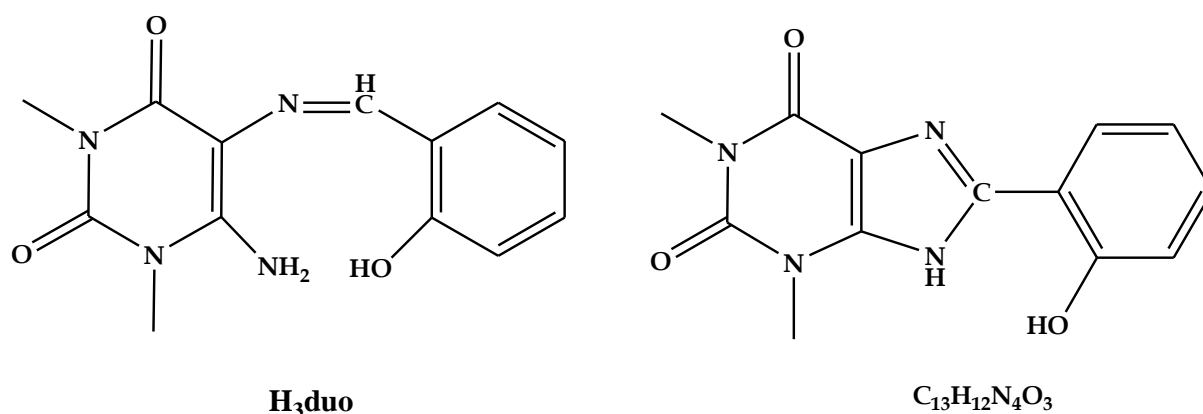

H_3**duo** $C_{13}H_{12}N_4O_3$

Figure 5.1: *Structures of H₃duo and the cyclized benzimidazole derivative, compound **1**.*

5.2 Experimental

5.2.1 5-Amino-6-[(Z)-(2-hydroxybenzylidene)amino]-1,3-dimethylpyrimidine-2,4-(1H, 3H)-dione (H₃duo)

A synthetic procedure was adopted from previously published work of Booysen *et. al.* [**7**]. A mixture of 5,6-diamino-1,3-dimethyl uracil (1.25 g, 7.34 mmol) and salicylaldehyde (1.1 cm^3, 11.0 mmol) in methanol (100 cm^3) was heated under reflux for 3 hours. The resultant orange solution was allowed to cool to room temperature and the yellow precipitate was filtered, yield = 60 %; m.p. 247 – 249 ˚C. IR (v_{max}/cm^{-1}): v(O-H) 3454; v(N-H) 3324; v(C=O) 1691; v(C=N) 1607; v(C=C) 1505. ^{1}H NMR (295K/ppm): 11.26 (br, s, 2H, *NH₂*); 9.78 (s, 1H, *H1*); 7.71 (d, 1H, *H2*); 7.24 (t, 1H, *H3*); 7.11 (br, s, 1H, *OH*); 6.90-6.83 (m, 2H, *H4, H5*); 3.44 (s, 3H, *C8H₃*); 3.17 (s, 3H, *C9H₃*).
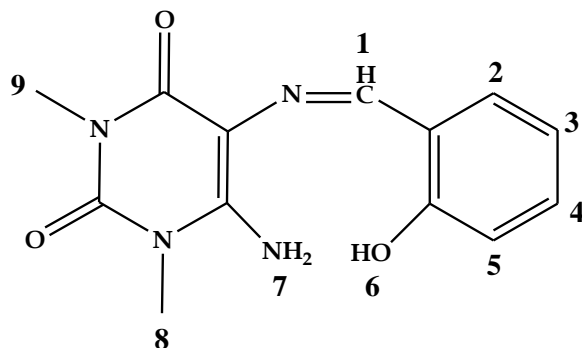

Figure 5.2: *Numbering scheme of H₃duo.*

5.2.2 8-(2-Hydroxyphenyl)-1,3-dimethyl-1H-purine-2,6-(3H, 7H)-dione (1)

The title compound was prepared by reacting H₃duo (234 mg, 85.48 μmol) and NH₄VO₃ (100 mg, 85.48 μmol) in 20 cm^3 methanol. A bright yellow precipitate was filtered, washed with methanol and dried under reduced pressure. Single crystals suitable for the X-ray diffraction study were obtained by recrystallization from an ethanol-dichloromethane (*v:v* = 1:1) mixture

which was left for several days at 5°C, yield = 64 %; m.p. 289.8 - 292.5 °C; IR (ν_{max}/cm^{-1}): ν(O-H) 3460; ν(N-H) 3323; ν(C=O) 1690; ν(C=N) 1609. ^{1}H NMR (295K/ppm): 8.01 (br, s, 1H, *NH*); 7.72 (d, 1H, *H9*); 7.22 (t, 1H, *H10*); 7.13 (br, s, 1H, *OH*); 6.92–6.74 (m, 2H, *H11, H12*); 3.18 (s, 3H, *CH$_3$,*); 3.18 (s, 3H, *CH$_3$*).
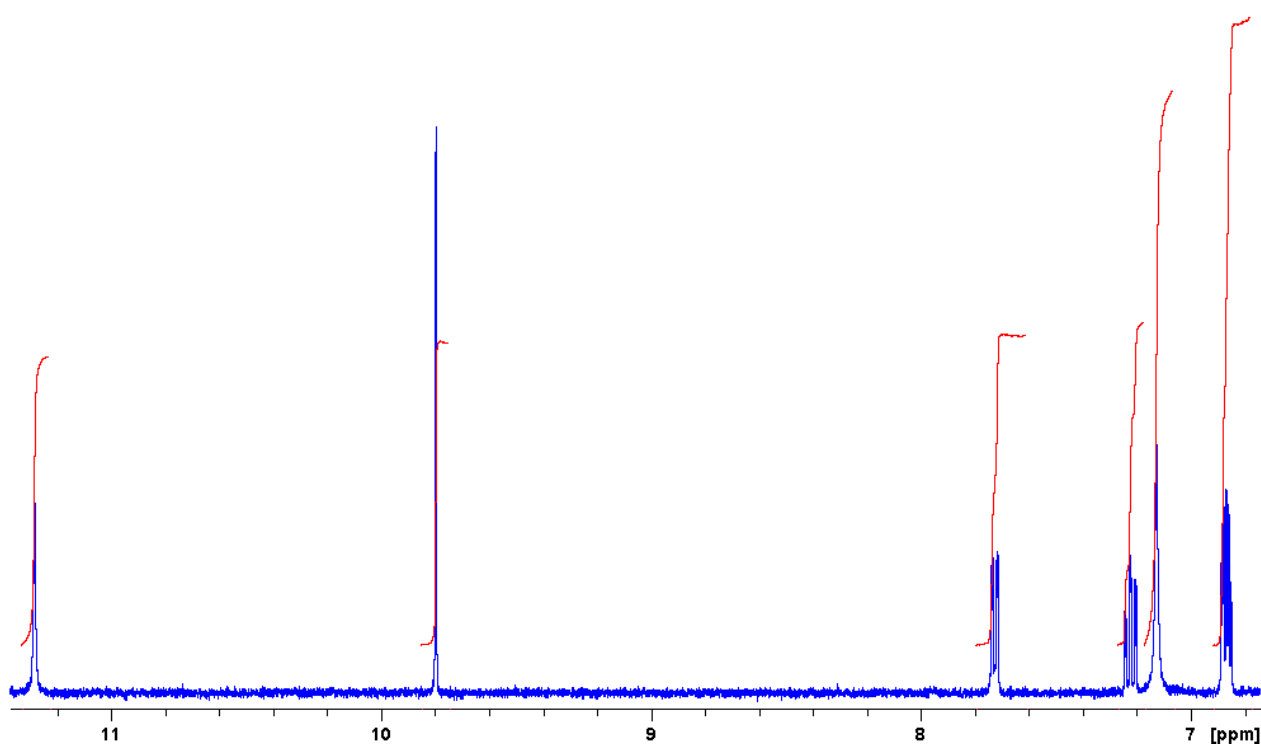

Figure 5.3: *^{1}H NMR spectrum of H$_3$duo in the range of 11.80 - 6.50 ppm.*

5.2.3   X-ray crystallography

The X-ray data was recorded on a Bruker Apex Duo equipped with an Oxford Instruments Cryojet operating at 100(2) K and an Incoatec microsource operating at 30 W power. Crystal and structure refinement data are given in **Table 5.1**. Selected bond lengths and angles are given in **Tables 5.2**. The data were collected with Mo Kα (λ = 0.71073 Å) radiation at a crystal-to-detector distance of 50 mm. Carbon-bound H atoms were placed in calculated positions (C-H 0.95 Å) and were included in the refinement in the riding model approximation, with U(H) set to

1.2U_{eq}(C). The H atoms of the methyl groups were allocated to rotate with a fixed angle around the C-C bond to best fit the experimental density [**8**]. The nitrogen-bound H atom was located on a difference Fourier map and refined freely.

5.3 Results and Discussion

5.3.1 *Synthesis and Spectral Characterization*

The product **1** was synthesized using a 1:1 molar ratio of the metal precursor, NH_4VO_3 and Schiff base ligand, H_3duo in refluxing methanol. The interest in this Schiff base arises from the biological relevance of uracil as a nucleotide base and its derivatives have shown various biological activities [**9**]. Yellow platelets suitable for X-ray analysis were grown from the slow evaporation of a dichloromethane-ethanol solvent mixture. This compound exhibits poor solubility in most organic solvents with the exception of DMF and DMSO. The IR spectra of H_3duo and its cyclized form are nearly identical where only minor shifts of the significant bands are observed (see **Figure 5.4**). For example, the v(C=O) vibrates at nearly identical frequencies [1691 cm^{-1} for H_3duo and 1690 cm^{-1} for **1**]. Another example is the C=N bands which are found at similar positions (1607 cm^{-1} for H_3duo and 1609 cm^{-1} for compound **1**).

The molecular transformation was more evident when comparing the ^{1}H NMR spectra of H_3duo and compound **1** (see **Figure 5.5**). Firstly, the absence of an imino proton was observed in compound **1** whereas in H_3duo this signal was originally observed as a sharp singlet at 9.78 ppm. Secondly, a broad singlet integrating for one proton at 8.01 ppm is assigned to the benzimidazolium proton of compound **1** which replaces the amino group found in the proton spectrum of H_3duo. Thirdly, all the phenolic moiety signals of compound **1** are similar as previously observed in H_3duo's NMR spectrum: the hydroxyl proton appear as broad singlets at 7.11 and 7.13 ppm for H_3duo and **1**, respectively while the aromatic protons appear as a doublet, a triplet and a multiplet integrating to 1, 1 and 2 for both compounds. Metal-induced cyclization of Schiff bases are a common phenomena. For example, upon coordination of the Schiff base ligand 2-(2-aminophenyliminomethyl)-4*H*-chromen-4-one (H_2pch) to the *fac*-[Re^I(CO)$_3$]$^+$ core, intra-ligand cyclization occurred between the amino nitrogen atom and the Schiff base carbon atom to afford a benzimidazole moiety, bzch which led to the isolation of a mononuclear

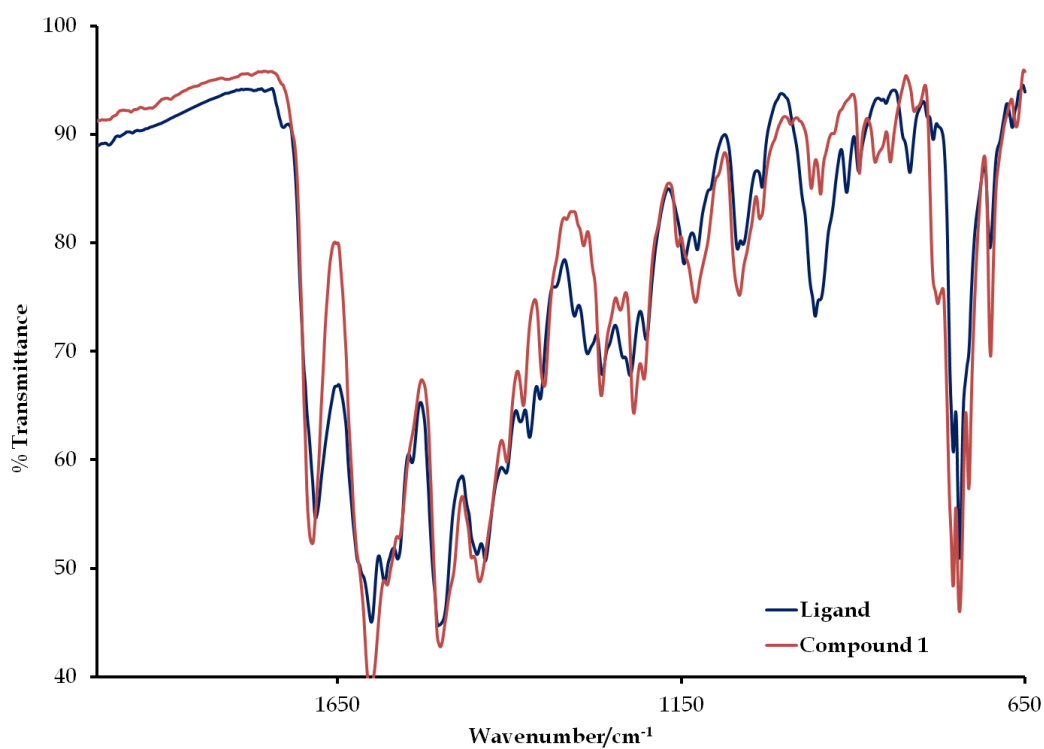rhenium(I) complex, *fac*-[Re(CO)₃(bzch)Cl] (**1**), where bzch = 2-benzimidazole-4*H*-chromen-4-one [**10**].

Figure 5.4: *Overlay IR spectra of the Schiff base ligand, H₃duo and compound **1**.*
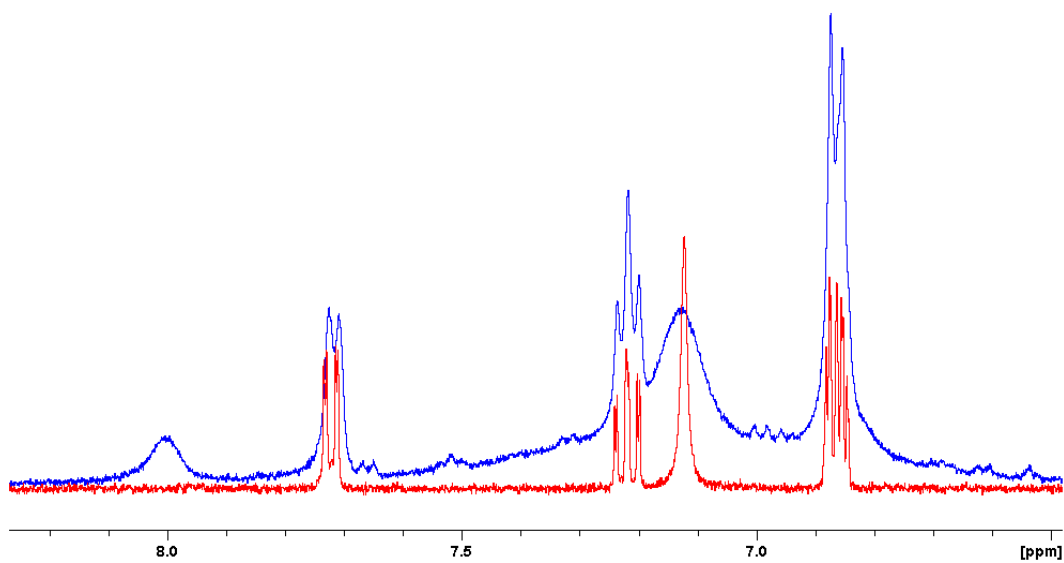

Figure 5.5: *Overlay ¹H NMR spectra of H₃duo (red) and compound **1** (blue).*

5.3.2 Crystal structure of compound 1

The molecule features a benzimidazole-inspired backbone comprised of a 6-amino-1,3-dimethylpyrimidine-2,4-(1*H*, 3*H*)-dione moiety which is annealed to a five-membered aromatic ring. This part of the molecule is essentially planar (r.m.s. of its fitted non-hydrogen atoms = 0.0205 Å). The small puckering amplitude ($t = 1.6°$) of the six-membered heterocyclic preludes a conformational analysis [11]. The least-squares planes defined by the atoms of the phenyl ring on the one hand and the benzimdazole-type ring system on the other hand enclose an angle of 0.45(10)° (see **Figure 5.6**). Both C-N-C angles in the five-membered heterocyclic are similar in value with 106.25(15)° and 104.41(15)°, with the smaller value found on the non-protonated nitrogen atom. However, these angles are smaller in value than the corresponding ones in hopoxanthinium monohydrate (invariably above 108°) where both nitrogen atoms bear a hydrogen atom [12].
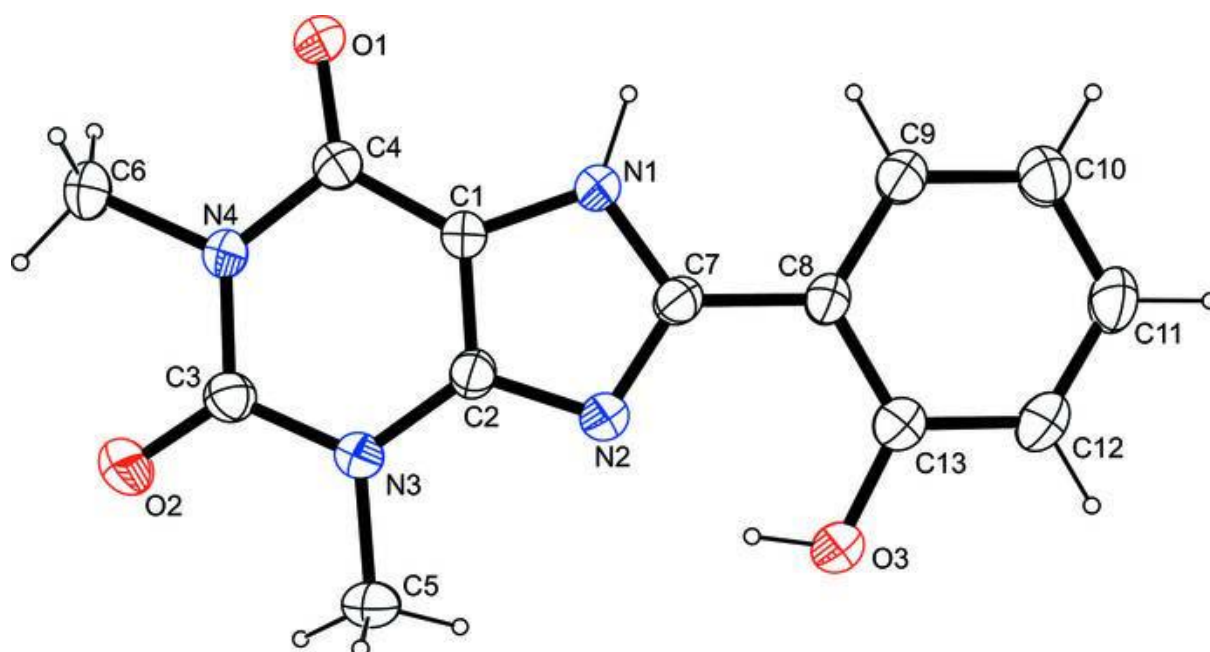

Figure 5.6: *The molecular structure of compound **1** with atom labels and anisotropic displacement ellipsoids (drawn at 50% probability).*

In the crystal structure, intra- as well as intermolecular hydrogen bonds and C-H⋯O contacts whose range falls by more than 0.1 Å below the sum of van-der-Waals radii of atoms

participating are observed. While the intramolecular hydrogen bonds are exclusively made up by the proton of the hydroxyl group as donor and the non-protonated nitrogen atom of the five-membered heterocyclic, intermolecular hydrogen bonds are solely apparent between the amino group and one of the double-bonded oxygen atoms (see **Table 5.3**). The C-H····O contacts can be separated in two groups: while one of the nitrogen-bound methyl groups forms a C-H····O contact involving the oxygen atom of the hydroxyl group, one of the aromatic C-H groups acts as donor for the double-bonded oxygen atom that is already part of the N-H····O type hydrogen bonds. In terms of graph-set analysis, the descriptor of the classical hydrogen bonds is $S(6)R^2_2(10)$ on the unitary level. For the C-H····O contacts, a $R^2_2(16)R^2_2(18)$ descriptor on the same level is needed for description. In total, the molecules are connected to chains [110]. The shortest intercentroid distance between two aromatic systems was measured at 3.7771(11) Å (see **Figure 5.7**). The packing of the compound **1** in the crystal is shown in **Figure 5.8**.
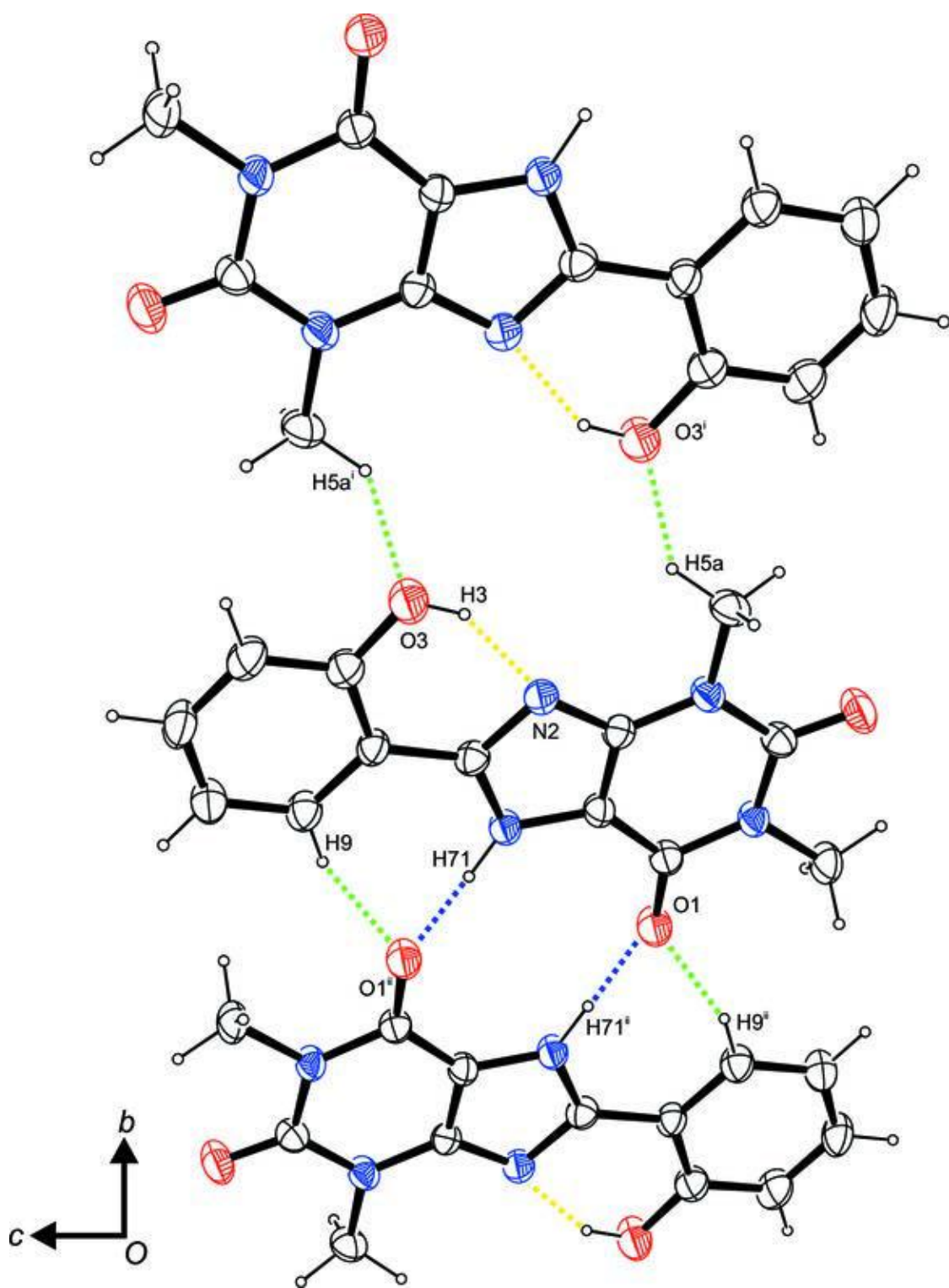
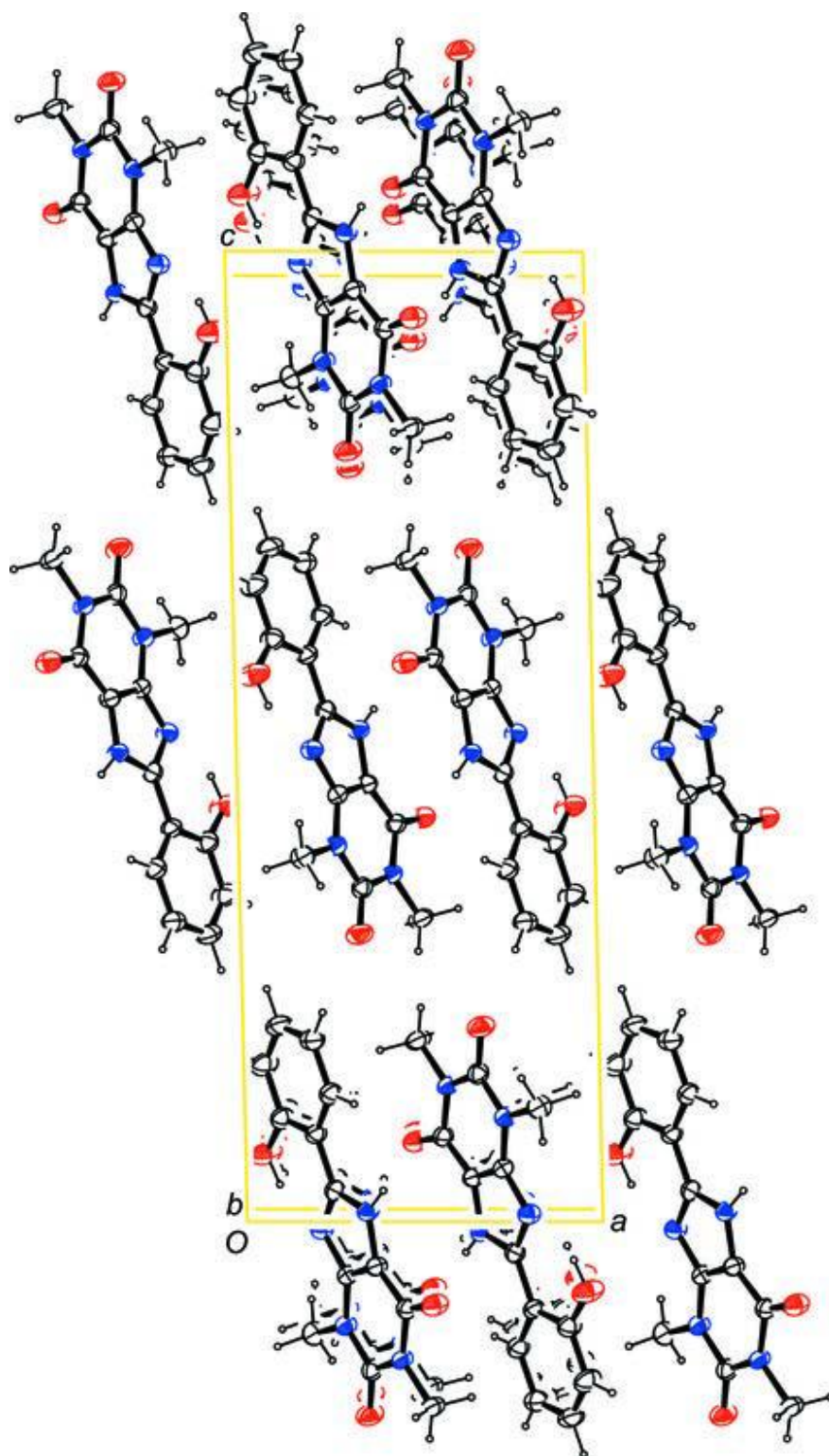**Figure 5.7**: *Intermolecular contacts viewed along [-100].*

Figure 5.8: *Molecular packing diagram of the compound, viewed along [010] (anisotropic displacement ellipsoids.*

89

5.4   References:

1.   Niralwad K.S., Shingate B.B., Shingare M.S., *Tetrahedron Lett.*, 2010, **51**, 3616.

2.   Lloyd L., *Handbook of Industrial Catalysis*, Springer, 2011.

3.   Mandadapu S.R., Gunnam M.R., Kankanamalage A.C.G., Uy R.A.Z., Alliston K.R., Lushington G.H., Kim Y., Chang K., Groutas W.C., *Bioorg. Med. Chem. Lett.*, 2013, **23**, 5941

4.   Szymańska A., Szymczak M., Boryski J., Stawiński J., Kraszewski A., Collu G., Sanna G., Giliberti G., Loddo R., Colla P. L., *Bioorg. Med. Chem.*, 2006, **14**, 1924.

5.   Sadaphal S.A., Kategaonkar A.H., Sapkal S.B., Shingate B.B., Gill C.H., Shingare M.S., *Bull. Cat. Soc. India*, 2009, **8**, 131.

6.   Jadhav G.R., Shaikh M.U., Kale R.P., Gill C.H.*, Chinese Chem. Lett.*, 2009, **20**, 292.

7.   Booysen I.N., Ismail M., Gerber T.I.A., Akerman M., Van Brecht B.J.A.M., *S. Afr. J. Chem.*, 2012, **65**, 174.

8.   Sheldrick G.M., *Acta Cryst*., 2008, A**64**, 112.

9.   Khan G.S., Shah A., Rehman Z., Barker D., *J. Photochem. Photobio. B: Biol*., 2012, **115**, 105.

10. Booysen I.N., Ismail M.B., Munro O.Q., *Inorg. Chem. Commun.*, 2013, **30**, 168.

11. Cremer D., Pople J.A., *J. Am. Chem. Soc*., 1975, **97**, 1354.

12. Schmalle H.W., Hanggi G., Dubler E., *Acta Cryst*., 1990, C**46**, 340.

Table 5.1: *Crystal and structure refinement data*

Chemical formula	$C_{13}H_{12}N_4O_3$
Formula weight	272.27
Temperature (K)	200
Crystal system	Monoclinic
Space group	$P2_1/c$
Unit cell dimensions (Å, °)	$a = 8.6418(5)$
	$b = 5.9415(3)$
	$c = 23.4475(10)$
	$\alpha = 90$
	$\beta = 91.275(2)$
	$\gamma = 90$
Crystal size (mm)	0.41 x 0.10 x 0.05
$V(\text{Å}^3)$	1203.62(11)
Z	4
Density (calc.) (Mg/m^3)	1.502
Absorption coefficient (mm^{-1})	0.11
$F(000)$	568
θ range for data collection (deg)	2.4-27.2
Observed reflections $[I>2\sigma(I)]$	$-11 \leq h \leq 11$ $-7 \leq k < 6$ $-31 \leq \ell \leq 27$
Independent reflections	2975
Data/Restraints/parameters	2975/0/188
Goodness of fit on F^2	1.01
Observed R, wR^2	0.049, 0.124
R_{int}	0.043

Table 5.2: *Selected bond lengths [Å] and bond angles [°]*

O1-C4	1.237(2)
O2-C3	1.213(2)
O3-C13	1.351(2)
N1-C7	1.355(2)
N2-C7	1.346(2)
N2-C2	1.351(2)
N3-C2	1.371(2)
N3-C3	1.382(2)
N3-C5	1.461(2)
N4-C4	1.396(2)
N4-C3	1.402(2)
N4-C6	1.474(2)
C1-C2	1.361(3)
C1-C4	1.410(3)
C13-O3-H3	109.5
C7-N1-C1	106.25(15)
C7-N1-H71	126.1(13)
C1-N1-H71	127.6(13)
C7-N2-C2	104.41(15)
C2-N3-C3	119.72(16)
C2-N3-C5	121.03(15)
C3-N3-C5	119.14(15)
C4-N4-C3	126.42(15)
C4-N4-C6	116.97(15)
C3-N4-C6	116.61(15)
C2-C1-N1	105.66(16)
C2-C1-C4	122.63(17)
N1-C1-C4	131.69(17)
N2-C2-C1	111.80(16)

Table 5.3: *Hydrogen bond lengths[Å] and angles[°].*

D-H⋯A	D-H (Å)	H⋯A (Å)	D⋯A (Å)	D-H⋯A (°)
1 O3-H3•••N2	0.84	1.86	2.611 (2)	148
2 N1-H71•••O1	0.97	1.78	2.746 (2)	175.4 (19)
3 C9-H9•••O1	0.95	2.37	3.294 (2)	164
4 C5-H5A•••O3	0.98	2.58	3.234 (2)	124

Chapter 6

Conclusion and Future work

The main aim of this research project was to design, synthesize and characterize novel di/oxidovanadium complexes with various N-donor heterocyclic ligands. This class of ligands proved to be versatile chelators for stabilizing the central atom in its oxidation states +III, +IV and +V while also conferring unique and rare coordination geometries. As proposed, all the ligands utilized coordinates as monoanionic bidentate chelators with the exception of 2-mercaptophenyl-1*H*-benzimidazole (Hsbz) which dimerized upon reaction with vanadyl sulfate. Furthermore, the formulated paramagnetic vanadium complexes yielded characteristic ESR spectra in solution and in the solid state (for $[VO(obs)_2]_n$). In addition, the electronic properties of the metal complexes resemble that attained for their free-ligands.

The anti-diabetic testing of the oxovanadium compounds with 2-pyridylbenzimidazole (see Chapter 3) will be conducted. This biological testing study will involve the investigation of the glucose lowering capability of the respective complexes against various cell lines (*e.g.* pancreas). The vanadium compounds that exhibit optimal activity will be injected into Streptozotocin-diabetic (STZ) rats for the further advancement of the biological studies. This will establish a solid basis for the biological testing of the isolated metal complexes in Chapter 4.

From a coordination chemistry point of view, future work entails the exploration of *bis*-heterocyclic ligands (see **Figure 6.1**) towards the $[VO_2]^+$ and $[VO]^{2+}$ cores. This will also provide an interesting comparative study between the structure-activity relationships between the mono- and *bis*-heterocyclic chelators. In addition, the glucose lowering effects of the resultant complexes will be explored. Additional motivation is that these *bis*-heterocyclic ligands have shown rich coordination chemistry with an array of transition metals, as shown by their stabilization capability of the *fac*-$[Re^I(CO)_3]^+$ and acidic $[Re^VO]^{3+}$ metal cores [1].

Interestingly, the attempted coordination of a Schiff base derived from 5,6-diamino-1,3-dimethyl uracil, showed no coordination but instead cyclized to form the heterocyclic compounds, see Chapter 5.
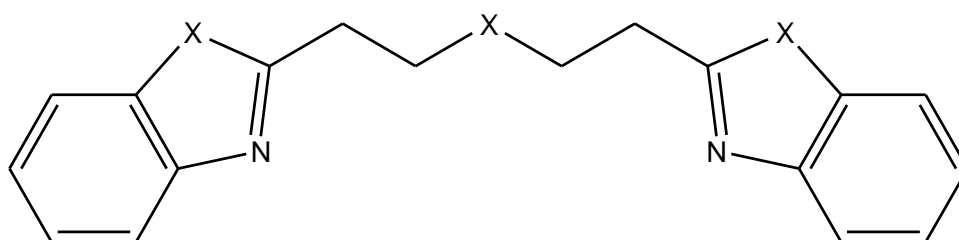

Figure 6.1: *Generic structure of the bis-heterocyclic ligands.*

Reference

1.   Gerber T.I.A., Potgieter K.C., Mayer P., *Inorg. Chem. Comm.*, 2011, **14**, 1115.